Novel seasonal application of low-level solar concentration to contribute to net-zero buildings

by

Gurneet Kaur Khattra

A Thesis Submitted to the Faculty of Graduate Studies of
the University of Manitoba
in Partial Fulfilment of the Requirements of the Degree of

MASTER OF SCIENCE

Department of Mechanical Engineering
The University of Manitoba
Winnipeg, Canada

Acknowledgements

I specially thank my advisor Dr. Eric L. Bibeau for giving me the opportunity to conduct this research as part of his research group. I sincerely admire and acknowledge his desire and commitment to the development of renewable energy and share in his vision for a greener and better future. I would also like to thank Doug Smith who contributed to the development of the Sunflower design used in this thesis. I also thank members of the examining committee for their time in reviewing my thesis and the feedbacks I received to further develop this work. I acknowledge the invaluable support of Seongtaek Oh throughout my research and Jessica Wilson who led the way to set up a flexible data entry approach for the user in Python. My peers at the Renewable Energy Research Group were also crucial to make this project a reality by creating a respecting, exciting and supportive work environment. This work would also not have been possible without the financial support from the University of Manitoba (IGSES), and M. Sc. Program funding. Finally, I thank my parents, Mr. & Mrs. Singh, and my sister for their continuous prayers and support. I thank my husband, Gagandeep Singh, my friends Inderjit Singh and Ekamdeep Singh for their continuance encouragement and support. Last not the least I thank the almighty for giving me strength to carry out my work with sincerity.

Abstract

Due to excessive fossil fuels consumption, the concentration of carbon dioxide is predicted to be approximately 500 ppm by 2050, impacting global biodiversity for generations. Increasing the percentage of recent solar energy use—sun, wind, hydro, and biomass—to address our global energy needs is of fundamental importance. With buildings representing nearly 38% of global emissions, solar energy can contribute to reduce impact: increasing the productive use of solar insolation from building grounds using reflective tracking mirrors, referred to as Sunflower, is a critical component. To this effect, a Sunflower model is developed from first principles to evaluate the productive use of low-level solar magnification from building grounds and roof tops. This model predicts the solar insolation incident onto a user chosen target with many Sunflowers to contribute to net-zero buildings. The model inputs are flexible, for example, change in number of Sunflower mirrors and their target specifications, including seasonal relocation to optimally reduce energy demand in a building, are part of user inputs. The model utilizes a single ray-tracing method to evaluate the solar irradiation redirected onto the building using low-cost solar tracking mirrors. This model developed in Python is based on solar angles and weather data to calculate the redirected hourly solar flux onto a chosen target. Using NREL's Solartrace program based on the Monti-Carlo method, model results are validated within an error of 2.35%. The Sunflower model is then applied to predict the displaced energy in an outdoor pool heating application. The pool heating approach using Sunflower bypasses second law inefficiencies as the pool is heated by the irradiations directly from sun without the use of an intermediate thermal fluid. Multiple case scenarios are established to evaluate the optimal mirror angles to increase the solar intensity for a given seasonal configuration. The Sunflower model predictions for applications in Winnipeg, Manitoba (Latitude 49.9^{o}) using 10 Sunflowers shows that seasonal pool heating load can be reduced by 67%, with a yearly GHG savings of 5.1 tons of CO_{2eq}. For this case, the average yearly solar intensity ratio for a single Sunflower with a horizontal target is 1.81, and averages 1.50 during summer months when solar insolation is higher. For a similar application in the remote community of Arviat, Nunavut (Latitude 61.1^{o}), currently depending on diesel fuel, pool water heating requirements can be reduced by 40% using 15 Sunflowers.

Table of Contents

List of Tables

List of figures

Nomenclature

English symbols

A	Surface area
B	EOT input
C	Heat capacity
EOT	Equation of time
F	Direction vector
HHV	High heating value
GHG	Greenhouse gases
g_h	Evaporated water
t	Solar time
h_c	Convective heat transfer
M	mass
K	Thermal conductivity
L	Thickness
LST	Local standard time
T_Z	Time zone
L_{local}	Local latitude
T_P	Target position
SF	Sunflower position
I_B	Direct normal irradiance
G_B	Direct normal solar energy on target
Q	Energy
Q_{SF}	Solar energy from Sunflower
I_{SF}	Solar flux from Sunflower
$I_{g,h}$	Global horizontal irradiance
$I_{d,h}$	Diffused horizontal irradiance
Qb	Direct normal energy on target
p	Pressure

p_{ws}	Vapor saturation pressure
$\dot{Q}$	Heat transfer rate
Q_d	Diffused solar irradiance on target
RH	Relative humidity
T	Temperature
t	Time
Q_R	Reflected solar energy on target
Q_T	Total irradiance on target
N	Day of the year
$\widehat{SF\_o}$	Vector of Sunflower's orientation
V	Volume
v	Wind velocity
$\dot{q}$	Heat flux
q_{si}	Total solar energy
DNI_{di}	Direct solar energy
DNI_{SFR}	Sunflower reflected solar energy
GHI_{di}	Diffused solar energy
T_P	Target position
SF	Sunflower position
X	Humidity ratio
X_S	Saturation humidity ratio
PCM	Phase changing materials
COP	Cost of performance
GBA	Generalized blocking area
$PMMA$	Polymethyl methacrylate
A_i	Anisotropy index
f	Modulating factor
R_b	Beam radiation tilt factor
$Q_{T\text{-}SF}$	Total irradiance on target without Sunflower
Q_{T+SF}	Total irradiance on target with Sunflower

Q_{ratio}	Intensity ratio
g_h	Amount of evaporated water per hour
h_{we}	Evaporation heat of water
CWEED	Canadian weather energy and engineering
LEED	Leadership in energy and environmental design

Greek symbols

Δ	Difference
ε	Plate angle
∇	Differential operator
$\mathcal{E}$	Emissivity coefficient
Δ	Solar declination angle
A	Hour angle
χ	Solar zenith angle
Σ	Stephan Boltzmann constant
ζ	Solar azimuth angle
θ_i	Incidence angle
θ_h	Horizontal angle of Sunflower
θ_v	Vertical angle of Sunflower
α_s	Sunrise and sunset hours
$\hat{S}$	Sunlight vector
θ_0	Angle of reflection
Θ	Evaporation coefficient
$\delta_{Solartrace}$	Solar declination angle in Solartrace
$\omega_{Solartrace}$	Hour angle in Solartrace
$\alpha_{Solartrace}$	Solar azimuth angle in Solartrace
$\gamma_{Solartrace}$	Solar zenith angle in Solartrace

1. Introduction

1.1. Global energy scenario

The world population is estimated to be 9.7 billion by 2050, which represents a 33% increase from the 2016 population census of 7.7 billion [1]. Rapid development and industrialization are increasing energy demand. Future global energy consumption is depended on the development of technology, economic trends, demographic change, and availability of resources that drive energy use. The United States Energy Information Administration forecasts that the increase in global energy consumption is expected to surge up to 30%, from 575 BTU Quadrillion (169 PWh) in 2015, to 736 BTU Quadrillion (216 PWh) in 2040 [2]. A considerable percentage of this upsurge will be from Non-Organization for Economic Co-Operation and Development (Non-OECD) nations than Economic Co-Operation and Development (OECD) nations, due to economic growth, easy access to the energy market, and increased population [16]. Figure 1 represents the energy demand growth by OECD and Non-OECD.

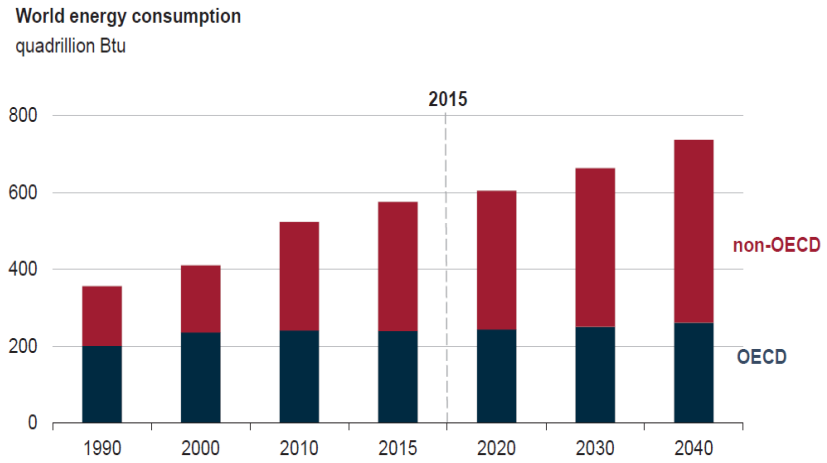

Figure 1: Past and projected global energy demand by OECD and Non-OECD from 1990-2040

According to the International Energy Agency, the total primary energy supply in 2018 was mainly from oil, coal, natural gas, representing 84% of the energy supply [3]. Figure 2 shows the breakdown of energy resources. Most of the energy is driven by fossil fuels and there is growing concern about its impact on the environment and sustainability. The global average atmospheric

carbon dioxide in 2018 was 407.8 parts per million (ppm) [3]. Carbon dioxide levels are much higher now than at any point in almost 1 million years.

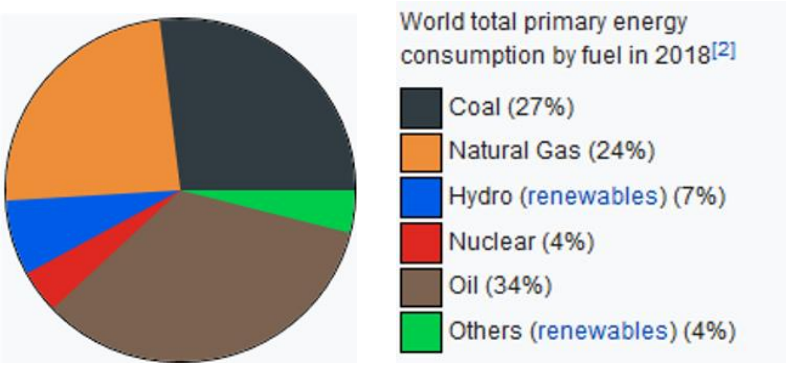

Figure 2: World total energy consumption by fuel in 2018

In 1980, the ppm concentration of carbon dioxide was nearly 340 ppm and presently the concentration is 418 ppm [4], as shown in Figure 3. The expected ppm concentration of carbon dioxide in 2050 is 500 ppm [4]. We are entering an era where human caused carbon dioxide will decisively impact every aspect of life and biodiversity. Since our increased dependency on fossil fuel will boost the concentration of CO_2, we may exceed as high as 685 ppm in the next few decades [6]. Increasing the reliance for renewable energy, enhancing the efficiency of energy systems, and lastly lowering the energy demand can decrease the concentration of CO_2. The most feasibly and viable solution to curb the emission levels is to further explore and implement the usage of renewable energy resources (solar, wind, hydro, and biomass), improved efficiency of the power-systems, battery storage developed systems, and other related technologies to reduce carbon emissions.

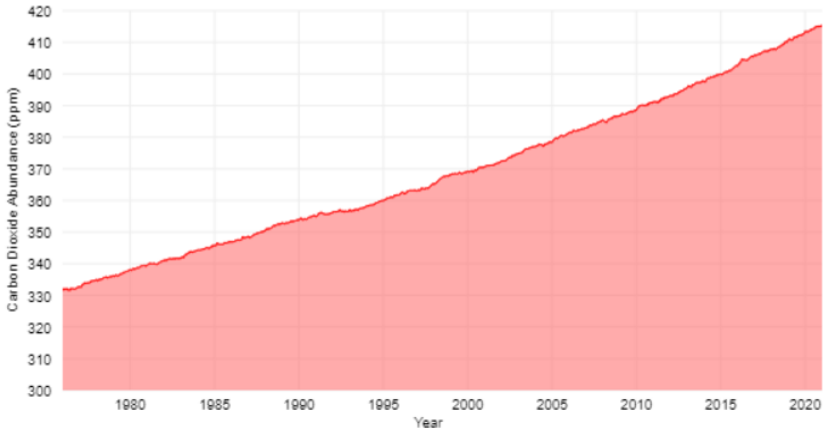

Figure 3: Part per million of carbon dioxide from 1975 to 2020

1.2. Renewable energies

As the global increase in energy consumption continues this will result in energy security and environmental sustainability issues unless either energy demand decreases, or there is a switch to renewable energies. Peak oil production and subsequent exhaustion of reserve will add pressure on the oil-exporting [2]. Policy makers need to take practical measures to eliminate the reliance on fossil fuels. Surpassing a critical concentration of CO_2 will affect developing countries more than developed ones due to higher populations. Some studies showed that if all fossil fuels on the earth are combusted then the ice of Antarctica will disappear, hypothetically resulting in the 200 feet rise in the sea levels [4], enough to submerge most of the major cities.

The world energy demand is projected to increase by 30% by 2040 [2]. Due to the rising concern of greenhouse gases (GHG) and fossil fuel depletion, the world needs transition to alternative resources of energy and technology, which would be more efficient, environment-friendly, economical, and available than fossil fuels. Renewable energies such as solar, wind, biomass, and hydro present a solution to reduce the amount of GHG emission and guarantee future energy security. Renewables can replace fossil fuels [2]. However, there is some debate on the reliance, cost, and life span of renewable energies being encouraged by topics on economic viability, fuel compatibility with present technologies, and even environmental consideration. Further research needs to be done to suppress these debates.

However, to solve climate change problem, it is important to focus on the Renewable Energy Ratio (RER), as the benchmark which qualifies the percentage of primary energy is derived from recent solar radiation. The Renewable Energy Ratio is defined as the ratio of percent of renewable energy to the total energy. Our research group focuses on THE RED CUP approach to increase RER to solve climate change where:

- THE are the energy requirement for Transportation, Heating and cooling, and Electricity.
- RED are the levers that can increase RER by adding Renewables, increasing energy Efficiency, and decreasing energy Demand.
- CUP are the scales to apply change which stands for Community, Utility, and People.

For example, THE RED CUP approach finds it relevant to apply small concentrating mirrors for buildings to solve climate change as it increases **R**enewables and improves **E**fficiency of current technologies at the **P**eople scale.

1.3. Low-level solar concentrators mirrors

Low concentrating solar reflectors referred as “Sunflower”, are two-axis solar tracking reflective mirrors that redirect sunlight onto a user-selected target to obtain solar intensity/magnification of about 1.5x to 10x for building applications. Such mirrors are yet to be in use. The Sunflower is a two-axis solar tracking device. Unlike current solar magnification technologies, both the target and Sunflower can literally be placed at any location, as per user selection and constraints, even if far from being optimal. Small solar reflectors are made viable, in part, by the considerable cost decrease in electronic components like motor controllers, and 3-D printer technology advancements, and small direct current stepper motors. These reflectors work by redirecting the Direct Normal Irradiance (DNI) onto a selected seasonal target surface allowing new distributed solar applications to address climate change at the people scale. It can be used for numerous applications, including residential pool heating and space heating by intensifying the solar energy on Phase Change Material (PCM) windows. The development of such Sunflower device is being developed within our research group in renewable energy at the University of Manitoba with numerous potential applications found.

A Sunflower comprises of a dome shaped tracking device and moving mirrors to reflect the suns' irradiation onto a fixed target. The firmware is uploaded to an Arduino board which activates two direct current (DC) motors to enable the device to track the sun using the variation of light intensity onto six low-cost optic-sensors arranged around a vertical stem. One motor is for zenith solar tracking, and the other motor is for azimuth solar tracking. Each motor's powers a cylindrical worm screw shaft. Each worm shaft is mated with a worm gear that matches with the motion of Sunflower for each axis. As each motor tracks the sun in the two polar axes, the mirror is directly geared to move 2:1 in the azimuth and 1:1 in the zenith to remain focused onto the target. The plane mirrors, as shown in Figure 4, are the major components which turn to keep reflecting sunlight toward a pre-determined target, compensating the sun's apparent motion in the sky. The circular area of all four mirrors is presently 1 m^2. The mirror material is Macao SAR Aluminium with a reflective efficiency of 95% [17]. To redirect the light towards the target, the reflective surface of the mirror is kept perpendicular to the bisector of the angle between the direction of the sun and the target, as seen from the mirror. The target is stationary relative to the heliostat, so the light is reflected in a fixed direction [19]. The unique reflector our research group designed, while not yet completed, accomplishes the design goal. The manufacturing cost target is $50 per unit.

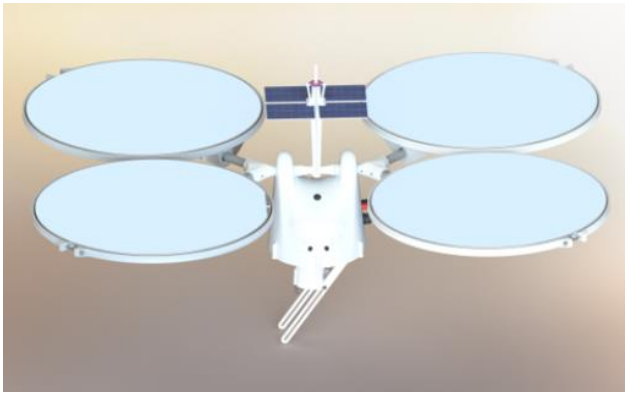

Figure 4: Sunflower during prototype configuration with 4 smaller mirrors. The system uses 2 motors to move the stem that tracks the sun and move the mirror using direct gearing. Mirrors are made of flexible reflective fabric to reduce weight and shipping package size. Such a design approach reduces costs but limits the mirrors to be constrained to a relatively small-scale in the order of 1 m^2. The four mirrors can be adjusted to approximate a concave of convex reflection surface.

1.4. Problem statement and hypothesis

The extra-terrestrial solar flux that intersects the earth's surface is 1351 W/m^2 [27], which globally means that 4.3 quintillion joules [5] of solar radiation intersects the earth's every hour, which is nearly 10,000 times more energy than the world presently consumes. Direct solar radiation energy can be used to address our transportation, heating/cooling, and electricity needs (THE). Various technologies use direct solar radiation to generate usable energy. The problem is the relatively low energy density of direct solar radiation. The usefulness of many solar technologies could be increased if the solar radiation was increased. The hypothesis of this research is that redirecting sunlight using small 2-D tracking mirrors to achieve relatively low solar concentration ratios onto a chosen building target to increase the solar intensity can contribute to solve climate change. Our research group has found at least 20 building applications of Sunflower mirrors to contribute to climate change. However, nothing can be achieved until a Sunflower model with flexible inputs is developed. Such model does not yet exist. Moreover, this is the only application in renewable energy where the application changes with seasons allowing to optimize the use of each Sunflower depending on building requirements.

In this research, once the Sunflower model is developed the analysis will be restricted to a pool heating application to demonstrate how small-scale mirrors can contribute to net-zero buildings. Canada has about 600,000 residential pools, and 60% of ground pools are heated. The typical period of pool heating is from May to September. The yearly energy usage of a swimming pool varies from 600 kWh/m^2 to 6,000 kWh/m^2 depending on pool area, period of operation, location, and weather [8]. Different types of active and passive technologies are used to achieve the required temperature. The active methods comprise electric, heat pumps, natural gas, propane, and solar heaters. Phase change materials and thermal insulation covers are examples of passive pool heating methods. Heat pumps are a popular method to heat pools [8], but pools are mainly heated using natural gas [9]. Approximately 10% of pool heating is done using solar heaters in Canada [10]. A worthwhile goal to address climate change is to determine by way of example the extent to which small-scale reflecting mirrors can reduce the energy requirement for pool heating in Canada. This can then be applied to many other applications, from heating greenhouses to increasing photovoltaic output of solar panels in winter months, to light pipes.

1.5. Objectives of research

The three objectives of this research are:

a) Develop a versatile predictive model using the Python coding language to calculate the solar intensity ratio obtained using small reflective mirrors assuming no objects are in the path of the solar rays and validate the model against Solartrace software that allows objects in the path. The model must be able to easily change the location, target, and application of each Sunflower.
b) Quantify the impact of Sunflower location, orientation, seasons, latitudes, and longitudes on the intensity ratio and magnification ratio.
c) Investigate the energy savings and GHG reduction possible using Sunflowers for pool heating in Winnipeg and Arviat locations.

1.6. Research methodology

The research methodology is schematically shown in Figure 5. A Sunflower model is required to be developed from first principles to predict the solar insolation for each seasonal application onto a target. The approach is to first

- use the formulation of equation of solar time including solar and local standard time, solar declination angle, hour angle, solar zenith angle, solar azimuth angle, incidence angle to track sun rays hourly at location of interest,
- allow to easily change inputs i.e., latitude and longitude of target, day, number of Sunflowers by developing a reusable library,
- change the Sunflower mirror position at any time during the year,
- calculate the intensity and magnification ratio, and
- validate the Sunflower model using the open-source program Solartrace, a Monti-Carlo ray tracing model developed by NREL which allow objects like trees in the path.

To be more specific, based on the sunlight vector, the direct normal irradiance data collected by Canadian Weather Energy and Engineering Datasets (CWEED) is given in the units of kJ/m^2. To redirect this normal irradiance towards the target, the angle of reflection is calculated assuming each Sunflower is focused onto the target by the user. The intensity ratio and the magnification

ratio of the energy on the target with and without a Sunflower is calculated. The model is then validated against NREL's Solartrace simulations. Furthermore, the horizontal surface is a target at 0° to the ground surface which is a pool in this application. Some solar irradiation is directly falling onto the target; some solar irradiations is redirected by the Sunflower mirrors onto the target. Figure 6 and Figure 7 show how the intensity of solar energy falling onto the target is increased by using a single Sunflower 2-D tracking mirror.

To calculate the total energy required for pool heating, the parameters for the pool target is given as an input to the Sunflower model. The developed Sunflower model calculates the total incident energy. The losses such as convection, conduction, radiation, and evaporation are included in the pool model to determine the total energy required to heat up the pool. Tables, graphs, and contour plots are automatically generated for each simulation case as part of the Sunflower model.

1.7. Research contributions

The research contribution is a *flexible* and *validated* model to predict the solar magnification using small-scale mirrors to contribute to net-zero buildings. To easily calculate the total energy gain by using Sunflower mirrors for many potential applications is the goal of this research. The research is performed into 2 steps.

- Step 1: Developing the generic Sunflower model to calculate the energy intensity, which can be applied to many applications to increase the solar intensity for net-zero buildings.
- Step 2: Apply the Sunflower model to residential pool heating to calculate the energy and GHG emission savings.

In Step 1, the developed solar energy tracking model allows the user to change the inputs as discussed in Section 1.6 for any applications, which vary seasonally. The Sunflower model can be applied, for example, to melt the paraffin wax in Phase Change Material (PCM) window for efficient space heating and provide sunlight in greenhouses to reduce power consumption and increase solar PV outputs. It is beyond the scope of this thesis to explain all the applications possible to address climate change using Sunflower mirrors.

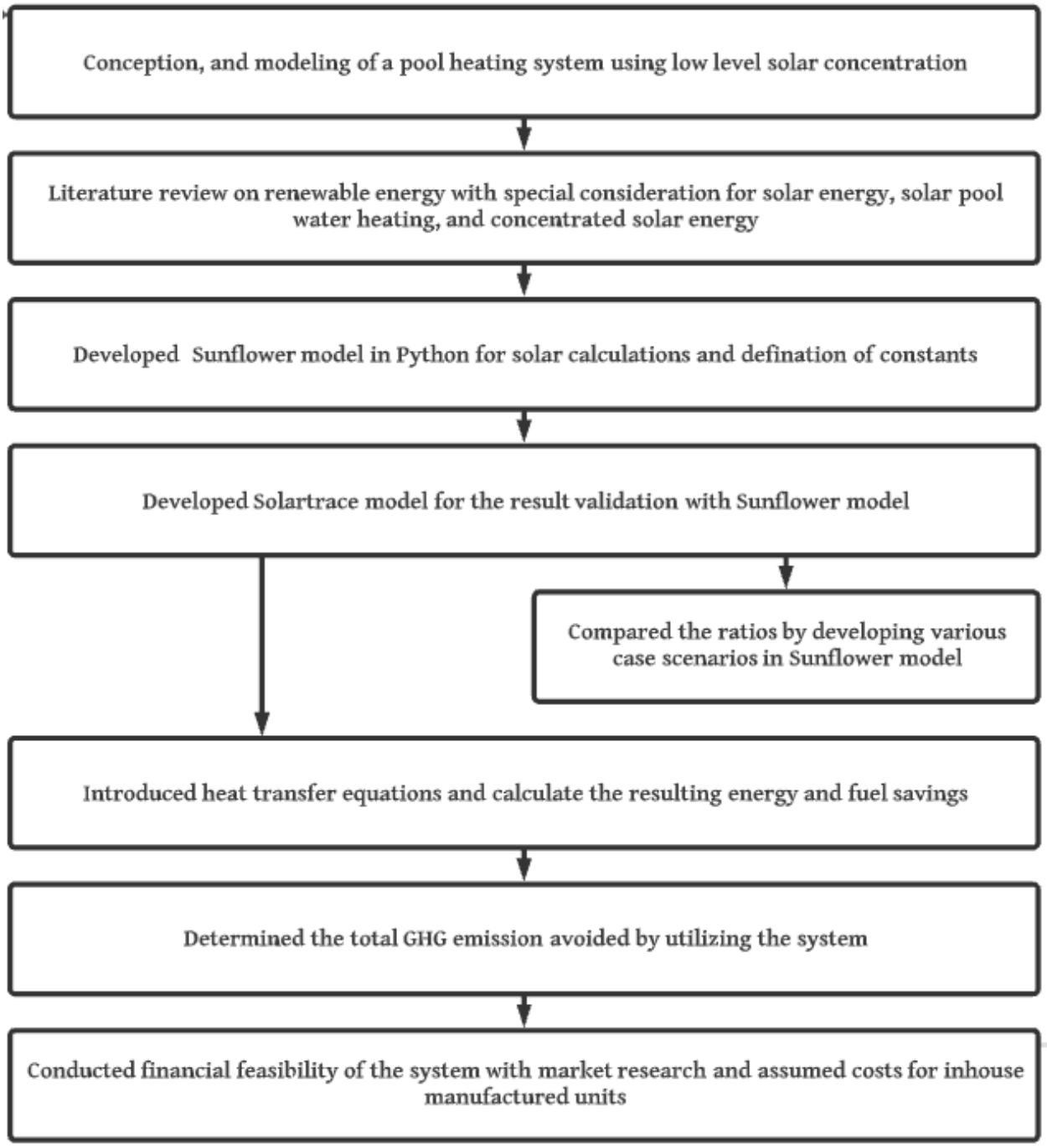

Figure 5: Research methodology to complete the project

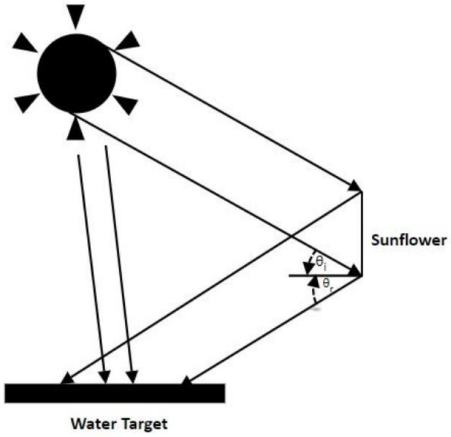

Figure 6: Using small-scale mirror to concentration sunlight onto a swimming pool water surface

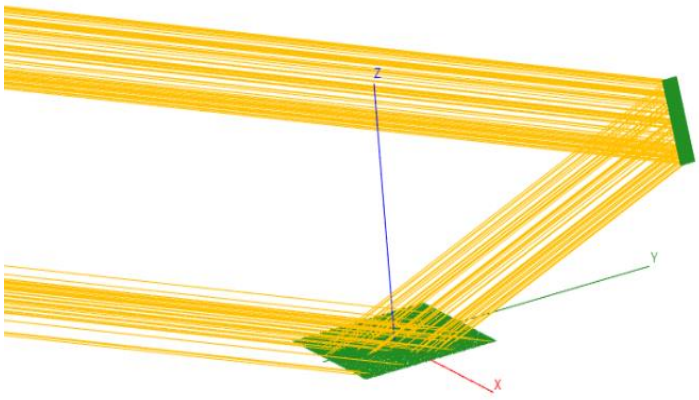

Figure 7: Visualization of the direct beam of the sun (with diffuse) and the redirect sunlight by one Sunflower mirror (without diffuse) as calculated using Solartrace program. Solar reflection is ignored. The lower green section is part of the pool surface, and the other green object is the Sunflower mirrors that redirects the direct beam onto the target while it tracks the sun using only 2 motors in total. The total solar energy onto the target is the direct beam from the sun and the reflected radiation from 1 to many Sunflowers.

In Step 2, the model is applied to demonstrate how to use Sunflowers for a residential pool heating application—the predictive model estimates the heating energy reduction and GHG emissions. The Sunflower model needs to give stakeholders insight of energy savings for implementing this type of pool heating system. Note that Step 2 must be repeated for every new application while Step 1 remains invariant.

Unlike any prior renewable energy applications, implementation of Sunflower allows user to change the application and thus the number of variables and unknowns are significant. Future optimization requires to develop a Sunflower model which assumes no interferences like trees so it can perform numerous calculations in a timely manner for all the potential applications. When obstacles are present then an add-on library similar to NREL's Solartrace is required.

1.8. Outline of thesis

In Chapter 2, the literature review is discussed. Some current applications based on heliostat are reviewed, including heat losses from a pool. Chapter 3 develops the methodology and explains the Sunflower model formulation. Subsequently, the validation of the results is investigated. Furthermore, the validated Sunflower model is used to investigate various scenarios such as different angles to find out the optimum combination of horizontal and vertical angles of each Sunflower with respect to the target. In Chapter 4, the assumptions and the characteristics of the pool water heating model are presented. The calculations and results of required energy, heat losses, total GHG savings, and cost analysis are shown. Lastly, the research conclusions, and recommendations established on the outcomes are presented in Chapter 5.

2. Background literature

2.1. Introduction

Concentrated solar energy is a promising approach to reduce fossil fuel consumption. It uses mirrors or lenses to concentrate the larger areas of low-density sunlight onto smaller areas of high-intensity sunlight. Figure 8 shows the tracking mechanism of a heliostat [22]. The orientation of the heliostat is determined by obtaining the normal vector of the heliostat. The normal vector of heliostat is calculated by the incident sunlight vector coming from the sun and the redirected sunlight vector from the heliostat going to the target.

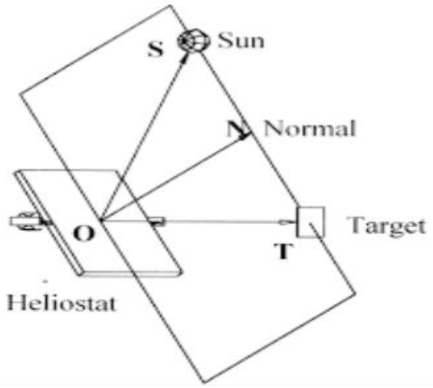

Figure 8: Tracking mechanism of heliostat from Reference [22]

Unlike traditional manually controlled heliostats, modern heliostats are controlled by computer programs. The direction of movement of a heliostat is defined by the equations based on the angle of Direct Normal Irradiance (DNI) relative to the earth's surface. Furtherly, these heliostat systems use astronomical theory to calculate the sun's direction with respect to the mirrors. The embedded program calculates the direction of required angle bisector for the given direction of the target. The control signals of the calculated angle by embedded program are then sent to the motors for the alignment of heliostat's mirrors. This process is repeated to keep mirrors effectively oriented [20]. For a Sunflower, tracking is performed using a trial-and-error approach to eliminate the shadow cast by a vertical step onto six low-cost optical sensors. During the sun tracking, the four light-weight mirrors are also moved as the motors are directly linked to the Sunflower mirrors.

2.2. Mechanical heliostat structure design

Zhang et al. [21] discussed the design of a high-performance heliostat having a motor gearbox drive system. The wind and gravity load on heliostats are accomplished by placing a heliostat isolated in a Concentrated Solar Power (CSP) plant. The schematic structure of a heliostat with forces and moments is shown in Figure 9. For the mirror and dimension design procedure, the suitable size, heliostat curvature, and area format of the heliostat are required to be considered. The mechanical guide structure is designed considering those parameters of low-cost and robustness to withstand the wind stress at a higher angle of attack. The motor-gearbox device is built on the electric drive ratings found from the former load analysis. This is because the product of the gearbox ratio and the motor's-built torque should be able to overcome the maximum wind load torque while driving the heliostat to accomplish precise solar tracking. Furthermore, the cost of heliostat can be higher compared to conventional means of power generation. However, such system offers thermal storage to increase load flow, making the technology more attractive.

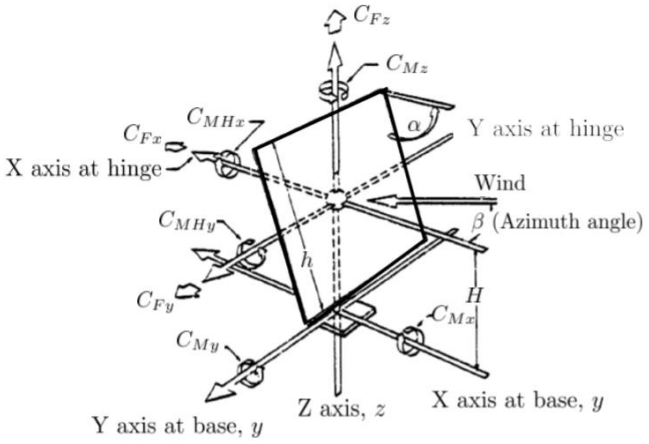

Figure 9: Illustration of hinge, azimuth moment of heliostat

Due to the multi-physics nature of the heliostat and the wide range of its design parameters, the designing of heliostats is a heuristic process. It requires simulation studies during the designing stages: validating the wind load analytical model, having access to the mechanical deformation of the heliostat's structure, and verifying its electrical motor-gearbox power performance, as shown in Figure 10. The following objectives are presented for low cost, high-performance heliostat.

- Robust: Capable of withstanding the wind load
- Precise: Efficient tracking operation
- Low-cost: Low cost of production, installation, maintenance of components
- Efficient: Providing energy savings with minimal power loss

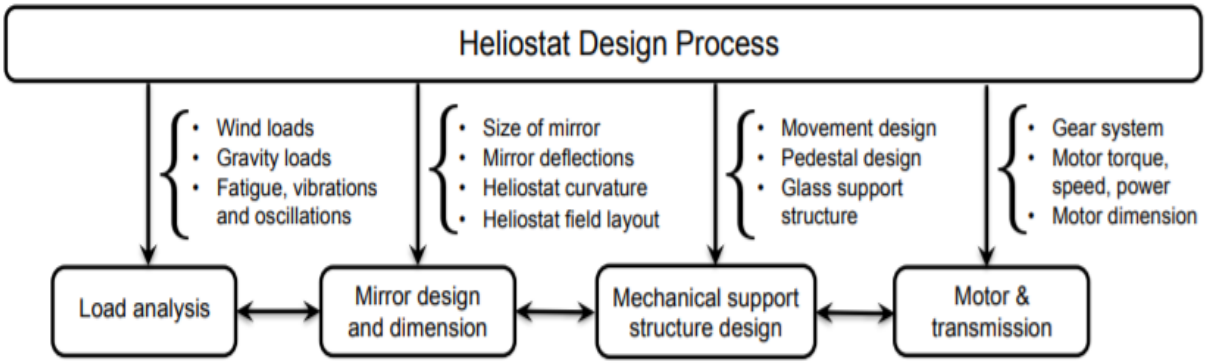

Figure 10: Flow chart of heliostat design process for concentrated solar power plants from Reference [21].

2.3. Cosine effect

Zhang et al. [22] defined the cosine effect of a heliostat as the cosine angle α formed between the solar radiation and the mirror normal line that reduces the effective sunlight receiving area of each heliostat mirror. This cosine effect is one of the critical reasons that causes energy loss in solar energy concentration systems. The cosine angle represents the ratio of the effective area to the real area of the heliostat's mirror. Figure 11 shows the schematic representation of the cosine angle. For Sunflower applications, cosine losses will be more prevalent as the end user selects the position of each Sunflower, and for building applications, there are numerous constraints: trees, garden, driveway.

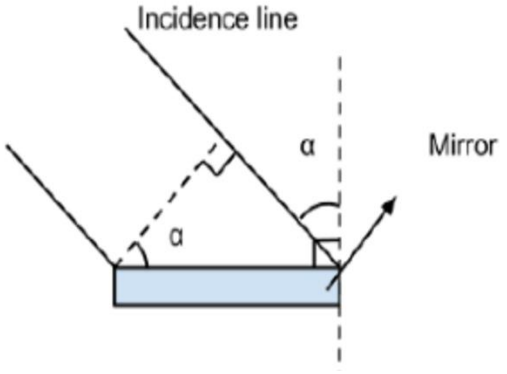

Figure 11: Cosine angle between incident line of solar radiation and normal line to the mirror. Here α is also the zenith angle of the sun that varies from +90° to -90° at sunrise and sunset and never crosses 0° at higher latitudes from Reference [22].

G. López et al. [23] described the cosine effect loss in a rotating and static heliostat field. The cosine loss can be minimized with the optimal arrangement of the heliostat. The study states that during the morning and the evening hours the cosine efficiency of the static and rotating field is 81% and 95% respectively. Table 1 shows the percentage amount of power loss due to misalignment or cosine effect [23].

Table 1: Percentage loss for misalignment of different angles [23]

Hours	α	Lost	α	Lost
1	0^o	0%	23.4^o	8.3%
2	1^o	0.02%	30^o	13.4%
3	3^o	0.14%	45^o	30%
4	8^o	1.00%	60^o	>50%
5	15^o	8.30%	75^o	>75%

2.4. Low-cost heliostat

Pfahl et al. [24] discussed the advantage of light-weight heliostat equipped with a rim drive. To achieve the required energy supply and controlled system, a 8 m^2-facet was developed. Figure 12 shows the low-cost heliostat structure balanced by using rim drives and horizontal axis for the

movement of mirrors. The heliostat structure consumes less energy due to the weight balanced moving parts and little shifting of the sandwich mirror. Further, the precise and efficient winch wheel cable drive system is used to move the rims. The diameter of the rims is kept large to achieve precise tracking with low-cost gears and motors. During night and in case of emergency, the linear stepper motor and actuators are incorporated with each rim drive to allow heliostat to stay powerless. An adjustable pin is installed at the shaft of the linear actuator to avoid the need of power during periods of no movements of rim. The primary advantage of this heliostat is its high energy efficiency as compared to many other models. Therefore, it requires smaller PV-cells.

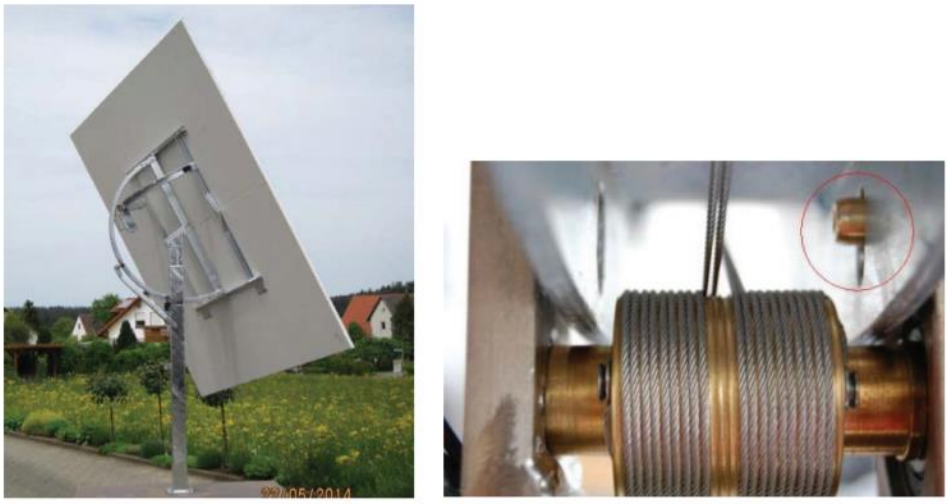

Figure 12: (a) Rim drive prototype with 8 m^2 mirror surface, and (b) winch cable drive system, locking position of the smaller rim drive with the red circle showing the adjustable pin, taken from Reference [24].

2.5. Wind loads on heliostats

Peterka et al. [25] discussed the structural and fatigue failures of heliostats due to the wind loads. The fatigue load of the heliostat is caused by the heavy wind loads than exceed the material capacity. Heliostats in power stations can be protected from wind loads by using upwind protection fences. The conclusions from the experiments are listed below:

- The effect of upwind blockage on the heliostat or wind fences can be accounted for by outlining a generalized blockage area. Therefore, the specific geometry can be ignored.

- Both mean and peak wind loads decrease significantly by increasing the generalized blockage area.
- The wind fences perpendicular to the wind are more effective than the fences at 45° to the approaching wind.
- Wind blockage structures of smaller length are more efficient than a single long fence.
- Wind drag and lift on single heliostat shows a remarkable sensitivity to wind turbulence within the expected scope for open fields.
- Square and circular heliostat have similar mean and peak wind load coefficients.

Such wind loads are an important issue for heliostat that remain yet unresolved. It has been suggested to use small, perforated holes in the fabric to reduce the drag which would affect the reflective coefficient.

2.6. Optical performance of concentrators

Algarue et al. [26] discussed that small-scale concentrator with moderate concentration ratios has the capability to replace expensive PV cells without compromising the overall output. The advantages of small-scale concentrators are light weight, modest size, and simple to install with no need of tracking. The authors utilized either refractive or reflective optical devices to concentrate the sun light on the target surface. By using advanced ray techniques, the research concluded that refractive and reflective concentrators have the same efficiency for concentration ratio up to ten, while in case of higher concentration ratio beyond ten, the performance of reflective concentrators is not efficient as compared to refractive concentrators.

Figure 13 shows the transparent cover of polymethyl methacrylate (PMMA) material of 1 mm thickness with 88% of transmissivity, and 95% reflectivity for all 3 reflective concentrators.

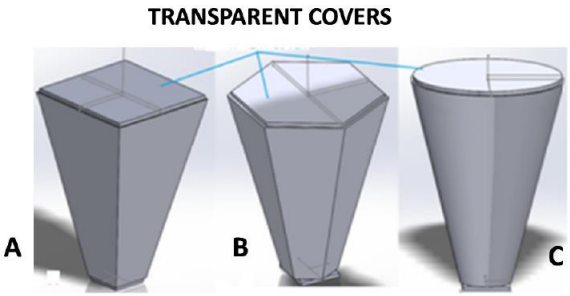

Figure 13: Three reflective concentrators of different shapes from Reference [26]

It is observed that in case of squared and hexagonal concentrators, the average flux of 3,500 W/m^2 is evenly distributed over the sunlight receiving area. However, for the circular concentrators, the average 20,000 W/m^2 flux distribution is concentrated at the centre and nearby area. Figure 14 represents the flux distribution over all three different shaped surfaces.

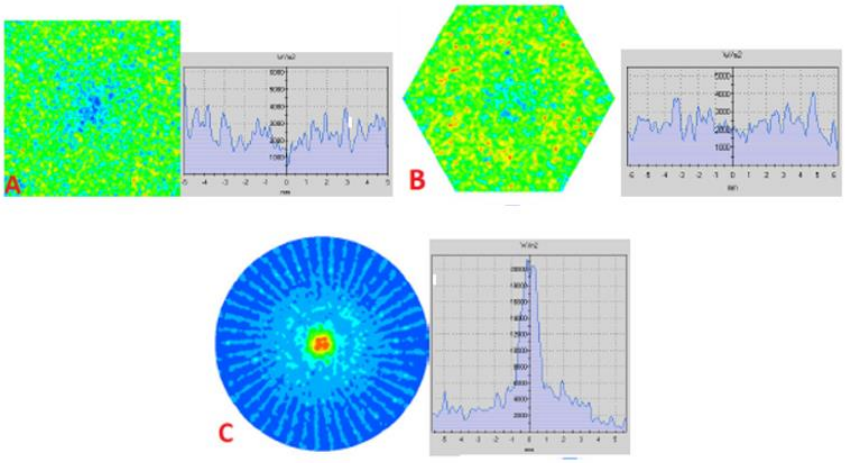

Figure 14: Flux distribution on the different shape receiver surfaces from Reference [26]

2.7. Low and high magnification

Concentrated solar power is based on several fundamental laws of physics and Second Law of Thermodynamics. Theoretically, the solar thermal efficiency of a heliostat is considerably higher because many reflecting mirrors are redirecting the solar energy. Heat losses from any surface are

directly relative to its surface area [27]. The heat losses are reduced if the mirror surface area is reduced.

Approximately 1,351 W/m^2 of solar radiation reaches the outer surface of earth's atmosphere, while a maximum of 1,000 W/m^2 reaches the earth's surface [27]. A heliostat can gather direct beam irradiation and transmit the energy over considerable distance without losses. Some of the major advantages of using low magnification concentrator are:

- Low magnification heliostat is cheaper in cost because it requires less amount of material to build.
- Since the height of low magnification heliostats is less than 5 feet, it is comparatively less probable to be destroyed by wind loads as compared to higher magnification heliostats that are taller in height. Here, wind forces can be addressed with fencing.
- Smaller sized heliostats can reflect solar concentrations at smaller sites irrespective to the conventional solar energy systems.
- Small heliostats are easy to install and relocate.

It is such advantages that Sunflower seeks to employ to permit the over 1 billion residential and commercial houses/buildings worldwide to productively use distributed solar radiation more effectively.

2.8. Residential pool heating methods

Mousia and Dimoudi [28] stated that every season, the average energy required to heat up a pool is 2456 kWh/m^2, and 1,827 kWh/m^2 when the pool is covered by a thermal insulated material [28]. The author concluded that the energy required is higher in traditional pool heating methods as compared to advanced methods by using phase change materials for pools.

Table 2 shows the thermal properties of various materials used in thermal insulation covers from Reference [43, 44, 45].

Table 2: Thermal properties of material used in thermal insulation covers

Names	Density (kg/m^3)	Thermal conductivity (W/m·K)	Specific heat (kJ/kg·K)
Polyvinyl chloride	1100 - 1450	0.13 - 0.28	1.0 [43]
High-density polyethylene	930 - 970	0.46 - 0.52	2.3 [43, 44]
Low-density polyethylene	910 - 940	0.33	2.3 [43, 44]
Unnamed plastic	-	0.08 [45]	-

The technologies utilized for pool heating are categorized into two categories: active and passive heating technologies. The different types of pool heating technologies are discussed in the following sections.

2.8.1. Conventional pool heating techniques

The commonly used conventional techniques in pool heating are electric and oil/gas heaters. Electric pool heater converts electric energy into heat energy to increase pool water temperature, whereas oil/gas heater use oil or gas to heat the pool [29]. Figure 15 demonstrates the schematic diagram of electric and oil/gas heaters for pool heating.

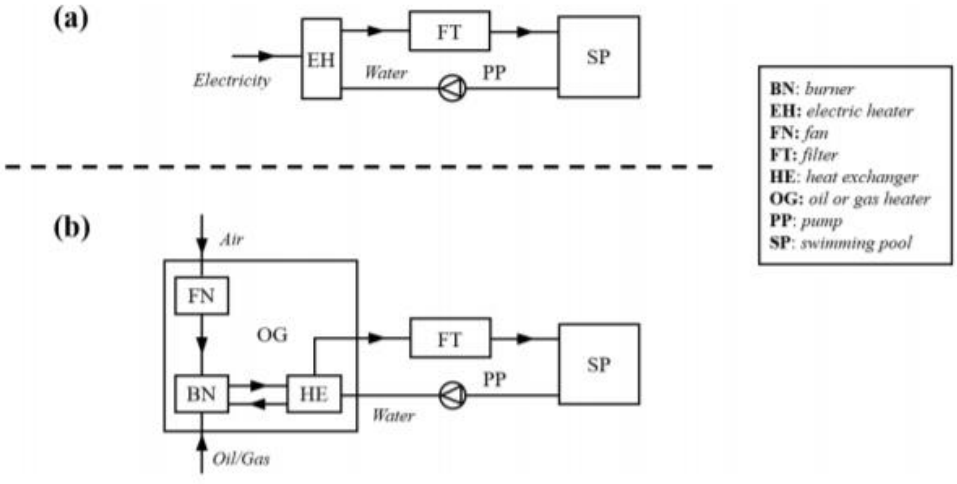

Figure 15: Schematic diagram of (a) electric and (b) oil/gas heaters for swimming pool heating applications from Reference [29]

For oil/gas heaters, heat exchanger, fan, and burner are included. The ambient air is the input into the burner and mixed with the oil. After this mixture is burnt, and heat is transmitted to the pool through a heat exchanger via a pumped fluid like glycol.

2.8.2. Solar collector technology

Solar collector technology is also widely used for pool heating systems due to its lower operating cost as compared the other pool heating methods. The solar energy works as an input to heat up the water in this system. To adopt this method, various studies have been conducted over the years. Croy et al. [30] conducted a study using solar collector in Germany. This research showed that solar collector system is more economically competitive than conventional systems [30]. In India, a study shows that the cost savings by using solar collector are up to 53.3% compared to conventional systems [31]. However, research conducted in the United States, concluded that the system might not be economically feasible over a period of 10 years [32].

2.8.3. Heat pump technology

Heating the pool water by using a heat pump is also a commonly used technology. This system consists of a fan, evaporator, condenser, compressor, and expansion valve. The ambient air is cycled by the fan which exchanges the heat with refrigerant in the evaporator. The compressor increases the pressure of refrigerant from the evaporator. This high pressurized refrigerant is the input to the condenser that further transfers the heat to the cold pool water. The refrigerant leaving the condenser will be the input to the expansion valve and thus the pressure of refrigerant will be reduced for the next cycle. Figure 16 shows the schematic of heat pump system.

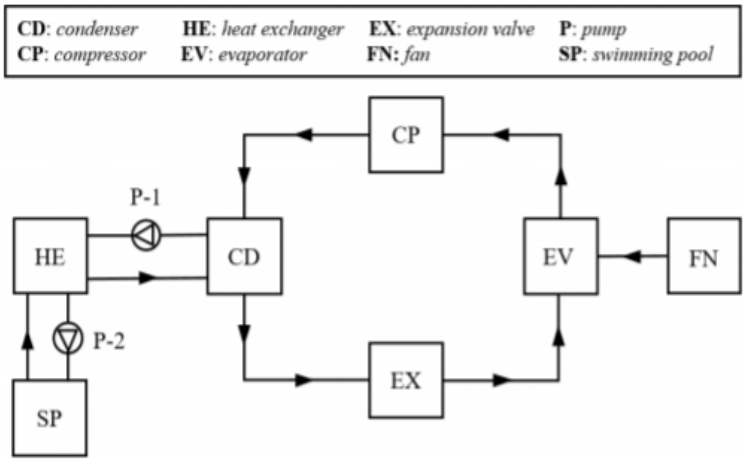

Figure 16: Pool heating system with air-source heat pump from Reference [29]

Greyvenstien et al. [33]. designed a heat pump system for pool heating purpose in South Africa. The writers concluded that the heat pump pool system is more cost-effective than solar panels. It might be due to the initial cost of solar panels. Chan et al. also claimed that based on their study for a five-star hotel in Hong Kong, the energy cost for pool heating system using heat pump with a Coefficient of Performance (COP) of 3.5 can be reduced by HK $275,700 in a ten-year cycle as compared to other conventional pool heating systems [34].

2.8.4. Phase change material storage technology

Phase change materials (PCM) is an energy storage system used in passive pool water heating technology. It stores energy during minimal demand and peak renewable generation period and discharge the energy during high demand and low renewable generation period [35, 36, 37]. Compared to other energy storage mediums, PCMs have a high energy storage capacity and approximately steady temperature during transition. Zsembinszki et al. [38] compared the two ways of applying PCMs in pool heating systems; PCM panels are installed in the swimming pool walls, and PCM storage tanks are used to supply heat for pool water. The writers concluded that the later method is more effective since the discharging time of stored heat can be managed effectively [29, 38].

2.9. Cost comparison of pool heating methods

Table 3 and Table 4 compares the estimated initial cost and operating cost per year of different pool heating methods [12]. Here, the preferable average pool size is considered between 3 to 6 m wide, 6 to 12 m in length, and 1.2 m in depth [11]. The initial cost and the operating cost of pool heating is the total cost of pool operation for its lifetime.

Table 3: Estimated pool-heater installation cost for 5 m 10 m pool

Type of heater	Heater cost ($)	Additional material and labour ($)	Total cost ($)
Natural gas	2,900	2,000	4,900
Heat pump	5,900	500	6,400
Solar	3,200	1,800	5,000

Table 4: Typical pool-heater operating cost for 5 m 10 m pool per year

Type of heater	Heater cost ($)	Additional material and labour ($)	Total cost ($)
Natural gas	1,100	100	1,200
Heat pump	400	100	500
Solar	0	50	50

2.10. Challenges with solar panel heating systems

To reduce environment impact and to reduce operating costs, users are adopting solar heating systems. Solar panels are installed either on the roof or on the surrounding ground area of the building. To achieve 15% to 20% of efficiency, the sunlight collector surface area of solar panels is normally 80% [13] of pool surface area for effective heating of the pool water [7]. Additionally, to accomplish the most effective tilt angle in case of flat roofs, angle mounts are required to incline tilt of the solar collectors [14].

Furthermore, there is no global warming emission directly linked to energy production from solar

panels, but there are GHG production at various stages of the solar panels' life cycle, including during manufacturing, material transportation, installation, maintenance, discharging and dismantlement [15].

2.11. Heat transfer losses

A comprehensive heat transfer model is a requirement to analyse the performance of pool heating system. The required energy to increase the temperature of pool water is considerably higher than the specific heat value over the operating period. To achieve a thermal equilibrium state, heat transfer from high temperature mediums to low temperature mediums are required to be balanced. The followings are the various forms of heat loss in pool heating systems [39].

- **Evaporative heat loss:** The conversion from pool liquid water into water vapour to establish a mass equilibrium with the unsaturated air at the given partial pressure leads to evaporation heat losses. In this process, water molecules absorb heat which is used to evaporative pool water. Windy days increase the evaporative heat loss. Furthermore, the water must be replaced with colder city water when the pool water level becomes too low.
- **Convective heat loss:** The velocity of the air on windy days result in convective heat loss.
- **Conductive heat loss:** For below ground pools, the conductive heat loss occurs due to heat transfers from the water to the surrounding ground and air above the pool surface. Studies observed that conductive losses can be ignored but Govaer et al. [40] state that the conductive losses must be considered in case of moist air, and moist soil or ground.
- **Radiation heat loss:** The radiative heat loss is generated by the heat transfer between the pool water and the surrounding air in form of long-wave radiation.

A detailed discussion of heat losses is further addressed in Chapter 3.

2.12. Net-zero buildings

Net zero buildings require net zero energy consumption. It indicates that the total amount of energy used by the building is equivalent to the renewable energy produced on site. In some cases, energy is produced off-site with renewable sources. These buildings emit much less greenhouse gases as compared to conventional buildings. However, there is a need to cost-effectively increase the energy efficiency of buildings by retrofitting these buildings, and designing new buildings with

increasing Leadership in Energy and Environmental Design (LEED) ratings [18]. The installation of Sunflower or reflecting mirrors can contribute to reducing the need of energy from fossil fuels. Moreover, the reflective mirrors will be simple to install and replace.

3. Numerical methodology and preliminary results

A Sunflower model is developed in Python 3.6 version based on the fundamentals of direct beam solar radiation [61] to evaluate the benefits of implementing small scale reflecting mirrors to contribute to net-zero building buildings. Step 1 requires calculating the solar intensity ratio onto a target when using multiple Sunflowers to evaluate the solar insolation supplied by first assuming there are no objects in the path of the solar rays. The model then is validated by comparing results with the NREL Solartrace model which applies a Monti-Carlo method and can handle obstacles by linking to Google Sketch-Up. The Sunflower model developed in Python regards sunlight as a single solar energy ray, compared to Solartrace model that considers multiple solar rays and check if the are impacted by other surfaces, then the target. The results from these two models are the same when there are no obstacles and allow to validate results. The Sunflower model calculates the impact of Sunflower locations and their orientation with respect to the target for given latitudes, longitudes, solar angles, and insolation data. User inputs are developed by using a flexible approach that allows multiple seasonal changes to later optimize the energy contributions of Sunflowers to net-zero buildings. Applications in renewable energy are not normally subjected to changing applications throughout the year. It is important to develop the model to account the multiple applications as part of the Sunflower model methodology for Step 1.

The Sunflower model needs flexibility to calculate each application in Step 2. Applications examples include:

- Pool heating
- Heating rooms through windows with the option of using PCM
- Provide sunlight in greenhouses to reduce power consumption
- Separate the solar spectrum and optimize applications for various frequencies
- Increase solar PV output
- Increase solar thermal panel output

In this thesis, only the residential pool heating application is considered where the target is in a horizontal position. Here, the pool model calculates the pool heat losses such as conduction, convection, evaporation, and radiation. Further, the required heat energy to obtain the desired

temperature, the natural gas replacement, and GHG emissions for Winnipeg and Arviat are calculated. To develop the Sunflower pool model as an example of Step 2, assumptions are made to reduce the complexity of the model without significantly sacrificing the accuracy of the solution. Note that unlike other methods, pool heating using Sunflowers is not subject to the second law of thermodynamics until the solar rays hit the water surface.

3.1. Assumptions

- All the DNI are collimated, that the Sunflower always tracks the sun properly, all the reflected rays from the Sunflower reach the target, and that all reflection on the Sunflower surface is specular– mirror-like reflection of light from the surface—and the user input reflectivity factor accounts for rays lost due to diffusion, transmission, and absorption.
- The model also assumes that the Sunflower is a flat surface and that the values found based on the rays going from the centre of the Sunflower to the centre of the target are the same as the values across the area of each.
- It is assumed that there are no obstacles between each Sunflower and the target.
- The pool surface is assumed flat without waves.
- The four Sunflower mirrors are coplanar.

3.2. Step 1: Calculating the solar intensity

To develop the Sunflower model, the relation between the sun's position and mirrors traction is calculated. The global centre is considered as target location. The solar energy that falls onto the target is comprised of:

1. Direct beam and diffuse solar insolation are falling onto the target. Solar reflection is not considered in the model.
2. The direct beam energy is redirected onto the target by each Sunflower to increase the intensity of solar energy onto the target.

The sun's apparent position in the sky is caused by the orbiting phenomenon of earth, and thus various equations have been developed to accurately describe the sun's position. This position depends on factors including location of the observer, observer's latitude and longitudinal site,

time of the day, and the day of year. By using these parameters, a series of solar angles can be calculated to estimate the sun's location in the sky. The solar angle equations such as equation of time, hour angle, zenith angle, and sunset and sunrise times are based on the developed formulation of solar insolation. Equations of the solar angles were implemented as functions in Python code for the Sunflower model.

3.2.1. Equation of time (EOT)

The EOT equation is used to calculate the solar time. This is a correction factor in minutes for the inconsistent spin of the earth that varies day by day throughout the year. It can be calculated by:

$$EOT = 9.87\sin(2B) - 7.53cos(B) - 1.5\sin(B) \tag{3.1}$$

where B is defined by:

$$B = 360\frac{(d-81)}{365} \tag{3.2}$$

where d represents the number of days of the year.

3.2.2. Solar time and Local Standard Time (LST)

Solar time is based on the sun's position in the sky and the location of observer on ground, whereas LST is the time based on the time zone of observer's location. A conversion from LST to solar time in hours is as follows:

$$t = LST + \frac{EOT}{60} + \frac{4L_{local}}{60} - t_{zone} - DS \tag{3.3}$$

where *DS* is daylight saving hour. If daylight savings time is considered for a location, then DS is equal to 1.

3.2.3. Solar declination angle (δ)

The solar declination angle locates where the sun's irradiations are normal to the longitude angle between Tropic of Cancer to Tropic of Capricorn to mark the year. There are many variations for these approximate equations. The Sunflower model used Spencer's formula for its high accuracy having an error less than 0.035°.

$$\delta = \frac{180}{\pi}[0.006918 - 0.399912\cos(\Gamma) + 0.070257\sin(\Gamma) - 0.006758\cos(2\Gamma) + 0.000907\sin(2\Gamma) - 0.002697\cos(3\Gamma) + 0.00148\sin(3\Gamma)] \quad (3.4)$$

where Γ is calculated in radians and is calculated by:

$$\Gamma = \frac{2\pi(d-1)}{365} \quad (3.5)$$

3.2.4. Hour angle (α)

The hour angle is based on the earth's rotation each day. This means that since the earth rotates by 360° in 24 hours, the hour angle changes by 15° per hour. The hour angle is defined to be negative in the morning, 0° at solar noon, and positive in the afternoon.

$$\alpha = \frac{360}{24}(t-12) = 15(t-12) \quad (3.6)$$

3.2.5. Solar zenith angle (χ)

The solar zenith angle is the angle between the vertical and the direct beam solar rays and is calculated by:

$$\cos\chi = sin\delta\ sin\Phi + cos\Phi\ cos\delta\ cos\alpha \quad (3.7)$$

The inverse of cosine can be used to find the solar angle between the ground and the direct beam.

3.2.6. Solar azimuth angle (ζ)

The solar azimuth angle is defined as the angle clockwise between the projection of the sunlight's vector onto the horizontal plane and due to south direction. It is also defined as the clockwise angle from the south, but the model uses the north as the 0° point. The azimuth angle is calculated in degrees by:

$$\zeta = 180° + [sign\ of\ \alpha] \cos^{-1}\left[\frac{\cos\chi \sin\phi - \sin\delta}{\sin\chi \cos\phi}\right] \tag{3.8}$$

3.2.7. Incidence angle (θ_i)

The incidence angle is the angle between the normal of the flat target and the sunlight vector. The cosine of this angle is defined by:

$$\begin{aligned}\cos\theta_i = \sin\delta \sin\phi \cos\beta + \sin\delta \cos\phi \sin\beta \cos\zeta_s + \cos\delta \cos\phi \cos\beta \cos\alpha \\ - \cos\delta \sin\phi \sin\beta \cos\zeta_s \cos\alpha - \cos\delta \sin\beta \sin\zeta_s \sin\alpha\end{aligned} \tag{3.9}$$

The simplified version is:

$$\cos\theta_i = \cos\chi \cos\beta + \sin\chi \sin\beta \cos(\zeta - \zeta_s) \tag{3.10}$$

3.2.7.1. Sunrise and sunset hours

The time of sunrise and sunset for each day is calculated by considering that during sunrise and sunset the zenith angle is equal to 90°. From this, the hour angle for sunset is calculated by:

$$\alpha_s = |\cos^{-1}[-\tan\delta \tan\phi]| \tag{3.11}$$

It is the absolute value because the hour angle at sunset is always positive. The hour angle at sunrise can be calculated by:

$$\alpha_r = -\alpha_s \tag{3.12}$$

Using Equation 3.6, the solar time at sunrise and sunset can be calculated. Equation 3.3 can be used to calculate the LST at sunrise and sunset.

3.2.8. Sunlight vector ($\hat{S}$)

The vector of sunlight directing from the origin of the target to the sun is calculated as follows:

$$\hat{S} = \begin{bmatrix} x_s \\ y_s \\ z_s \end{bmatrix} = \begin{bmatrix} \sin\zeta \sin\chi \\ \cos\zeta \sin\chi \\ \cos\chi \end{bmatrix} \tag{3.13}$$

Because of the way the components are calculated, it is a unit vector. The magnitude should therefore be equal to one where:

$$\left|\hat{S}\right| = \sqrt{x_s^2 + y_s^2 + z_s^2} \tag{3.14}$$

3.3. Step 1: Location and orientation of target and Sunflower

Given the position of the face of the target, the directed beam energy from the sun, the direction of the direct solar rays, and the solar energy incident onto the target can be calculated. This incident energy onto the target surface and each Sunflower's mirror surface is required to be calculated hourly.

The energy from the sun is into three parts: DNI, diffuse irradiance, and reflected irradiance. Using meteorological data collected for the area of interest, these three components can be calculated to varying degrees of accuracy. Direct beam irradiance is simply the component of DNI incident to the surface that can be calculated by multiplying DNI by the incidence angle. The diffuse irradiance is calculated by considering horizon brightening, circumsolar diffuse, and isotropic diffuse. The ground reflected irradiance is calculated by using the isotropic model. For calculating the energy incident on the Sunflower's surface, only the DNI component is considered to redirect the energy as mirrors cannot redirect diffuse (circumsolar and isotropic). Reflection energy from the ground is ignored for the Sunflower.

3.3.1. Target position (T_P)

The following equations are used in the Sunflower model to calculate the target position relative to the origin (global centre). The input file contains vertical distance (v_T), horizontal distance (h_T) and azimuth angle of target (ζ_T) for the current target. The azimuth angle of target is the angle measured from the north and increases by ging clockwise. This angle represents in which horizontal direction the target is located relative to the origin. The target position in [east-north-height] coordinate system is calculated in the model as:

For $\zeta_T \leq 90°$:

$$T_P = \begin{bmatrix} x_T \\ y_T \\ z_T \end{bmatrix} = \begin{bmatrix} h_T & \cos(90 - \zeta_T) \\ h_T & \sin(90 - \zeta_T) \\ v_T & \end{bmatrix} \tag{3.15}$$

For $\zeta_T > 90°$:

$$T_P = \begin{bmatrix} x_T \\ y_T \\ z_T \end{bmatrix} = \begin{bmatrix} h_T & \cos(450 - \zeta_T) \\ h_T & \sin(450 - \zeta_T) \\ v_T & \end{bmatrix} \tag{3.16}$$

3.3.2. Sunflower position (SF)

The position of the Sunflower is based on the target positioning. The input file contains v_{SF}, h_{SF} and ζ_{SF} for the Sunflower relative to the target. The azimuth angle of Sunflower is the angle measured from the north and increases by ging clockwise. This angle represents in which horizontal direction the Sunflower is located relative to the target The Sunflower position in [east-north-height] coordinate system is calculated in the model similarly to the target position, except for an additional step of adding the coordinates of the target position to the calculate the coordinates.

For $\zeta_{SF} \leq 90°$:

$$SF = \begin{bmatrix} x_{SF} \\ y_{SF} \\ z_{SF} \end{bmatrix} = \begin{bmatrix} h_{SF} & \cos(90 - \zeta_{SF}) \\ h_{SF} & \sin(90 - \zeta_{SF}) \\ v_{SF} & \end{bmatrix} + T_P \tag{3.17}$$

For ζ_{SF} > 90°:

$$SF = \begin{bmatrix} x_{SF} \\ y_{SF} \\ z_{SF} \end{bmatrix} = \begin{bmatrix} h_{SF} & \cos(450 - \zeta_{SF}) \\ h_{SF} & \sin(450 - \zeta_{SF}) \\ v_{SF} & \end{bmatrix} + T_P \tag{3.18}$$

3.3.3. Vertical (θ_v) and horizontal angle (θ_h) of Sunflower Location

The sunflower position can also be defined by using another method. The inverse tangent of vertical distance and horizontal distance between target and Sunflower can be used to find the vertical angle. The angle between the horizontal surface and the vector directing from the Sunflower to the target is calculated as follows:

$$\theta_v = \tan^{-1}\left(\frac{v_{SF}}{h_{SF}}\right) \tag{3.19}$$

Figure 17 shows, the target is located at the centre. The horizontal angle (θ_h) is measured from the south of the target which is located at 0°. The angle increases counterclockwise. The vertical angle (θ_v) is between the horizontal ground and the centre of Sunflower. It increases with the increment in the height of Sunflower and decreases by lowering the height of Sunflower. The Sunflower does not follow the same reference points as the solar angles.

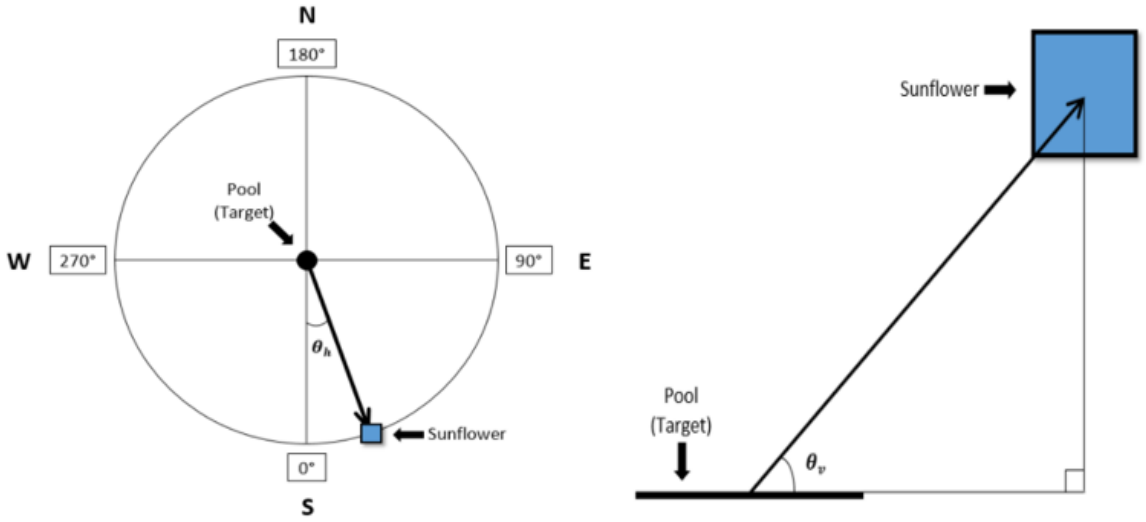

Figure 17: Horizontal angle θ_h and vertical angle θ_v of Sunflower location

The horizontal angle (θ_h) of Sunflower's location is defined as the angle measured from the line between the south of the target and the pool and the line between the centre of Sunflower and the pool. The angle increases by going counterclockwise. It differs from the azimuth angle of Sunflower by 180°. The concept of horizontal angle of Sunflower location originates from the facing direction of Sunflower to the sun. For example, when the azimuth angle of Sunflower is 180° (or at south of target), the horizontal angle of Sunflower location is 0°, and the Sunflower faces north where the target is located. When the sun is located at south of the target (ζ=180°), the Sunflower is highly effective when located at north of the target (θ_h =180°).

3.3.4. Direction vector between Sunflower and target (*F*)

The direction vector from the Sunflower to the target is calculated by:

$$F = \begin{bmatrix} x_F \\ y_F \\ z_F \end{bmatrix} = T_P - SF = \begin{bmatrix} x_T - x_{SF} \\ y_T - y_{SF} \\ z_T - z_{SF} \end{bmatrix} \tag{3.20}$$

The magnitude of this vector is determined by:

$$|F| = \sqrt{x_F^2 + y_F^2 + z_F^2} \tag{3.21}$$

The unit vector is:

$$\hat{F} = \frac{F}{|F|} \tag{3.22}$$

3.3.5. Angle of reflection (θ_o)

The angle of reflection is the angle at which the direct beam solar irradiance is reflected off from the Sunflower mirror to reach the target. To find the angle of reflection, the angle between two vectors (2θ), i.e., the sunlight vector and the vector between Sunflower and the target is calculated by using linear algebra. For the reflection the angle of incidence (θ_i) between the sunlight vector ($\hat{S}$) and the normal vector on the Sunflower mirror plane ($\widehat{SF\_o}$) is equal to the angle of reflection

(θ_o) between the normal vector of Sunflower and the target ($\hat{F}$) vector. Figure 18 shows the angle of incidence (θ_i) and angle of incidence (θ_i). Therefore, the angle of reflection is calculated by:

$$\theta_o = 1/2 * \cos^{-1}\left(\hat{S} \cdot \hat{F}\right) \tag{3.23}$$

3.3.6. Vector of Sunflower's orientation ($\widehat{SF\_o}$)

The orientation of the Sunflower is the normal vector of the Sunflower mirror plane. The normal vector of Sunflower is half of the vector sum of two vectors, i.e., vector $\hat{S}$ (sunlight vector) and $\hat{F}$ (vector between the location of target and location of Sunflower). Using this relationship between the normal vector of the Sunflower and the two vectors $\hat{S}$ and $\hat{F}$, the vector of Sunflower's orientation is defined by:

$$\widehat{SF\_o} = \begin{bmatrix} x_{\widehat{SF_o}} \\ y_{\widehat{SF_o}} \\ z_{\widehat{SF_o}} \end{bmatrix} = \begin{bmatrix} \frac{(x_{\hat{S}} + x_{\hat{F}})}{2 * \cos\theta_o} \\ \frac{(y_{\hat{S}} + y_{\hat{F}})}{2 * \cos\theta_o} \\ \frac{(z_{\hat{S}} + z_{\hat{F}})}{2 * \cos\theta_o} \end{bmatrix} \tag{3.24}$$

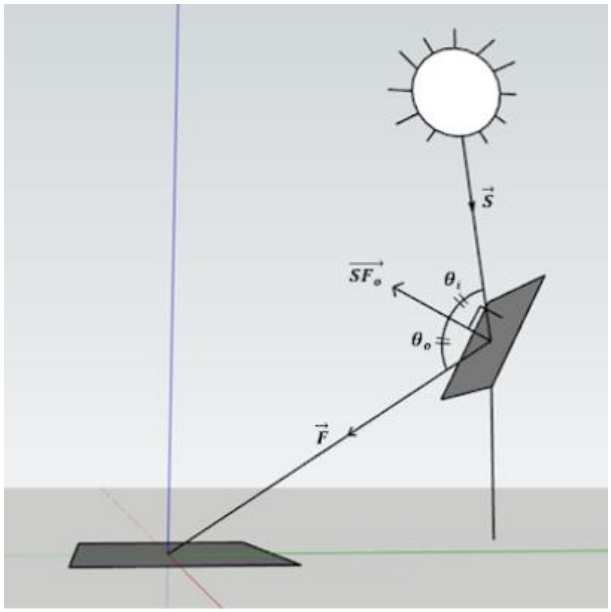

Figure 18: Demonstration of Sunflower orientation vector

By using the Sunflower orientation vector, the Sunflower can reflect sunlight onto the target without misalignment of redirected sunlight from Sunflower. The orientation vector allows Sunflower to focus onto the target all the time a sit tracks the sun.

3.3.7. Projected areas (A_1, A_2, A_3)

To calculate the flux on the target, the projected area for three different locations is required. A_1 is the projected area of sunlight that reaches the Sunflower. It is calculated by:

$$A_1 = A_{SF} \cos \theta_o \tag{3.25}$$

A_2 is the projected area of sunlight rays reflected off from the Sunflower and is equal to the projected area of incidence light onto the Sunflower. It is calculated by:

$$A_2 = A_1 \tag{3.26}$$

A_3 is the projected area of sunlight rays reflected off from the Sunflower that reaches the target's surface. It is calculated by:

$$A_3 = \left|\frac{A_2}{\sin(\beta + \alpha_{SF})}\right| \tag{3.27}$$

3.4. Step 1: Meteorological data

For this research, CWEEDS 2014 hourly data is used to determine the solar irradiance throughout the year. CWEEDS data records various meteorological conditions for a location for each hour of single day over the course of many years. Here, 2014 is the most recent year considered. However, the year can be changed through the user input files. The data of interest is the solar irradiance data for Winnipeg. The hours recorded in the CWEEDS data are LST, not solar time. The irradiance data is broken up into four different components to estimate the solar energy on a surface. Each of these components are collected for the hour at which they are recorded, for example the data at hour 5 is the total irradiance collected from hour 4 to hour 5. When determining the solar angles for this time interval, the time used is the halfway point, so for the example, a LST of 4.5 would be used. Note that if sunrise and sunset occur during a one-hour time interval, the data still represents the average during that one hour.

The solar components are all measured in kJ/m^2 and consists of the extra-terrestrial irradiance (I_{ext}), Global Horizontal Irradiance (GHI), Diffuse Horizontal Irradiance (DHI), and Direct Normal Irradiance (DNI):

1. I_{ext} represents the horizontal component of the irradiance received outside of the earth's atmosphere,
2. GHI represents the total irradiance received by a horizontal surface,
3. DHI represents the total diffuse irradiance received by a horizontal surface, and
4. DNI represents the total direct normal irradiance received on a surface perpendicular to the sun's rays.

3.4.1. Direct normal irradiance (I_b)

The data collected by CWEEDS is given in the units of kJ/m^2 integrated over one hour. This needs to be converted into W/m^2 to be used for the calculations by:

$$I_b = \frac{G_b(1000\ J/kJ)}{3600\ s/hr} = \frac{G_b}{3.6} \tag{3.28}$$

3.4.2. Global horizontal irradiance ($I_{g,h}$)

The $I_{g,h}$ is calculated from the CWEEDS data similarly to how I_b was calculated.

$$I_{g,h} = \frac{G_{d,h}(1000\ J/kJ)}{3600\ s/hr} = \frac{G_{g,h}}{3.6} \tag{3.29}$$

3.4.3. Diffuse horizontal irradiance ($I_{d,h}$)

The $I_{d,h}$ is calculated from the CWEEDS data similarly to how I_b and $I_{g,h}$ was calculated.

$$I_{d,h} = \frac{G_{d,h}(1000\ J/kJ)}{3600\ s/hr} = \frac{G_{d,h}}{3.6} \tag{3.30}$$

3.5. Step 1: Solar energy from sun and Sunflower

The equations used to calculate the solar energy from the sun and Sunflower on the target are shown as follows:

3.5.1. Solar energy from Sunflower (Q_{SF})

For the solar rays that contact the Sunflower face to hit the target, θ_o must be less than 90°. If it is greater than 90° it means that the sun is past sunset.

If θ_o < 90°:

$$Q_{SF} = I_b(r_{SF})(a_T)(A_{SF})\cos\theta_o \tag{3.31}$$

If $\theta_o \geq 90°$:

$$Q_{SF} = 0 \tag{3.32}$$

3.5.2. Solar flux from Sunflower (I_{SF})

The solar flux that is redirected to the target from the Sunflower is not calculated in the Sunflower model. However, to calculate the solar intensity in flux maps, the Solartrace model is calculating the solar flux The following equation can be used:

$$I_{SF} = \frac{Q_{SF}}{A_3} \tag{3.33}$$

3.5.3. Direct normal solar energy on target (Q_b)

The direct normal sunlight rays only hit the surface of the target if θ_i is less than 90º. If θ_i is greater than 90º it means that the sunlight rays are hitting at the back of target surface. Therefore, the energy obtained from direct normal irradiance is calculated based on the incidence angle.

If $\theta_i < 90°$:

$$Q_b = (A_T)(a_T)I_b \cos\theta_i \tag{3.34}$$

If $\theta_i \geq 90°$:

$$Q_b = 0 \tag{3.35}$$

3.5.4. Diffuse and reflected solar energy on target (Q_d)

The diffuse solar energy hitting the target is estimated from the CWEEDS data of the diffuse on a horizontal surface using the HDKR model (HDKR combines the Hay, Davis, Klutcher, and Reindl models). This model incorporates circumsolar, horizon brightening, and isotropic diffuse energy. The diffuse solar energy is calculated by:

$$Q_d = (A_T)(a_T)I_{d,h}\left\{(1 - A_i)\left(\cos^2(\beta/2)\right)\left[1 + f\sin^3\left(\beta/_2\right)\right] + A_i R_b\right\} \tag{3.36}$$

where A_i is the anisotropy index calculated when I_{ext} is not equal to zero by:

$$A_i = \frac{I_{g,h} - I_{d,h}}{I_{ext,h}} \tag{3.37}$$

If $I_{ext,h}$ is equal to zero, then A_i is set equal to zero and f is the modulating factor calculated when $I_{g,h}$ is not equal to zero by:

$$f = \sqrt{\frac{I_{g,h} - I_{d,h}}{I_{g,h}}} \tag{3.38}$$

If $I_{g,h}$ is equal to zero, then f is set equal to zero. R_b is the beam radiation tilt factor calculated when $\cos\chi$ is not equal to zero by:

$$R_b = \frac{\cos\theta_i}{\cos\chi} \tag{3.39}$$

If $\cos\chi$ is equal to zero, then R_b is set equal to zero.

The reflected solar energy (Q_r) from the surroundings is estimated to hit the target from the CWEEDS data is based on the isotropic sky model, which is the most used model to estimate this value. This model is defined by:

$$Q_r = (A_T)(a_T)(\rho)I_{g,h}\sin^2\left(\beta/_2\right) \tag{3.40}$$

3.5.5. Total irradiance on target without Sunflower (Q_{T-SF})

The total irradiance energy on the target is comprised of direct normal (Q_b), diffuse (Q_d), and reflected (Q_r) except the energy redirected from the Sunflower onto the target. The irradiance energy is calculated by:

$$Q_{T-SF} = Q_b + Q_d + Q_r \tag{3.41}$$

3.5.6. Total irradiance on target with Sunflower (Q_{T+SF})

The total irradiance energy (Q_{T-SF}) on the target including the energy redirected from the Sunflower (Q_{SF}) onto the target is calculated by:

$$Q_{T+SF} = Q_{T-SF} + Q_{SF} \tag{3.42}$$

3.5.7. Intensity ratio (Q_{ratio})

The intensity ratio is defined as the ratio of the energy on the target with Sunflower and without the Sunflower. It is the total gain of energy and is calculated by:

$$Q_{ratio} = \frac{Q_{T+SF}}{Q_{T-SF}} \tag{3.43}$$

If Q_{T-SF} is equal to 0, then Q_{ratio} is defined by:

$$Q_{ratio} = 0 \tag{3.44}$$

3.6. Step 1: Energy intensity estimation using ray-tracing method in Solartrace

NREL Solartrace is a software that models concentrating solar power systems using Monte-Carlo ray-tracing methods. The Monte-Carlo method uses the approach of projecting the large number of particles into a confined region. Since each particle follows its own arbitrary path, it is a statistical method. For solar energy analysis, sunlight can be described as a combination of large number of solar rays. Monte-Carlo method can be applied by considering the solar rays as particles. In ray-tracing, the analysis of each solar ray's behaviour is available, therefore more complex interactions of rays with multiple objects can also be analyzed. In Solartrace ray-tracing, an assigned number of rays are projected from the sun and are traced through the defined system. Depending on requirements, the obstacles can be added and removed in ray-tracing. As the rays are traced through, various optical interactions such as reflection and refraction occur. Depending on the angle of the solar rays, the reflectivity, refraction index number, and energy intensity on any specific portions in any surface area can be estimated.

To define the Solartrace ray-tracing model for energy intensity estimation, firstly, the direction of the solar rays is defined, followed by the setting of optical properties, aperture shape, and surface contour for different optical objects in Solartrace. Further, the location and orientation of the

objects in the model are also to be defined in Solartrace. Finally, the number of rays to project and the number of rays to interact with the optical objects are assigned.

Seeding is the distribution of solar rays when the solar rays are projected. There are more than 1,000 different seeding methods available in the Solartrace. For this research only one seeding method is selected because analysis of using multiple seeding methods requires large amount of computational time to run the ray-tracing model to obtain results.

Using the built-in feature of the script engine for automation of ray-tracing, an algorithm is developed to calculate the solar energy intensity for redirected sunlight and direct sunlight onto the target for the whole year. The equations used in Solartrace are the same as the equations as used in Sunflower model. However, for the Solartrace model, the built-in functions of the Solartrace script engine are used for the equations to calculate the solar energy intensity for the whole year

3.6.1. Optical properties of objects

Optical properties are defined before creating each object in the Solartrace model. After creating each object, optical properties can be assigned for each object, i.e., aperture shape, surface contour, location, and orientation. The Solartrace model uses Fresnel equations for the calculation of reflection and refraction at surface interfaces [41]. Reflectivity can vary anywhere between 0 and 1. For reflective mirrors, since most of light is reflected away, 0.95 reflective value is selected.

3.6.2. Solar ray direction

The model considers the position of Sunflower with respect to the target, the orientation of the target, and the position of the sun and its DNI as an input. To determine the most effective usage of Sunflower reflective mirrors, the position and number of reflective mirrors required to provide the amount of solar energy are determined. Further, the model was adapted to calculate the combined concentrating effect of up to 20 Sunflowers. The position of each Sunflower can be changed independently by using the three parameters, i.e., the Sunflower's azimuth angle, view angle of observer, and the Sunflower's horizontal distance from the target.

To define a unit vector of solar rays, the following equations are introduced in the Solartrace program manually.

$$\delta_{Soltrace} = \arcsin\big(0.39795 * cos\big(0.98563(d - 173)\big)\big) \tag{3.45}$$

$$\omega_{Soltrace} = 15(t - 12) \tag{3.46}$$

$$\alpha_{Soltrace} = \arcsin(sin(\delta_{Soltrace}) * sin(L) + cos(\delta_{Soltrace}) * cos(\omega_{Soltrace}) * cos(L)) \tag{3.47}$$

$$\gamma_{Soltrace} = \arccos\left(\frac{sin(\delta_{Soltrace}) * cos(L) - cos(\delta_{Soltrace}) * sin(L) * cos(\omega_{Soltrace})}{cos(\alpha_{Soltrace})}\right) \tag{3.48}$$

The direction unit vector of solar rays is defined as

$$x = -\sin(\gamma_{Soltrace}) * \cos(\alpha_{Soltrace}) \tag{3.49}$$

$$y = \sin(\alpha_{Soltrace}) \tag{3.50}$$

$$z = \cos(\gamma_{Soltrace}) * \cos(\alpha_{Soltrace}) \tag{3.51}$$

3.6.3. Aperture shape and surface contour of objects

In Solartrace, different aperture shapes and surface contours can be created. All the objects in the Solartrace model are selected to be square and flat.

3.6.4. Ray-tracing parameters

To perform the ray-tracing, the number of rays is to be selected. By default, the number of rays is 10,000. However, as the number of ray intersections increases, the result becomes more accurate and closer to reality. Therefore, in the Solartrace model, 100,000 positive ray intersections are

selected for validation. Note that during sunrise and sunset, the aperture area of the reflective surface of mirror and the surface of pool water is close to zero. To make sure 100,000 rays hit the small aperture area, a maximum of 10,000,000,000 rays are selected to be generated.

3.6.5. 3D scatter plot of ray intersections, flux map and statistical information

Before running the model in the script engine of Solartrace to estimate energy intensity for the year, ray-tracing can be run by selecting a certain time to confirm if the automation of ray-tracing is operating as intended. The result of running ray-tracing for a selected hour is visualized using a 3D scatter plot of ray intersections with various objects, and flux map on planar objects.

The 3D scatter plot of ray intersections shows how each solar ray is projected from the sun to the reflective surface of mirror and to the pool surface. Figure 19 shows the scatter plot at a certain hour. This flux map also shows the distribution of power per unit area flux over the planar surface of objects. The unit of flux is in W/m^2.

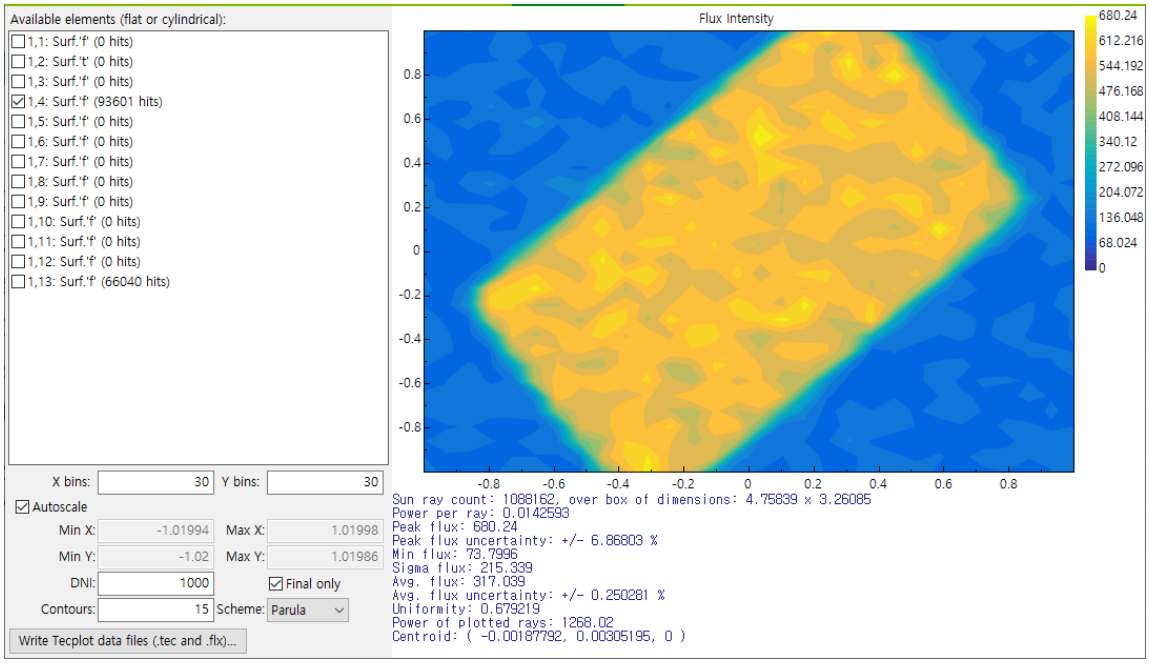

Figure 19: Flux map of pool water surface including solar rays from the reflected surface of mirror using Solartrace

Under the flux map, the statistical information with peak flux and average flux can also be observed. For estimation of energy density, the average flux is used. In Figure 19, the orange region shows higher flux compared to the blue region due to the projection of the reflective surface of reflective mirror. However, the average flux shown in the flux map shows the blue region that only includes rays directly from the sun. To find the average flux in the orange region, the coordinates of the flux map need to be changed into the centre region where the blue region is not included. Therefore, the average flux is calculated only in the centre region where $-0.05 < x < 0.05$ and $-0.05 < y < 0.05$. By using Equation 3.31, the average flux is multiplied by the projection area of the reflected solar rays coming from the reflective surface of mirror to calculate the intensity or energy. The resolution difference is because of the number of bins. Bin is a block cell of the flux map. When the number of bins in the flux map are smaller, the number of solar rays available entering each bin are greater because each bin is larger in size. The flux intensity value in the flux map is the average intensity of solar rays from each bin. Therefore, the colour variation depends on the size of each bin. The variation is more uniform when the number of bins is small. Despite the variation, the average flux intensity of solar rays is not affected because the average flux intensity value is the average of average values of each bin.

3.6.6. Location and orientation of reflective surface of mirror and target

To visualize the location and orientation of each object in the Solartrace model, Google SketchUp provides Solartrace plug-in to create Solartrace objects as shown in Figure 20.

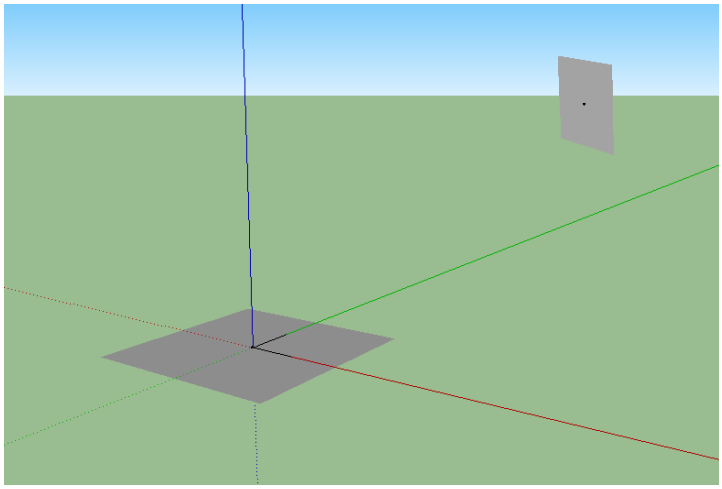

Figure 20: Google SketchUp for Solartrace geometry setting

As done in the Sunflower model, the reference coordinates (0, 0, 0) are assigned to be at the centre of the target. Based on the reference, the orientation of the reflective surface of the mirror is determined by Equations 3.14, 3.21, and 3.23. The coordinates of every Sunflower in the model to locate near the target is defined. Figure 21 from Sunflower model demonstrates all three coordinates of the Sunflowers.

	Segment 0
Location latitude [degrees]	49.9
Location longitude [degrees]	-97.14
Application	None
Day range	121 to 274
Position of target [x,y,z]	[0.0, 0.0, 0.0]
Number of sunflowers	10
Position of sunflower 0 [x,y,z]	[-2.39, 6.58, 0.5]
Position of sunflower 1 [x,y,z]	[-1.22, 6.89, 0.5]
Position of sunflower 2 [x,y,z]	[0.0, 7.0, 0.5]
Position of sunflower 3 [x,y,z]	[1.22, 6.89, 0.5]
Position of sunflower 4 [x,y,z]	[2.39, 6.58, 0.5]
Position of sunflower 5 [x,y,z]	[-2.57, 7.05, 1.5]
Position of sunflower 6 [x,y,z]	[-1.3, 7.39, 1.5]
Position of sunflower 7 [x,y,z]	[0.0, 7.5, 1.5]
Position of sunflower 8 [x,y,z]	[1.3, 7.39, 1.5]
Position of sunflower 9 [x,y,z]	[2.57, 7.05, 1.5]

Figure 21: Position coordinates of 10 Sunflowers in Solartrace. A segment is a unique set of data entries that do not change during a period.

The position of Sunflower 0 can be located by going to -2.39 units on x-axis or east-west distance, 6.58 units on y-axis north-south distance, and 0.5 units on z-axis. Figure 22 shows the top view of the model. The target is set to 1 m^2 for the purpose of demonstrating the model.

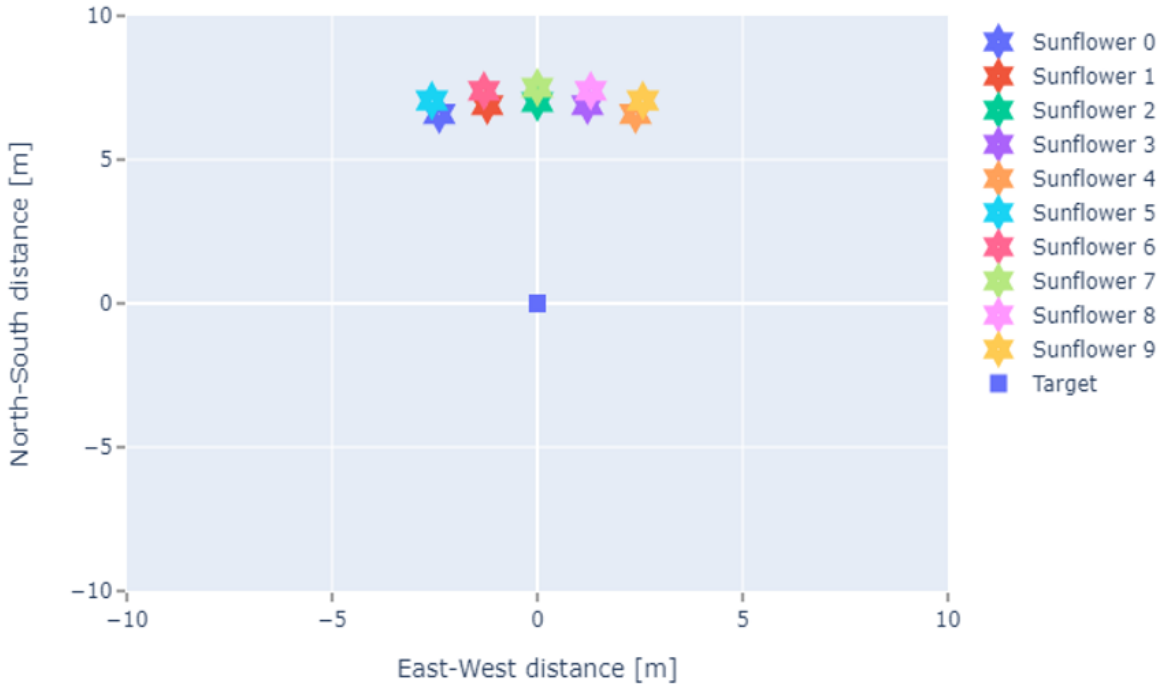

Figure 22: Top view of the placement of Sunflowers and target in Solartrace

3.7. Canadian solar resource

The solar resource is the essential factor in understanding the scope of solar energy production. The solar energy production is directly related to the solar irradiance at any location [42]. The potential of solar energy shifts as the season changes. Figure 23 shows the daily and yearly DNI and GHI values of Canada: annual range of DNI is from 584 kWh/m^2 to 1,899 kwh/m^2 whereas the yearly values of GHI ranges from 803 kWh/m^2 to 1387 kWh/m^2.

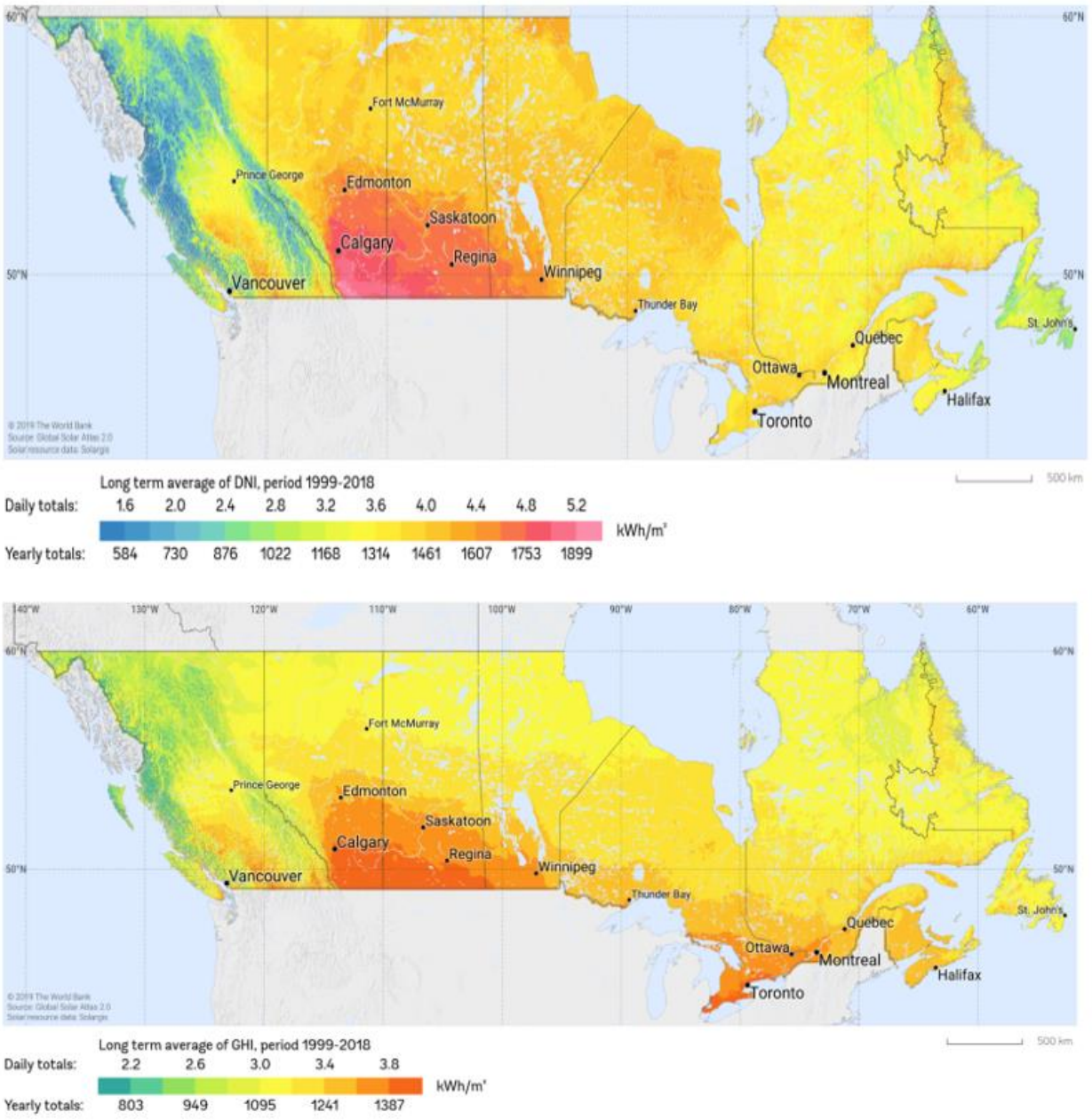

Figure 23: Solar resource maps representing annually average of daily DNI (top) and GHI (bottom) values of Canada from Reference [42]

Table 5 to Table 7 shows the daily and monthly average data for Winnipeg, Arviat, and Vancouver calculated by using RETScreen validation software.

Table 5: Daily and monthly solar irradiation in Winnipeg

Winnipeg	Daily total		Monthly total	
	$kWh/m^2/d$	$kJ/m^2/d$	$kJ/m^2/month$	$MJ/m^2/month$
January	1.4	5040	156240	156.2
February	2.36	8496	237888	237.9
March	3.76	13536	419616	419.6
April	4.9	17640	529200	529.2
May	5.77	20772	643932	643.9
June	6.15	22140	664200	664.2
July	6.33	22788	706428	706.4
August	5.26	18936	587016	587.0
September	3.61	12996	389880	389.9
October	2.21	7956	246636	246.6
November	1.3	4680	140400	140.4
December	1.05	3780	117180	117.2

Table 6: Daily and monthly solar Irradiation in Arviat

Arviat	Daily total		Monthly total	
	$kWh/m^2/d$	$kJ/m^2/d$	$kJ/m^2/month$	$MJ/m^2/month$
January	0.3	1080	33480	33.5
February	0.92	3312	92736	92.7
March	1.94	6984	216504	216.5
April	3.59	12924	387720	387.7
May	5.07	18252	565812	565.8
June	6.03	21708	651240	651.2
July	5.57	20052	621612	621.6
August	4.16	14976	464256	464.3
September	2.55	9180	275400	275.4
October	1.4	5040	156240	156.2
November	0.49	1764	52920	52.9
December	0.12	432	13392	13.4

Table 7: Daily and monthly solar Irradiation in Vancouver

Vancouver	Daily total		Monthly total	
	$kWh/m^2/d$	$kJ/m^2/d$	$kJ/m^2/month$	$MJ/m^2/month$
January	1.13	4068	126108	126.1
February	2.03	7308	204624	204.6
March	3.13	11268	349308	349.3
April	4.53	16308	489240	489.2
May	5.37	19332	599292	599.3
June	5.66	20376	611280	611.3
July	5.97	21492	666252	666.3
August	5.18	18648	578088	578.1
September	3.99	14364	430920	430.9
October	2.2	7920	245520	245.5
November	1.27	4572	137160	137.2
December	0.92	3312	102672	102.7

3.8. Input files

The variable inputs developed for the Sunflower model allow to change the application and positions of Sunflowers. In the Sunflower model, there are three major inputs: solar data, Sunflower position, and target position. Figure 24 shows the main input data file for the Sunflower model. The inputs of CWEEDS data for the location of interest and number of Sunflowers in the main input file are defined. Figure 25 shows the inputs for the range of days and the reflective index of the ground. Figure 26 and Figure 27 shows the location, orientation, properties of Sunflower, and target.

```
Cweed,            ./SolarData/Cweed/Winnipeg_CWEEDS.WY3,     #cweed data file
year,             2014,                                      #year of cweed data
Type,             CweedType,                                 #only CweedType supported currently
lat,              49.9,                                      #latitude
L,                -97.14,                                    #longitude
t_z,              -6,                                        #time zone
N_of_Seg,         1,                                         #number of different segments
N_of_S,           10,                                         #number of sunflowers in each segment
seg0,             ./InputData/Segment_0_case_v1.0pool.seg,       #path to segment file 1
run,              case_level1,                               #Purpose of run (in the title of each plot)
ID,               case_level1,                               #Unique set of letters and/or numbers to separate different runs in how the files are
saved
NSrange,          20,                                        #Distance North-South for map plot in meters
EWrange,          20,                                        #Distance East-West for map plot in meters
project,          CasesLevel1,                               #name of project for folder inside results
plot_type,        html jpeg png,                             #file types to save the plots as (choose html, png, or jpeg or any combo)
```

Figure 24: Main input data file: weather data, location, number of Sunflowers are determined.

```
n_start,          121,                                          #starting day of the year of sunflower use for segment
n_end,            274,                                        #ending day of year of sunflower use for segment
LST,              0,                                          #local standard time tht segment use starts
refl,             0.8 105 0.2 305 .8,                         #reflective index of the ground and day that it changes
LocSF,            ./InputData/SF_loc_case_v1.0.dat,           #SF location file path
Loctarget,        ./InputData/None_case_v1.0pool.app,             #target/application data file path
DS,               0,                                          #Daylight savings correction (if not used, put 0)
n_prepare,   3,                                       #Days to prepare pool water temperature to be desired temperature
T_desired,   25,                            #Desired temperature of pool water in deg C
```

Figure 25: Input data file for selecting the time period and reflective index

```
A_SF,                       1,              #Area of SF [m^2]
r_SF,                       0.95,           #reflectivity of SF
v_SF0,  0.5,                                #vertical distance from target to sunflower 0
v_SF1,  0.5,
v_SF2,  0.5,
v_SF3,  0.5,
v_SF4,  0.5,
v_SF5,  1.5,
v_SF6,  1.5,
v_SF7,  1.5,
v_SF8,  1.5,
v_SF9,  1.5,

h_SF0,  7,                                  #horizontal distance from target to sunflower 0
h_SF1,  7,
h_SF2,  7,
h_SF3,  7,
h_SF4,  7,
h_SF5,  7.5,
h_SF6,  7.5,
h_SF7,  7.5,
h_SF8,  7.5,
h_SF9,  7.5,

SF_az0, -20,                                #sunflower azimuth angle for sunflower 0
SF_az1, -10,
SF_az2, 0,
SF_az3, 10,
SF_az4, 20,
SF_az5, -20,
SF_az6, -10,
SF_az7, 0,
SF_az8, 10,
SF_az9, 20,
```

Figure 26: Sunflower location, orientation, and property input data file

```
abs,        1,                  #absorbability of target (aborbs all)
T_a,        32,                  #area of target
angle,      0,                 C#tilt angle of target
app,        None,               #application of the target (PV, None, Pool, Distill)
T_h,        0,                  #horizontal distance from this target to target 0 (always positive)
T_v,        0,                  #vertical distance from thsi target to target 0 (up is positive, down is negative)
T_az,       0,                C#azimuth angle of target surface in degrees (if no azimuth angle because horizontal, put 0)
T_azT0,     0,                  #azimuth angle of target in degrees from target 0 (if same position/is target 0, put 0)
```

Figure 27: Target location, orientation, and property input data file

3.9. Step 1: Intensity ratio with multiple reflective mirrors

Intensity ratio is defined as the summation of direct energy and redirected energy by the Sunflower mirrors of equal area to the target divided by the direct solar energy on the same surface. It is the output of the Sunflower reflective mirrors that how many times it is intensifying the solar energy based on the geographical location in that current hour. Large intensity ratios calculated near sunset and sunrise offer negligible contributions as the solar insolation are low at that time. The given set of equations listed in previous sections are used to calculate the intensity ratio for Winnipeg by

using CWEEDS 2014 solar data to demonstrate the output of the Sunflower model. The area of Sunflower mirrors and target is set to 1 m^2 with the Sunflower located 4 m north of the target, or 180^o horizontally of the target facing south, and at 2 m above from ground to form an angle of 26.5° by using Equation 3.19. This is the base configuration and comparisons are often made with this arrangement to assist the user to optimize the usage of Sunflower effectively with a Sunflower target retail price of $50 per m^2, maximising seasonal fossil fuel displacement and renewable energy generation for net-zero buildings is a priority.

3.9.1. Direct and redirected energy

The Sunflower model calculates the solar energy from the sun and redirected solar energy from each Sunflower. The sun rise hour, sunset hour, DNI, GHI are calculated by the Sunflower model. The reflected irradiations are zero in case of a horizontal target because there is no tilt between ground and horizontal target. The irradiations reflected from the ground are the reflective irradiations. The average intensity of direct solar energy per hour on target from the sun is 148 W. However, the average summation of direct solar energy from the sun and redirected energy from the Sunflower reflective mirror is 269 W, which is approximately 1.81 times more than the direct solar energy. Figure 28 shows the contribution of the sun and sunflower onto the target.

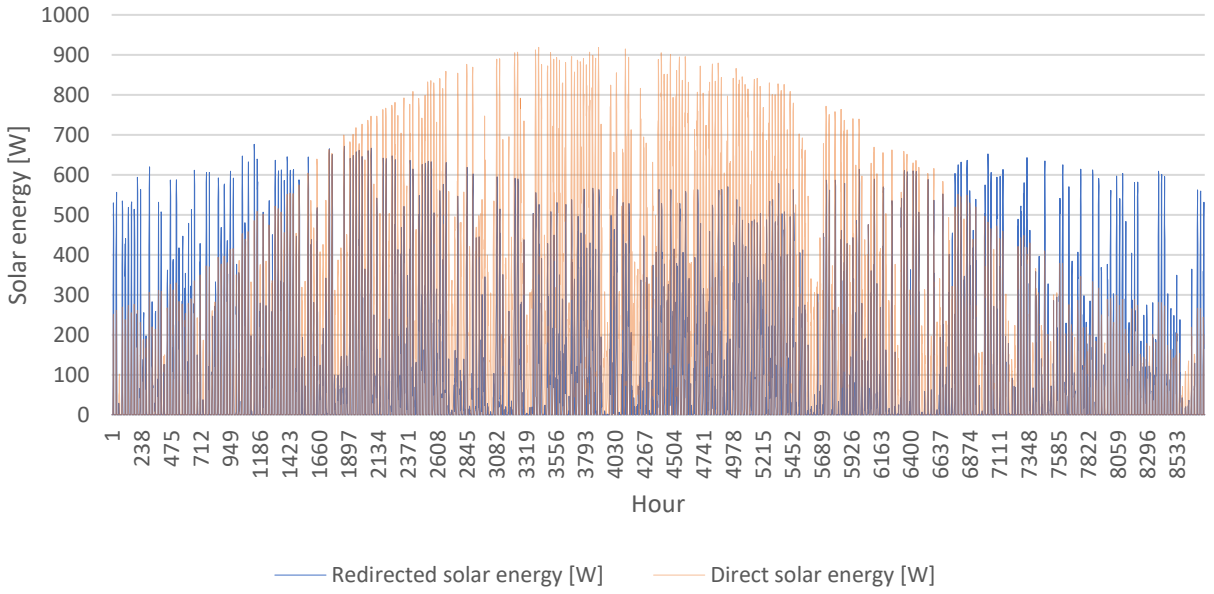

Figure 28: Direct and redirected solar energy from a single Sunflower when placed in the north of target, facing south, and forms an angle of 26.5° from the ground in Winnipeg

The redirect solar energy is almost double than the direct energy in winter months whereas the direct energy in summer months is higher than the redirected energy. The sun during the winter season is closer to the earth than during summer. Due to horizon of sun and the location of the Sunflower mirrors on earth's surface with respect to the sun, the output energy results increase during winter season.

3.9.2. Validation of intensity ratio

To validate the results from the Sunflower model, the location of the Sunflower is the same as the Solartrace model. Figure 29 shows the intensity ratio calculated by both models are close to each other. The yearly average ratio from Sunflower model is 0.897, which is validated by the Solartrace by giving the intensity ratio of 0.876. It is less than 1 because it includes the night-time hours where the intensity ratio is 0. After excluding the night-time hours consideration, the intensity ratio results by Sunflower and Solartrace models are 1.81 and 1.76 respectively. The percent error is 2.35%. The yearly average intensity ratio over the period is calculated from Equation 3.42.

Possible source of error is in the flux intensity analysis in ray-tracing. As previously mentioned in Section 3.6.5, the average flux intensity of solar rays can slightly change if the number of bins is changed. The greater number of incoming solar rays in ray-tracing model gives closer results to the Sunflower model calculations. In this case the selected number of solar rays was 100,000, whereas the result difference was even more when the selected number of solar rays was 10,000. The average intensity ratio in winter/spring month is noticeably greater than summer/fall months. Figure 29 shows the hourly intensity ratio from the Sunflower model and Solartrace over selected days.

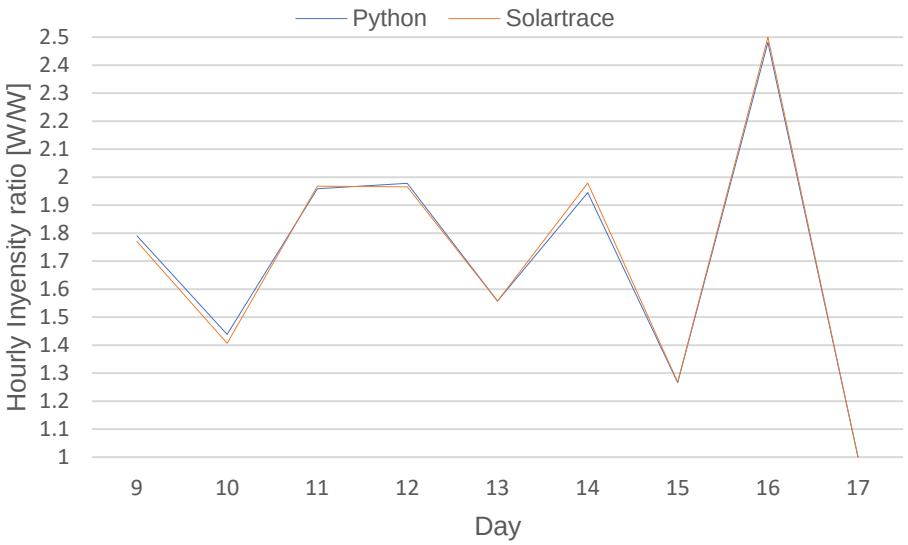

Figure 29: Validation of intensity ratio

Figure 30 shows the hourly intensity ratio from May 1 to October 1 where the intensity ratio reaches a maximum value of 1.6 for a few days during the selected period. However, for most of the days, the intensity ratio is near 1.3. Further, the intensity ratio decreases during sunrise and sunset time hours and on cloudy days. Overall, the average intensity ratio for the selected period is 1.5.

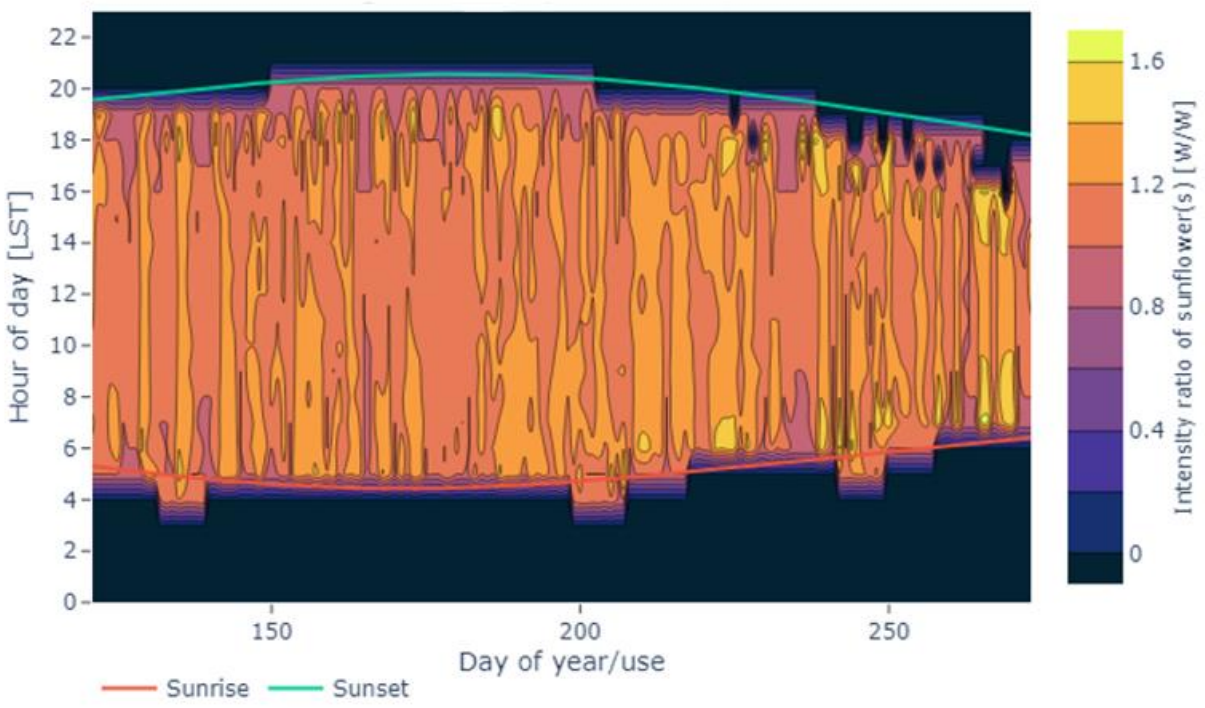

Figure 30: Hourly intensity ratio on target from May 1 to October 1 when Sunflower is placed in the north of target, facing south, and forms an angle of 26.5° from the ground

3.10. Step 1: Intensity ratio on different orientation of target

In the previous section, the hourly intensity ratio calculations are done on the horizontal surface. To increase the scope of the Sunflower for various energy applications, the calculations of average intensity ratio for each day are also performed at a tilted surface target at 50° to the earth's surface, vertical surface target, and horizontal surface target. Figure 31 shows the average intensity ratio on the different oriented targets. Here also, the Sunflower location is north of the target at 2 m height from ground level to form an angle of 26.5°.

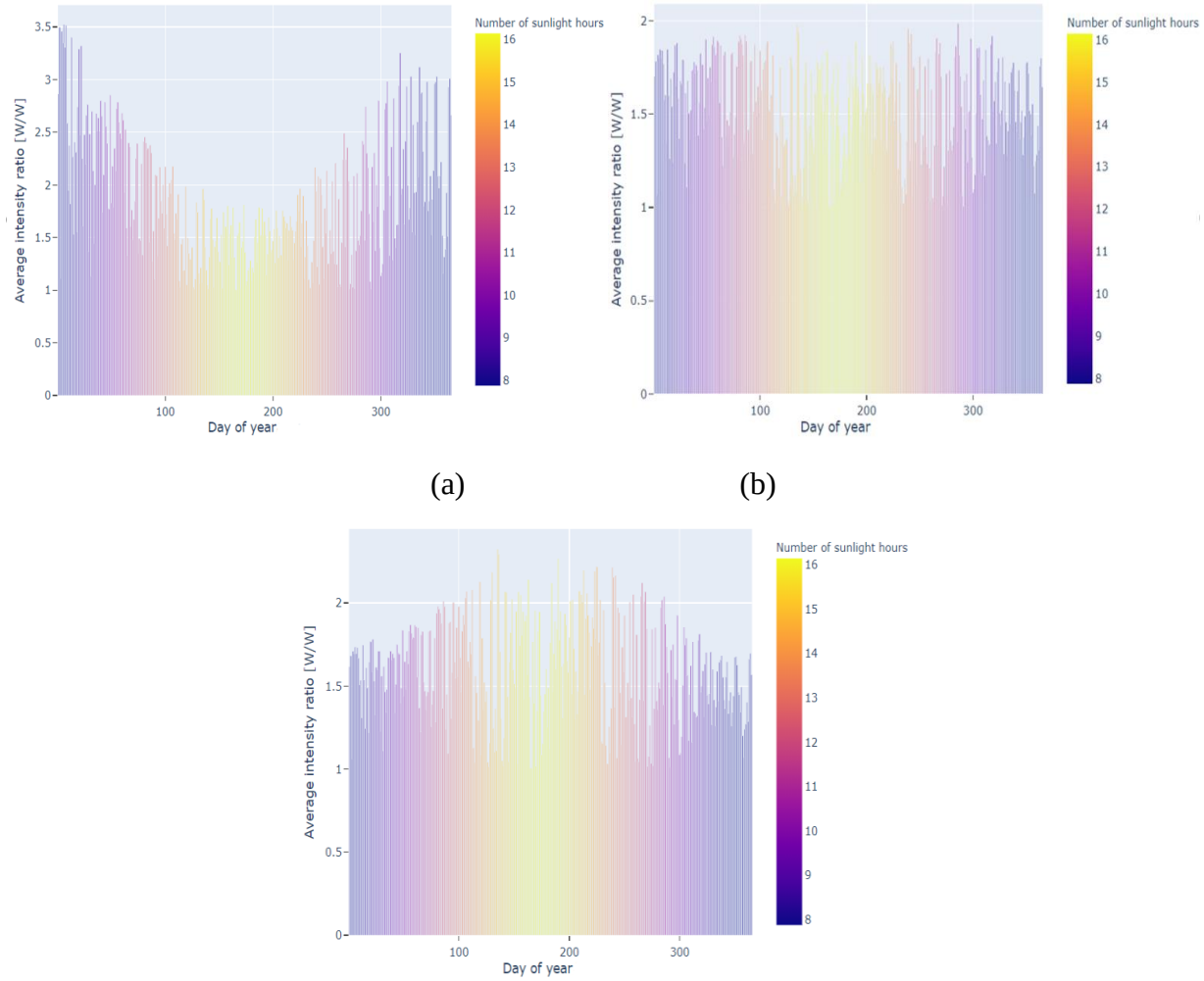

Figure 31: Average intensity ratio on (a) horizontal surface, (b) vertical surface, and (c) tilted surface at 50° to the ground surface, when Sunflower is placed in the north of target, facing south, and forms an angle of 26.5° from the ground

The intensity ratio for different target orientation varies due to the difference in direct and redirected energy from the sun on the different locations of the target surface. In case of the horizontal target, the average intensity in the fall/winter is sometimes greater than 3. The results shows that the increase in daily average intensity is due to the high intensity ratios in mornings and evenings hours. Since the horizontal target is flat, but the Sunflower is at an angle of 26.5° or 2 m above from ground level, the solar insolation on the target is low as compared to redirected

rays from the Sunflower. As the summer season begins, the intensity ratio for the morning and afternoon hours starts decreasing due to the lowering of the sun zenith.

The average intensity on tilted target is almost the same throughout the year, whereas the average intensity ratio is more during summer months compared to the winter months for vertical targets. Table 8 shows the average intensity ratio on different target positions.

Table 8: Average intensity ratio on different target positions when Sunflower is placed in the north of target, facing south, and forms an angle of 26.5° from the ground

Target position	Average intensity ratio [W/W]
Horizontal surface	1.81
Tilted surface at 50° to the ground	1.63
Vertical surface	1.77

3.11. Step 1: Magnification ratio

Magnification ratio of Sunflower is defined as the summation of direct energy and redirect energy by using multiple sunflowers divided by the direct energy on the same surface. To achieve the goal of making the Sunflower model user friendly, the effect of multiple Sunflower mirrors needs to be calculated. The case study has been divided into two different categories for horizontal surface, tilted surface, and vertical surface by using these target orientations:

- Target area of 1 m^2 with 10 m^2 Sunflower mirror area
- Target area of 10 m^2 with 1 m^2 Sunflower mirror area

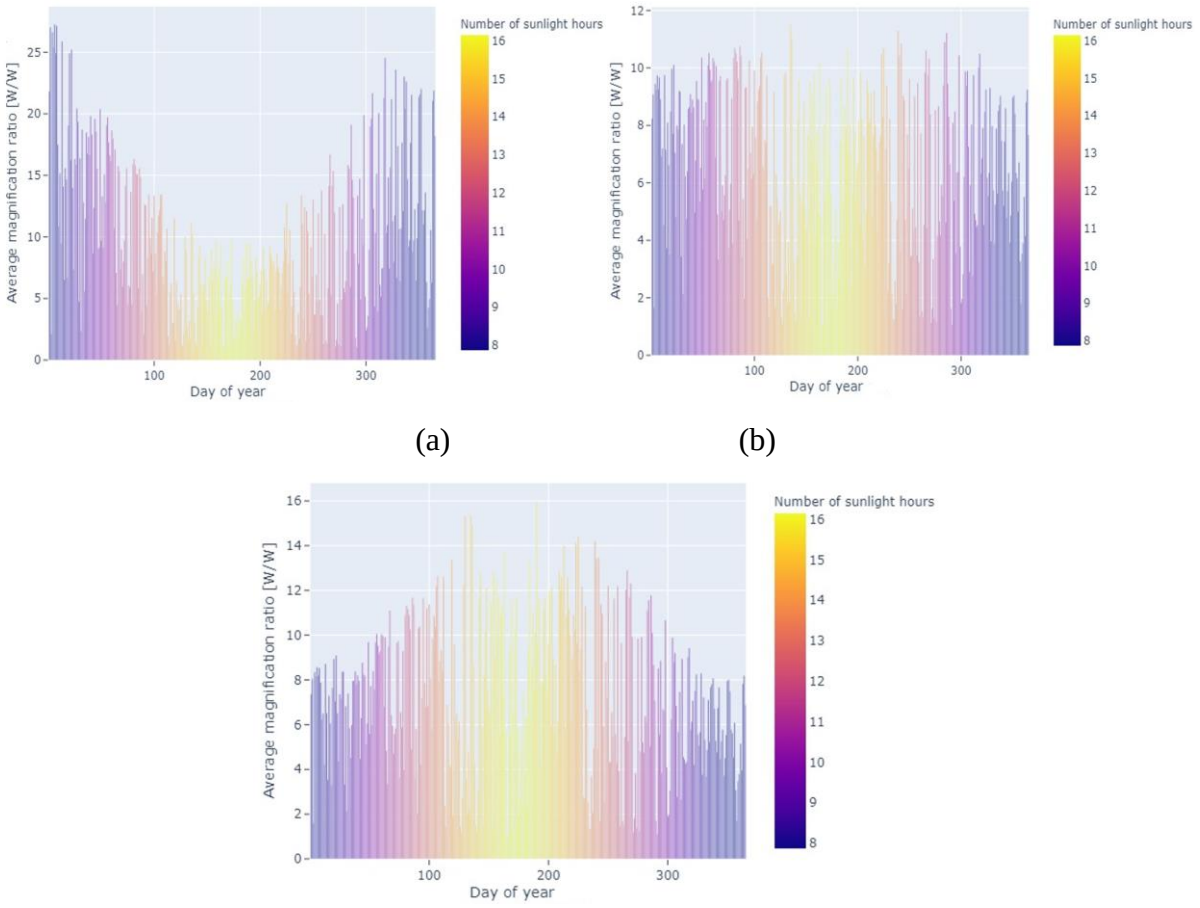

Figure 32: Average magnification ratio of 10 m2 Sunflower on (a) 1 m2 horizontal surface, (b) 1 m2 tilted surface, and (c) 1 m2 vertical surface when Sunflower is placed in the north of target, facing south, and forms an angle of 26.5° from the ground

The trend of average magnification ratio is same as the intensity ratio, but when the ten Sunflowers redirects energy onto the target, the magnification ratio increases by 10 times as shown in Figure 32. The second case scenario was established by keeping the target area ten times bigger than the actual Sunflower mirror area. The Sunflower mirror area is 1 m^2 whereas now the target area is 10 m^2. The average magnification ratio is same throughout the year. Figure 33 and Table 9 shows the average magnification ratio for all three targets.

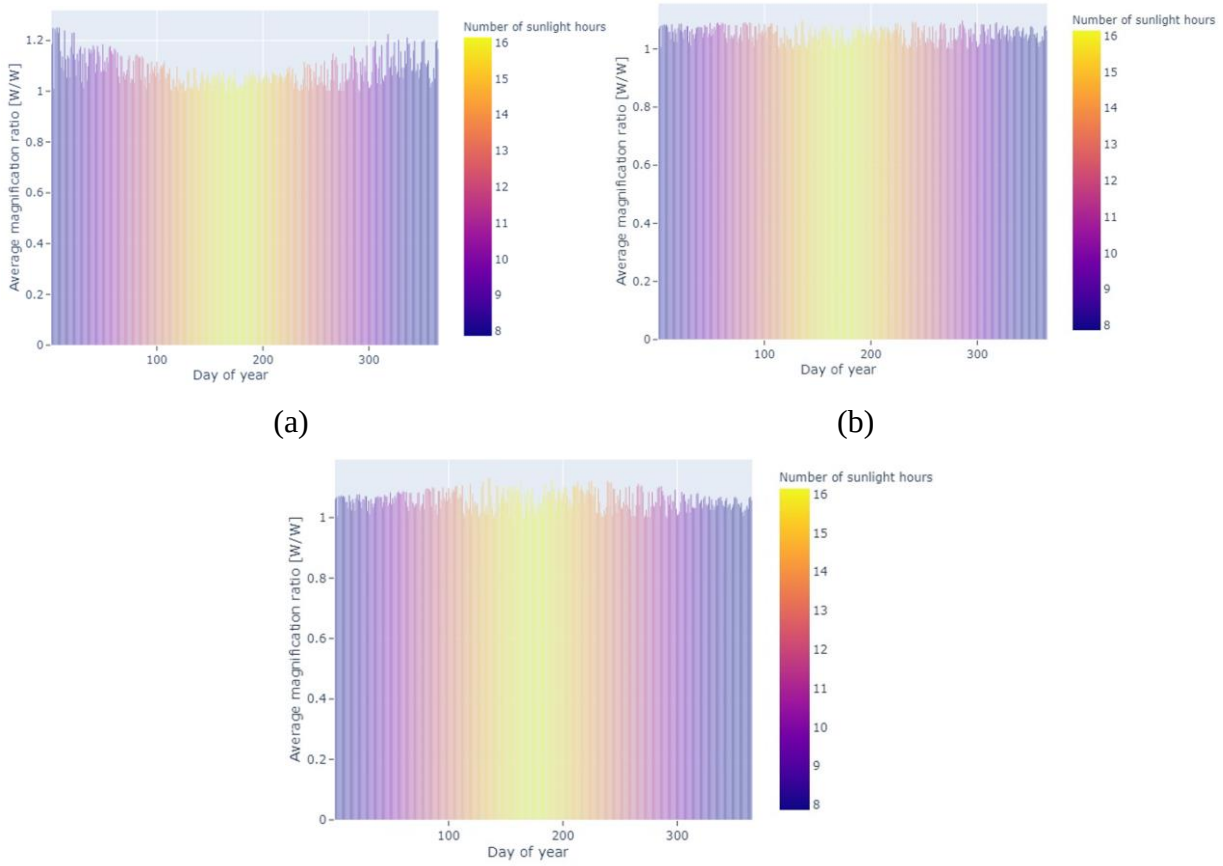

Figure 33: Average magnification ratio of 1 m2 Sunflower on (a) 10 m2 horizontal surface, (b) 10 m2 tilted surface, (c) 10 m2 vertical surface when Sunflower is placed in the north of target, facing south, and forms an angle of 26.5° from the ground

Table 9: Average magnification ratio for different target positions when Sunflower is placed in the north of target, facing south, and forms an angle of 26.5° from the ground

Target position	Average magnification ratio of 10 Sunflowers on 1 m^2 target [W/W]	Average magnification ratio of 1 Sunflower on 10 m^2 target [W/W]
Horizontal surface	9.79	1.08
Tilted surface at 50° to the ground	7.84	1.06
Vertical surface	9.35	1.07

3.12. Step 1: Impact of Sunflower location on intensity ratio

Each Sunflower can be placed in various locations with respect to the target. It has been found that the maximum output or the most optimum location of Sunflower as expected is when it is placed north of the target. However, since Sunflower applications are diverse and the landscape around buildings can make Sunflower placement difficult, it is important to include all possible locations. Moreover, each Sunflower can be placed significantly above or below the target. To find the difference, a case study has been conducted by placing the Sunflower on south, east, and west to the target. Figure 34 shows the daily average intensity ratio. It must be made clear that the user is restricted by elements like trees, buildings, fences, and gardens so that Sunflowers will often be located where they can rather than where they should.

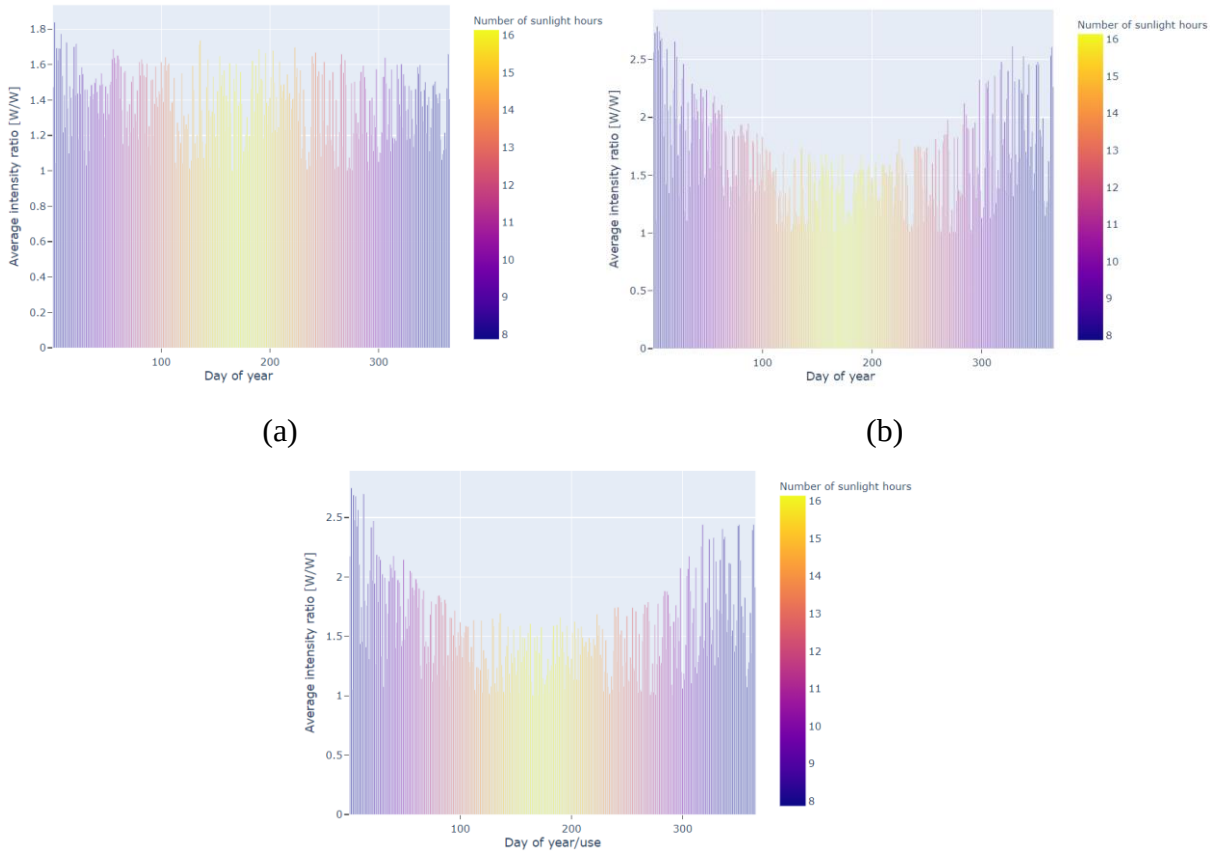

Figure 34: Average intensity ratio of Sunflower located at (a) south of horizontal target facing north, (b) east of horizontal target facing west, and (c) west of horizontal target facing east forms an angle of 26.5° from the ground

After finding the considerable difference among average intensity ratios by placing the Sunflower at different locations, the Sunflower is now placed 10^{o} towards east and west from north of the target to further examine the difference in average ratio. Figure 35 shows the new average intensity ratio values after making the minor change in the location of Sunflower. Table 10 shows the intensity ratio for various Sunflower locations.

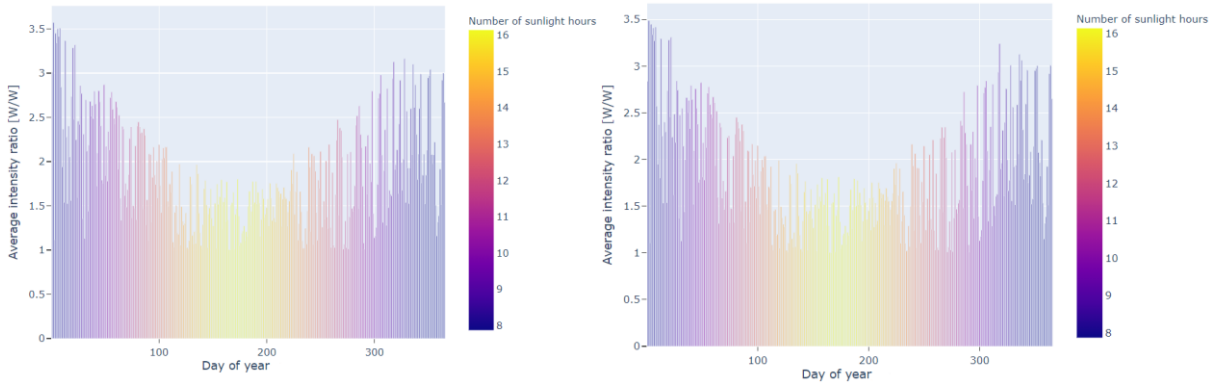

Figure 35: Average intensity ratio of Sunflower located at 10^{o} towards east (left), and 10^{o} towards west from north of horizontal target (right) forms an angle of 26.5° from the ground

Table 10: Average intensity ratio for various Sunflower locations

Sunflower location	Average intensity ratio on horizontal target [W/W]
North of target	1.81
South of target	1.39
East of target	1.59
West of target	1.60
10^{o} east from north of target	1.79
10^{o} west from north of target	1.80

3.13. Step 1: Impact of Sunflower height on intensity ratio

As described in the previous section, the location of Sunflower makes an impact on the intensity ratio. Figure 36 shows the total energy of redirected sunlight by the Sunflower at different heights or angles to the ground placed on south of horizontal target on a certain day. Before noon, the total energy on target is highest when the Sunflower is placed at 0.5 m height and 4 m horizontally from the centre of the target or at an angle of 7.1°, but after hour 14, the total energy on target increases when the Sunflower is placed at 2 m above ground level or an angle of 26.5°. This pattern follows throughout the year. It is concluded that the relation between Sunflower location and DNI direction impacts the output results. The lower height of sunflower is also beneficial as the wind loads are comparatively less than at higher heights as discussed in literature review section.

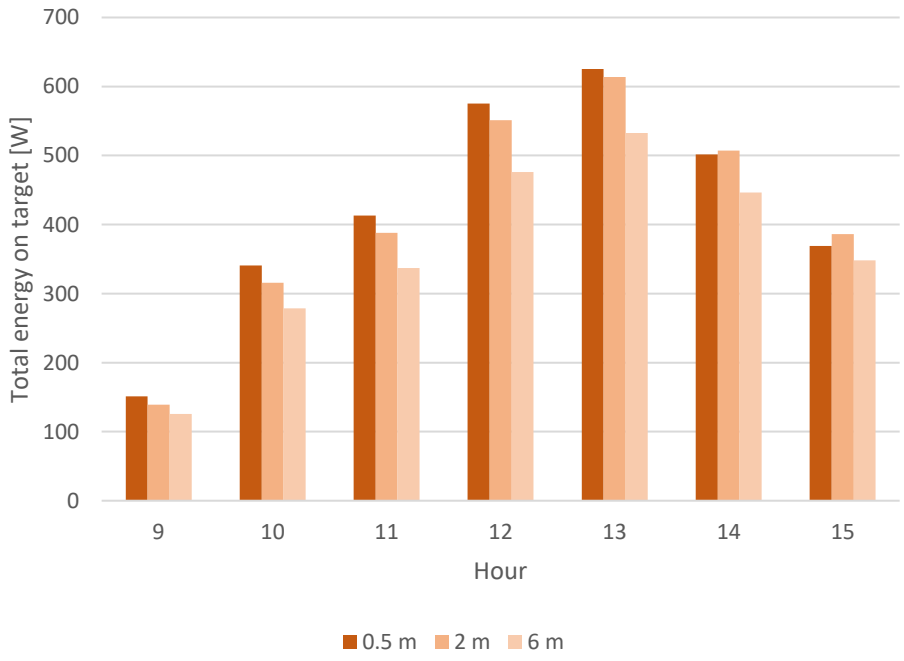

Figure 36: Total energy in W of redirected sunlight by the Sunflower at different heights placed on south of horizontal target on certain day when Sunflower is placed in the north of target, facing south, and forms an angle of 26.5° from the ground

It is found that the intensity ratio is higher when Sunflower is place at a lower height. Table 11 shows the average intensity ratio at different heights.

Table 11: Average intensity ratio at different heights placed on south of horizontal target on certain day

Height of Sunflower [m]	Average intensity ratio [W/W]
0.5	1.84
2	1.81
6	1.70

3.14. Step 1: Overall trend of intensity ratio

It is demonstrated in the previous section that intensity ratio is impacted by changing the vertical angle (height/length) of Sunflower location. To further investigate the overall changes in the intensity ratio, the Sunflower is set to different combinations of vertical and horizontal angles for each month of 2014. The definition of both angles is described in Figure 17.

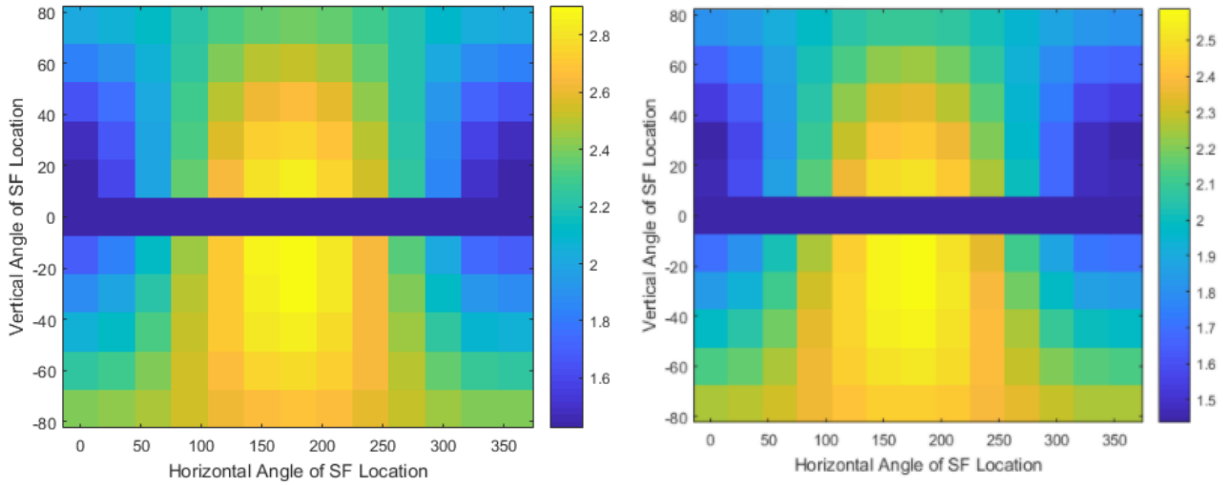

Figure 37: Average intensity ratio in January (left), and February (right) for various vertical and horizontal angles of Sunflower location

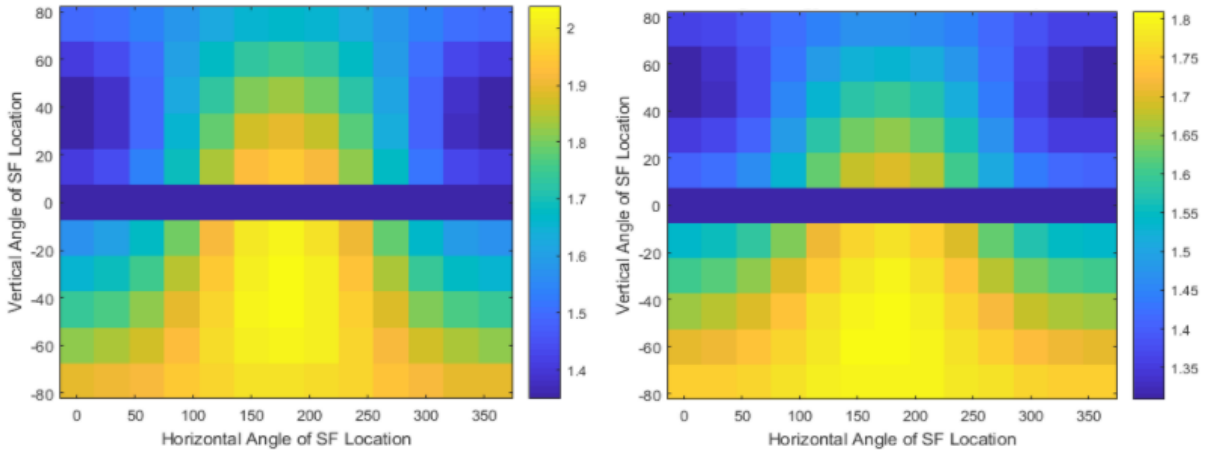

Figure 38: Average intensity ratio in March (left), and April (right) for various vertical and horizontal angles of Sunflower location

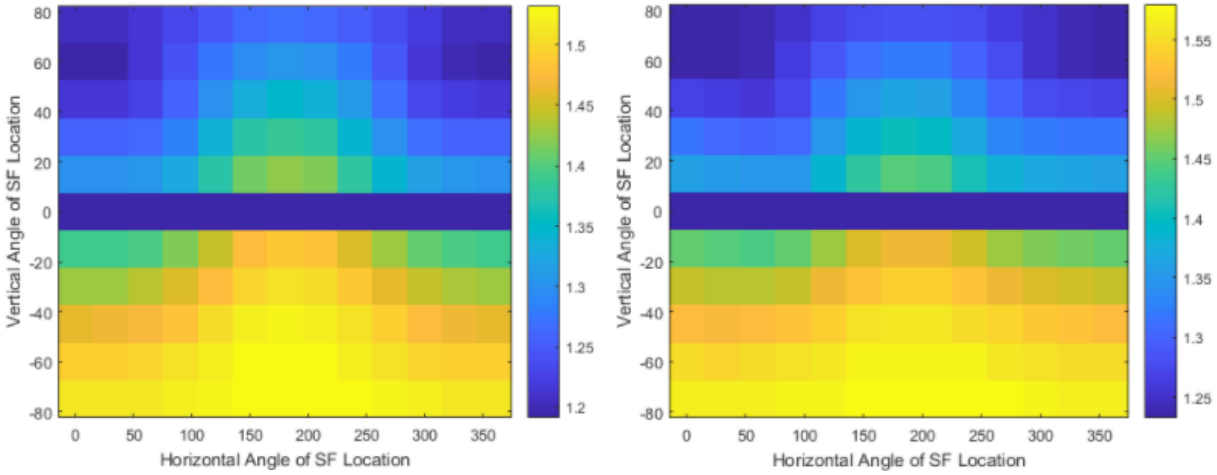

Figure 39: Average intensity ratio in May (left), and June (right) for various vertical and horizontal angles of Sunflower location

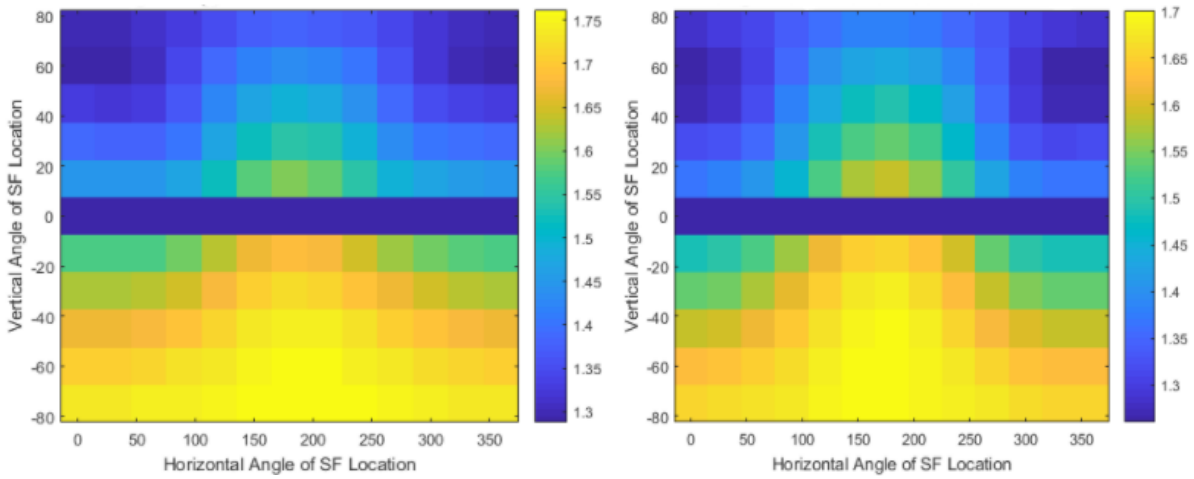

Figure 40: Average intensity ratio in July (left), and August (right) for various vertical and horizontal angles of Sunflower location

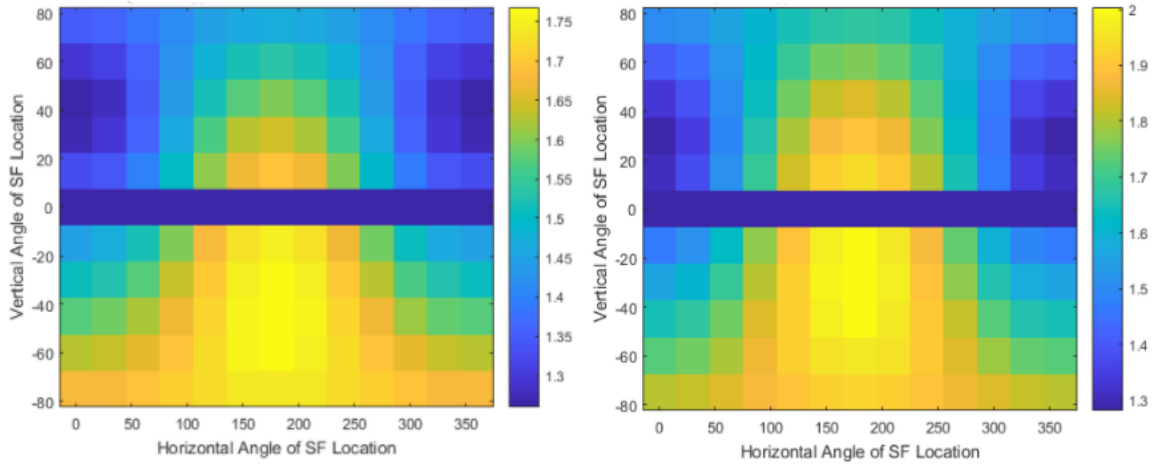

Figure 41: Average intensity ratio in September (left), and October (right) for various vertical and horizontal angles of Sunflower location

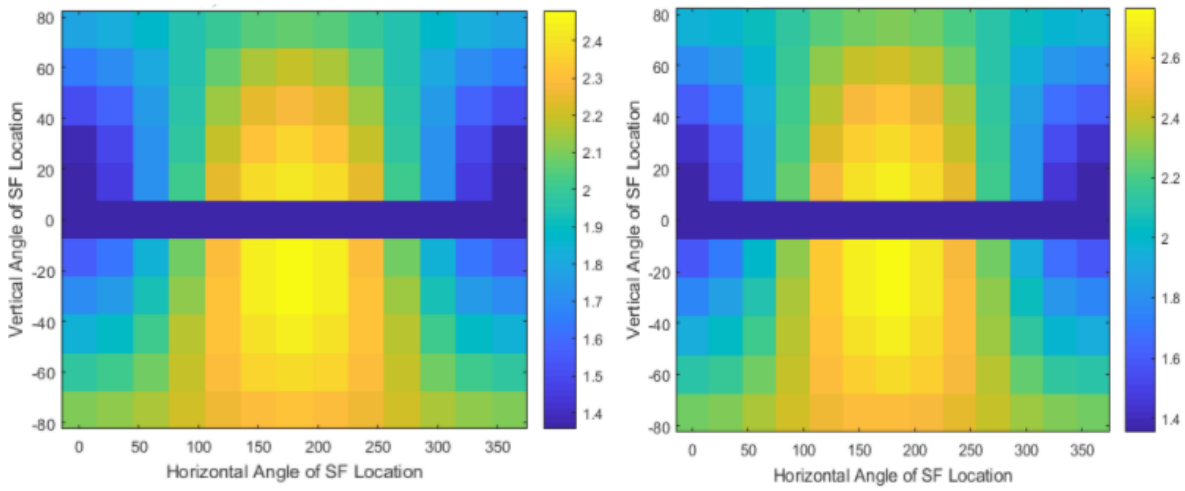

Figure 42: Average intensity ratio in November (left), and December (right) for various vertical and horizontal angles of Sunflower location

Figure 37 to Figure 42 demonstrates that when the horizontal angle of Sunflower location is 0°and the vertical angle is -80°, the average intensity ratio for January is approximately 2.3. This location of Sunflower would be useful in the case of space heating by increasing the solar radiation onto windows that have phase change material to heat up a room during winter season. When the vertical angle is 0° this means the target is at the same height as the Sunflower, the sunlight vector and the plane of Sunflower are parallel to each other and there is no redirected energy onto the target. For this combination the average intensity ratio on target is 1.0 for all months. In the cooler months the intensity ratio is considerably more than the warmer months for all possible combinations of vertical and horizontal angles.

3.15. Step 1: Intensity ratio at different latitude and longitude

To do the comparison of intensity ratios for different latitude and longitude, Vancouver (49.2°) and Arviat (61.1°) locations are compared to Winnipeg site. Additionally, these cities were also selected due to their different climate and weather conditions compared to Winnipeg. In the previous section the results for Winnipeg demonstrated the change in results due to change in Sunflower location and orientation. Figure 43 to Figure 45 demonstrates the daily average intensity of different target locations at Arviat and Vancouver. Table 12 shows the average intensity ratio on different target surfaces in Winnipeg, Arviat, and Vancouver.

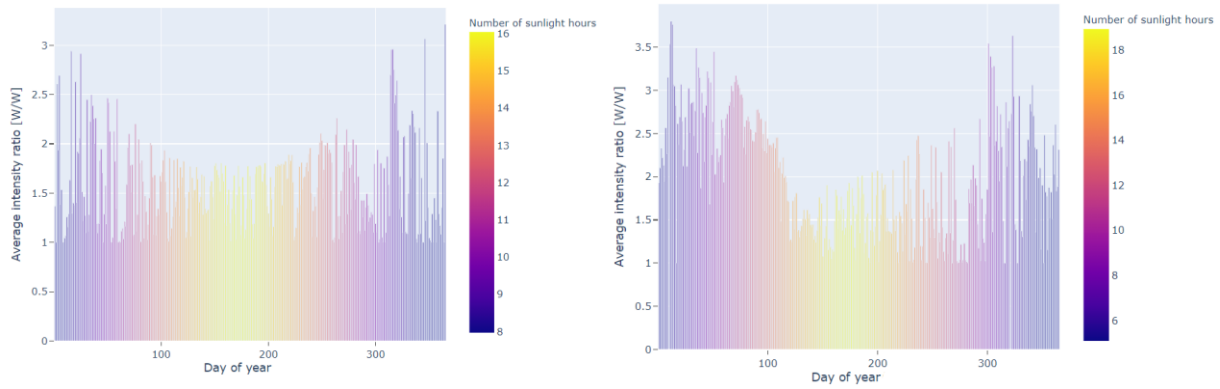

Figure 43: Average intensity ratio on horizontal target in Vancouver (left), and Arviat (right) when Sunflower is placed in the north of target, facing south, and forms an angle of 26.5° from the ground

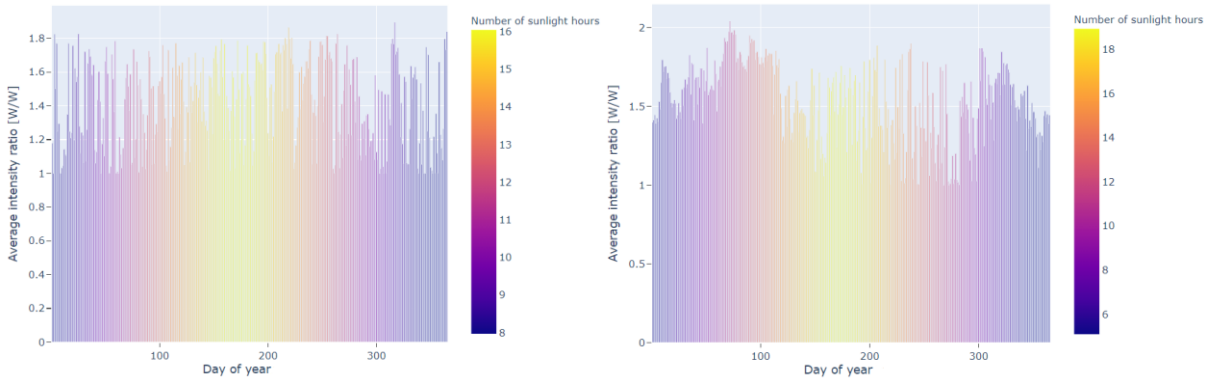

Figure 44: Average intensity ratio on tilted target in Vancouver (left), and Arviat (right) when Sunflower is placed in the north of target, facing south, and forms an angle of 26.5° from the ground

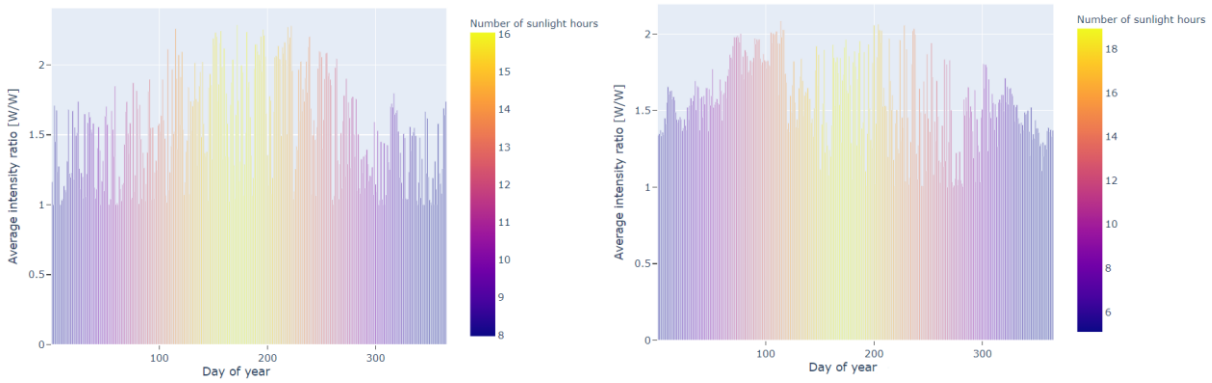

Figure 45: Average intensity ratio on vertical target in Vancouver (left), and Arviat (right) when Sunflower is placed in the north of target, facing south, and forms an angle of 26.5° from the ground.

Table 12: Average intensity ratio on different targets in various locations when Sunflower is placed in the north of target, facing south, and forms an angle of 26.5° from the ground

Location	Horizontal target	Tilted target	Vertical target
Winnipeg	1.81	1.63	1.77
Arviat	1.87	1.65	1.77
Vancouver	1.71	1.60	1.79

It is demonstrated that for Winnipeg, the highest intensity is for a horizontal target and least for the tilted target. As the average intensity ratio is the ratio of total energy on the target to the direct energy on the target, the results show that on average 1 m^2 of the horizontal target receives 148 W/h whereas 1 m^2 of the vertical target receives 156 W/h energy. The total average energy from sun and Sunflower on 1 m^2 of the horizontal target is approximately 269 W/h and vertical target receives about 277 W/h.

On the other hand, Vancouver has the greatest average intensity ratio for vertical target and least for tilted target. The 1 m^2 of the vertical target receives direct energy of 134 W/h and tilted target receives of 175 W/h. The total energy on 1 m^2 of the vertical target is 241 W/h and the tilted target receives 281 W/h. However, in all cases the differences are relatively small.

3.16. Step 1: Comparison of intensity ratio for each month for different latitude and longitude

To optimize the usage of Sunflower for various applications, the monthly intensity ratio is calculated and compared again for Winnipeg, Arviat, and Vancouver. Figure 46 to Figure 51 demonstrates the average daily intensity ratio for each month.

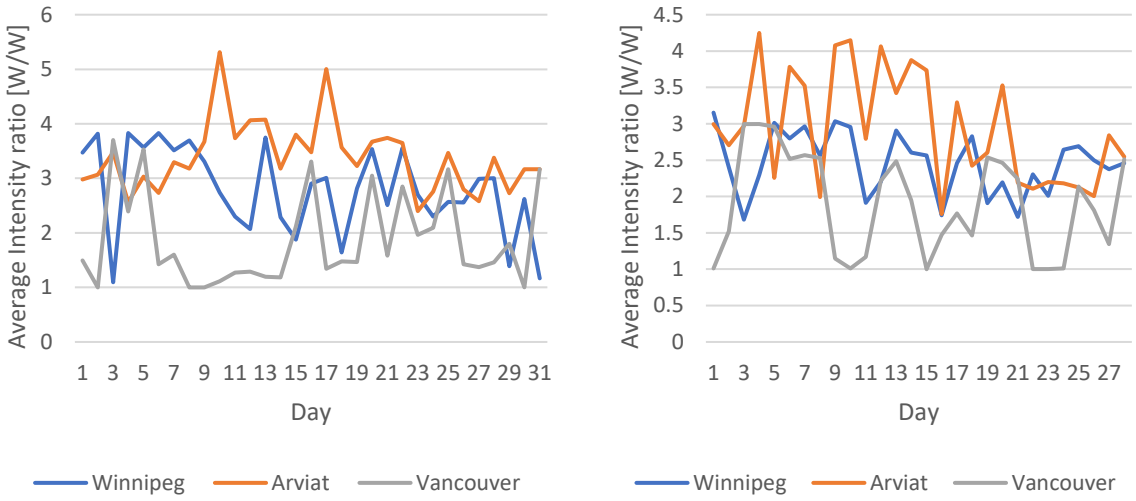

Figure 46: Intensity ratio comparison in January (left) and, February (right) when Sunflower is placed in the north of target, facing south, and forms an angle of 26.5° from the ground

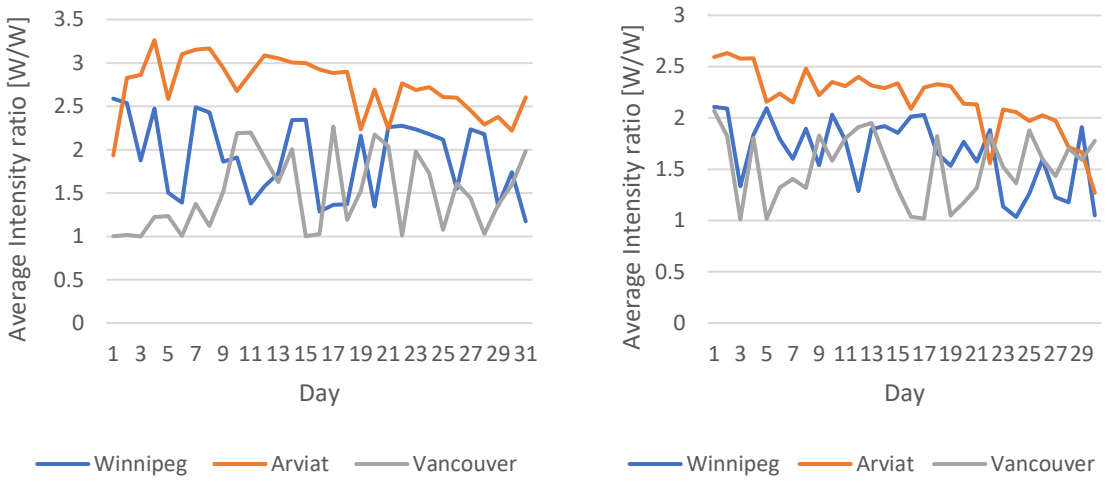

Figure 47: Intensity ratio comparison in March (left), and April (right) when Sunflower is placed in the north of target, facing south, and forms an angle of 26.5° from the ground

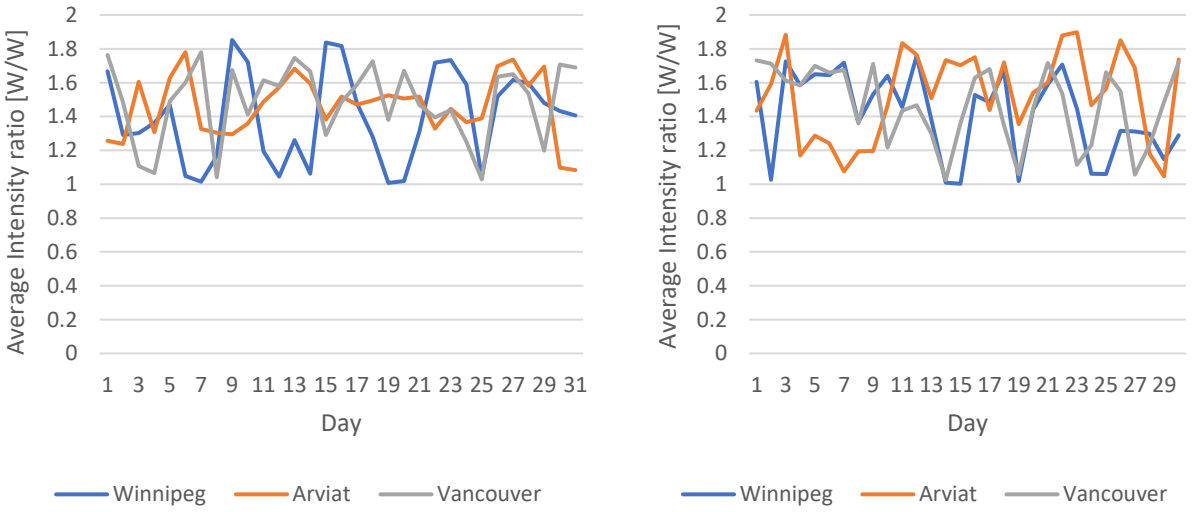

Figure 48: Intensity ratio comparison in May (left), and June (right) when Sunflower is placed in the north of target, facing south, and forms an angle of 26.5° from the ground

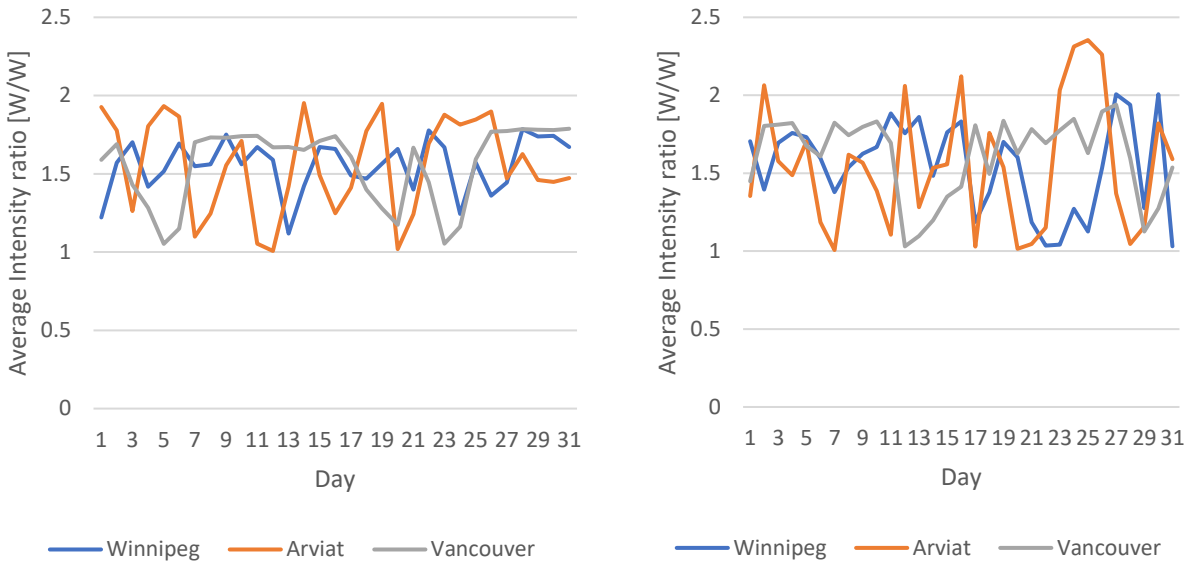

Figure 49: Intensity ratio comparison in July (left), and August (right) when Sunflower is placed in the north of target, facing south, and forms an angle of 26.5° from the ground

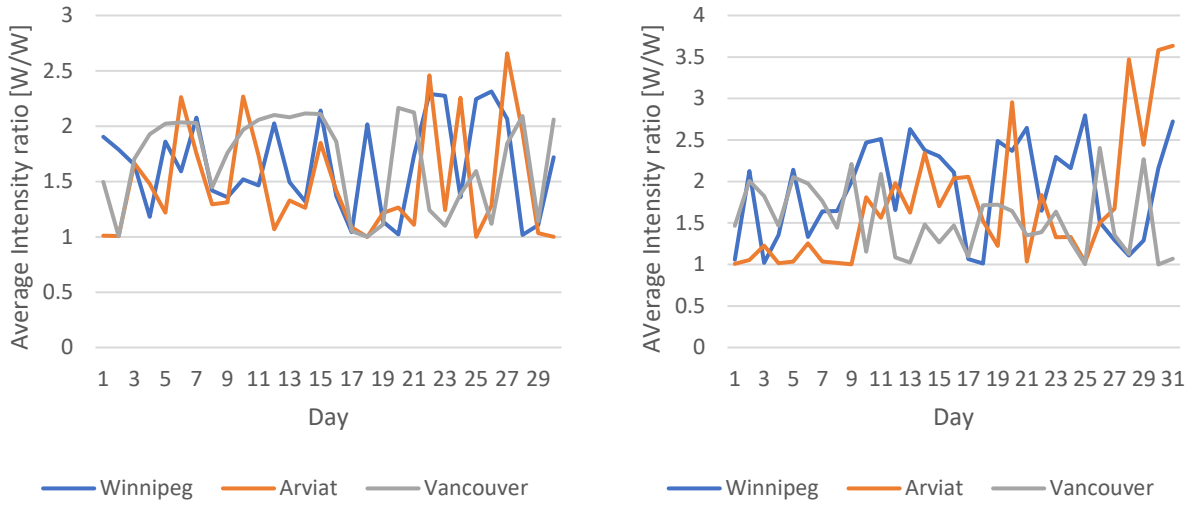

Figure 50: Intensity ratio comparison in September (left), and October (right) when Sunflower is placed in the north of target, facing south, and forms an angle of 26.5° from the ground

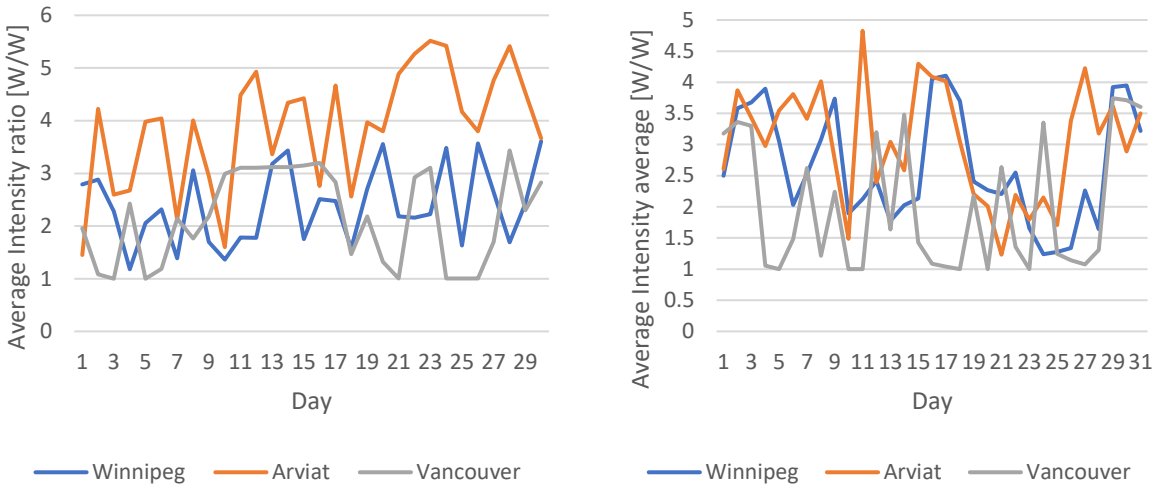

Figure 51: Intensity ratio comparison in November (left), and December (right) when Sunflower is placed in the north of target, facing south, and forms an angle of 26.5° from the ground

The average intensity ratio for fall and winter months are similar for Winnipeg and Arviat. However, there is substantial difference between intensity ratio of fall/winter and intensity ratio of summer/spring for both the cities. Table 13 shows that Vancouver has more consistent average intensity ratio throughout the year. High monthly values occur when the sun is lower in the horizon in winter months. The impact of clouds needs to be better understood as shown next.

Table 13: Monthly average intensity ratio for different locations when Sunflower is placed in the north of target, facing south, and forms an angle of 26.5° from the ground

Month	Winnipeg	Arviat	Vancouver
January	2.78	3.38	1.86
February	2.46	2.94	1.88
March	1.91	2.73	1.49
April	1.66	2.17	1.52
May	1.39	1.46	1.48
June	1.41	1.52	1.46
July	1.55	1.55	1.55
August	1.54	1.55	1.61
September	1.65	1.48	1.69
October	1.90	1.72	1.54
November	2.37	3.87	2.15
December	2.65	3.04	1.98

3.17. Step 1: Intensity ratio on sunny and cloudy day

As Sunflower can contribute to net-zero buildings, it is also important to find the difference between intensity ratio during sunny and cloudy days as Sunflower cannot reflect diffuse radiations in such weather conditions. Figure 52 demonstrates the DNI and intensity ratio on cloudy day and sunny day.

Day number 165 (cloudy) and 169 (sunny) in June are selected from the 2014 data set for Winnipeg to compare the intensity ratio of cloudy and sunny day. The intensity ratio on cloudy day is nearly 1. However, on sunny day, the intensity ratio is considerably higher during morning/evening hours, and nearly constant for remaining hours of the day. There is approximately 60% difference in intensity ratio for both the days. The diffuse irradiations are almost the same on both days.

This completes the description of Step 1 which is required before any net-zero building application is considered. The pool application will now be addressed in Step 2. Recall that Step 2it is different for each Sunflower applications and a custom add-on model is required. However, the Sunflower model for Step 1 is identical for all applications.

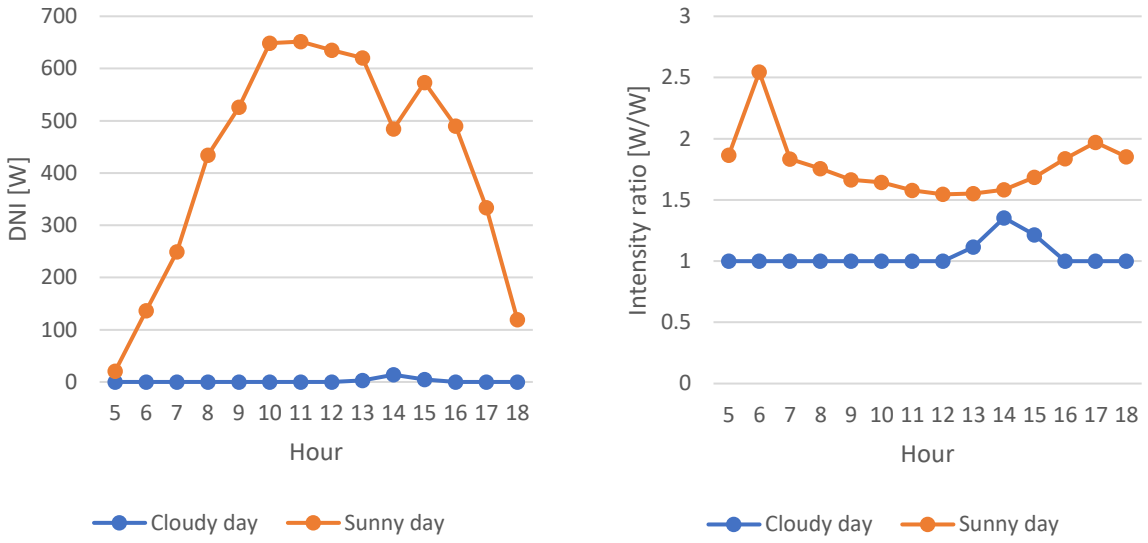

Figure 52: DNI in W (left), and intensity ratio (right) on cloudy day, and sunny day when Sunflower is placed in the north of target, facing south, and forms an angle of 26.5° from the ground

3.18. Step 2: Pool model key assumptions

For the pool model here are a list of key assumptions before the model is presented.

1. The temperature of the water for filling the pool is 25°C.
2. To decrease the heat losses, the material of the pool walls is fiberglass.
3. A pool cover is installed when the pool is not in use.
4. The pool is below ground.
5. The sky temperature is considered equal to air temperature to calculate radiation losses.
6. The hourly outside air temperature and wind speed is provided by the CWEEDS database.
7. Heat losses are dominated by evaporation.
8. The goal is to calculate the ratio of natural gas required with and without using Sunflower mirrors rather than trying to improve the accuracy of pool heat loss models.

3.19. Step 2: Pool model

The Sunflower model is now applied for heating the water of an outdoor below-ground pool which is a seasonal application with the target in a horizontal position and an application not subject to second law analysis. The developed Sunflower model calculates the heating energy requirement from May 1 to October 1 using in part the Engineering toolbox [62]. The total amount of direct and redirected energy onto the target is used to raise the temperature of the pool water. It is important to note here that there is no obstacle between direct and redirect solar energy from the Sunflower and pool. Based on the average residential pool dimension in Canada [46], Table 14 shows the parameters of the pool assumed for the Step-2 pool model.

Table 14: Parameters used for the pool model

Dimensions	Unit
Length	8.0 m
Width	4.0 m
Height (deep)	1.2 m
Volume of water	3,840 m^3

The total amount of energy required to raise the temperature is governed by [47].

$$Q_{required} = c_{water} * m_{water} * (T_{desired} - T_{initial}) \quad (3.52)$$

$Q_{required}$ is the amount of energy needed to achieve the required temperature change of the water. The constant (c_{water}) is the heat capacity of water, which is approximately 4.184 kJ/kg$^{\circ}$C. The mass of the pool water is represented by m_{water}. It is considered that the pool is filled with tap water at 25°C and the initial temperature of the water is 15°C. During operation, the air temperature is taken form CWEEDS dry bulb temperature of the location. The ΔT ($T_{desired} - T_{initial}$) is the temperature difference between desired temperature and the surrounding air temperature of the location. The desired temperature of water is set to 25°C. Since the pool is outside in an open area,

there is a temperature difference between the surroundings and the pool water. Figure 53 shows the pool energy losses.

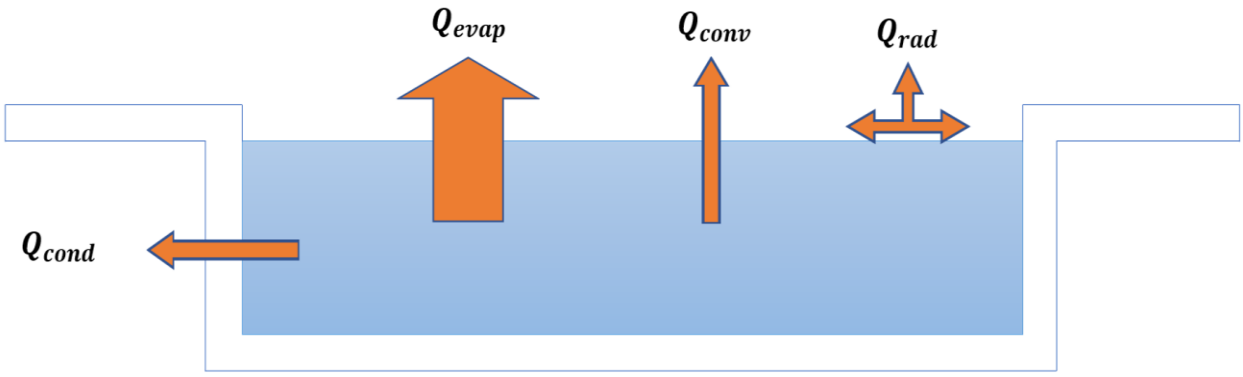

Figure 53: Various heat losses from below ground pool surface

Conduction heat losses: The conduction heat losses can be considered as transfer of energy from more energetic to the less energetic particles due to interactions between them. The heat loss rate by conduction through the pool walls and bottom with the ground is calculated by [48]:

$$Q_{conduction} = k_{fiberglass} * A_{pool\ tube\ surface} * \frac{\Delta T}{L_{thickness}} \tag{3.53}$$

where $Q_{conduction}$ in W/m^2 is the amount of heat loss through conduction. The parameter k is a constant thermal conductivity in W/mK. To reduce the conduction losses, the material for pool walls and floor is set to fiberglass in the Sunflower model with conductivity ($k_{fiberglass}$) of 0.04 W/mK [49]. The pool surface area ($A_{pool\ tube\ surface}$) includes the four walls and surface of pool. The ΔT is the temperature difference between desired pool water temperature and dry bulb temperature from CWEEDS of the location. The $L_{thickness}$ of wall is 0.95 cm. Since the pool is 1.2 meter deep below the ground, it is important to consider soil temperature to calculate the losses. It is assumed that the soil temperature up to 1 m depth is the same as the air temperature. Therefore, the air-dry bulb temperature is taken to calculate the losses through the ground, making this calculation apply to above ground pools also.

Convection heat losses: The heat losses in the form of energy between the surface and moving fluid due to temperature difference are convention heat losses. The convection heat loss happens because of the air velocity at upper interface and induced water flow due to buoyancy forces [50] which is ignored. The convection losses can be calculated by:

$$Q_{convection} = h_c * A * \Delta T \tag{3.54}$$

where $Q_{convection}$ is heat transferred per unit time in W/m^2. The convective heat transferred constant is h_c in W/(m$^{2^\circ}$C) and ΔT is the temperature difference between the fluid and surrounding surface. The convective heat transfer constant (h_c) is calculated by [51]:

$$h_c = 12.12 - 1.16v + 11.6\, v^{1/2} \tag{3.55}$$

The velocity of wind is represented by v and taken from the CWEEDS data to calculate the convection heat losses.

Radiation heat losses: Matter emits energy in the form of thermal radiation by virtue of its temperature. While the other mode of heat transfer requires the presence of medium material, radiation losses are transported by electromagnetic waves. The radiation losses occur on the surface of water to the surrounding by:

$$Q_{radiation} = \varepsilon\sigma(T_s^4 - T_{sur}^4) \tag{3.56}$$

where ε is the emissivity constant. It is a radiative property of the surface which provides a measure of how much energy is emitted by surface compared to a black body. The emissivity value of water is 0.95. The term, σ, is a Stephan Boltzmann constant with a value of 5.67 ×10^{-8} W/m^{2}K^4[52]. T_s is the pool water temperature and T_{sur} is the surrounding temperature which is the temperature of the sky. There are various types of equations for the relationship between sky temperature and air temperature [63]. Due to the complexity of various factors such as sky cloud cover, altitude of clouds, it's hard to estimate the sky temperature. According to Energy Star [64], the sky temperature can be assumed as the surrounding air temperature. Therefore, the developed

Sunflower model for pool heating considers dry bulb temperature taken from the CWEED for T_{sur} to calculate radiation losses.

Evaporation losses: As per the Engineering toolbox [60], evaporation occurs on the pool water surface for unsaturated air. During the evaporation, the water molecules absorb the heat from the pool water surface because the water molecules go through phase change from liquid to gas. The evaporation of pool water depends on the pool temperature, air temperature, air humidity, and air velocity above the water [53]. The maximum saturation pressure of the water vapor in moist air is dependable on the temperature of the air vapor mix [54]. The water vapor saturation pressure can be found by:

$$p_{ws} = 100\, e^{(77.3450 + 0.0057\, T - 7235\, /\, T)} / T^{8.2} \tag{3.57}$$

where p_{ws} is water vapor saturation pressure in Pa, T is the dry bulb temperature of the moist air in $^{\circ}$C. To know how much water can be evaporated, the relative humidity, the ratio of water vapor partial pressure to the water vapor saturation pressure is required. Since the partial pressure of water vapor is unknown, the following numerically curve-fitted empirical equation demonstrating the relation to find the relative humidity, RH, is used [55]:

$$RH = 100\, e^{\frac{cb(TD-T)}{(c+TD)(c+T)}} \tag{3.58}$$

TD is dew pressure in degrees Celsius. Constants c and d have values of 17.62 and 243.0, respectively. The humidity ratio can be expressed as the partial pressure of vapor in air to the partial pressure of the dry air. The water vapor pressure is modest as compared to the atmospheric pressure and the relation between the humidity ratio and the saturation pressure is almost linear [56]. The maximum saturation humidity ratio of saturated air at the same temperature as the water surface (XS), can be expressed as follows:

$$X_S = 0.62198 p_{ws} / (p_{a-} p_{ws}) \tag{3.59}$$

where p_{ws} is saturation pressure of water vapor and p_a is atmospheric pressure in pa. The humidity ratio of air (X) is calculated by:

$$X = 0.62198 p_{ws} RH / [p_{a-}(p_{ws} RH)] \quad (3.60)$$

In addition, the amount of evaporated water can be found by:

$$g_s = \Theta A (X_S - X)/3600 \quad (3.61)$$

where g_s is amount of evaporated water per second (kg/s) and $\Theta = (25 + 19v)$ is an evaporation coefficient (kg/m^{2}h) where v is the wind velocity taken from CWEEDS, A is the water surface area in m^2. Finally, the evaporation losses can be calculated by:

$$Q_{evaporation} = h_{we} g_s \quad (3.62)$$

where h_{we} is the enthalpy of water for phase change from liquid to gas set at 2,442 kJ/kg at 25°C. Because of the evaporation on the pool surface, as the water temperature decreases, the water depth also decreases. To maintain the water depth, water is required to be supplied by a pump. The effect of water supplied by the pump to the pool water temperature is negligible because it is assumed that the temperature of the supplied water by pump is the same as the pool water temperature. It is appropriate to make this assumption because the focus of this research is on the comparison of energy savings of pool heating by Sunflower to natural gas. This assumption is made in both systems: pool heating by Sunflower and pool heating by natural gas, so the overall output is not affected. The model calculates the energy requirements to achieve the desire temperature in the beginning of operating period, after that, the required energy is equal to the pool heat losses.

3.20. Step 2: Natural gas requirement and GHG savings for pool heating application

To accomplish the required energy to heat the pool the direct energy and Sunflower redirected energy is incorporated into the model calculated in Step 1. Furthermore, results are compared to

heating with natural gas and a heat pump. The required energy is taken from the natural gas to achieve the desired amount of energy and is calculated by:

$$Heat\ energy = \frac{1}{HHV_{natural}gas \times efficiency} \tag{3.63}$$

With the high heating value of natural gas taken as 55 kJ/kg [57] and the efficiency of the heat pump is taken as 90% [58].

The greenhouse gases (GHG) savings reduces as the fossil fuels are replaced by solar energy. The GHG savings are calculated by:

$$CH_4 + 2\,O_2 \rightarrow CO_2 + 2\,H_2O + \text{energy} \tag{3.64}$$

This completes the description of the Step-2 pool heating model application.

4. Results and discussion

4.1. Heat losses and required energy to heat up the pool

The heat losses from the pool water are due to the temperature difference between surrounding air and pool water occurs in different heat transfer forms. The model shows that evaporation heat losses dominate compared to other means of heat losses, as described in the literature review. The radiation and conduction losses are minimal as compared to convection and evaporation. Figure 54 demonstrates the different types of heat losses on July 15.

Figure 54: Different types of pool heat losses for July 15 in Winnipeg

Figure 55 shows the heat losses per hour throughout the operating period of pool heating from May 1 to Oct 1 for Winnipeg. To prevent high losses due to high velocity of wind, it is considered that the pool is located near to the fencing area in the backyard. The wind speed is decreased by 3 m/s from the CWEED 2014 wind data. Additionally, it is recommended that the pool must be

covered with insulated pool covers when not in use. The heat losses are set to zero during night-time, sunset, and sunrise hours.

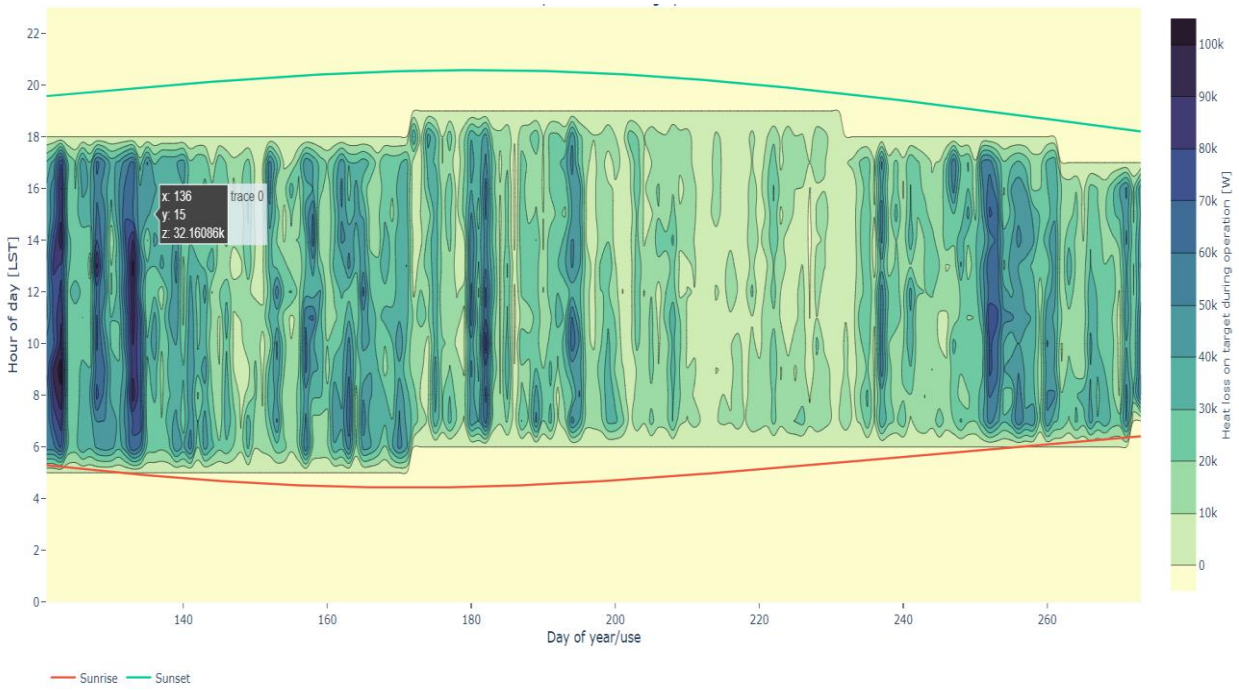

Figure 55: Heat losses per hour throughout the operating period of pool heating between May 1 to Oct 1.

The total amount of energy required to heat up the pool is the sum of initial energy to get the desired temperature and the heat losses. For Winnipeg, the model is simulated with several case scenarios. It is found that by using 10 Sunflowers, a desirable result can be achieved. Figure 56 shows the daily required energy, natural gas requirement, direct energy, and redirect energy from 10 Sunflowers to satisfy the energy demand. The required natural gas is below zero (negative) because the provided direct and redirected energy is more than the requirement to get the desired pool temperature.

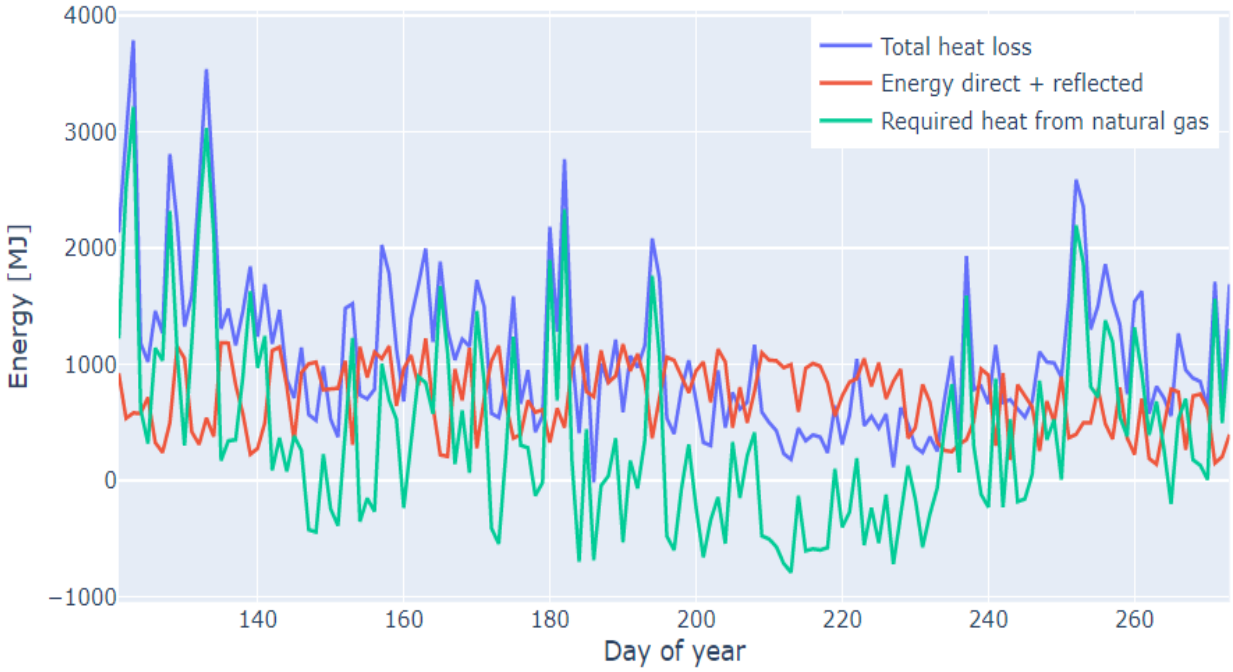

Figure 56: Hourly heat losses, total energy provided by 10 Sunflowers, and required natural gas

In the beginning of May, the energy demand is maximum and decreases by June/July. The total energy required to heat up the pool is 45.7 MW seasonally and the energy provided by 10 Sunflowers is 30.05 MW. The total energy replacement is 67%. Figure 57 demonstrates heat losses, the direct and redirect energy from 10 Sunflowers, and extra energy.

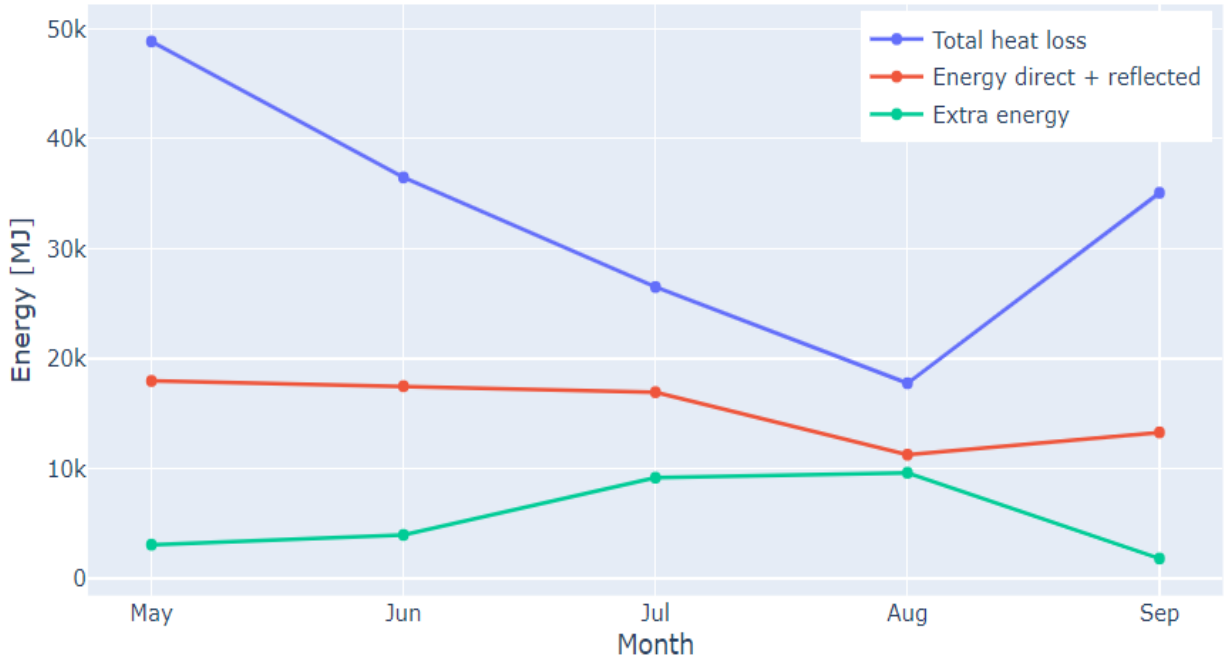

Figure 57: Average monthly heat losses, required energy and extra energy for pool heating

4.2. Natural gas and GHG emissions

The proposed system utilizes solar energy to heat the pool water. The system has also been compared with the natural gas usage for pool heating. It is found that the 48% of natural gas is replaced with solar energy. Figure 58 shows the average monthly natural gas usage with and without proposed model.

The comparison analysis of both the case scenarios, when only natural gas is heating the pool and when Sunflower is primary source to heat the pool is conducted. The GHG savings are calculated by the Sunflower model. The natural gas is producing 9.6 tCO_{2eq} seasonally, but when the natural gas and solar energy are heating the pool water, it produces the 5.1 tCO_{2eq} throughout the period. Figure 59 demonstrates the comparison of CO_2 generated when Sunflower is used and when it is not used.

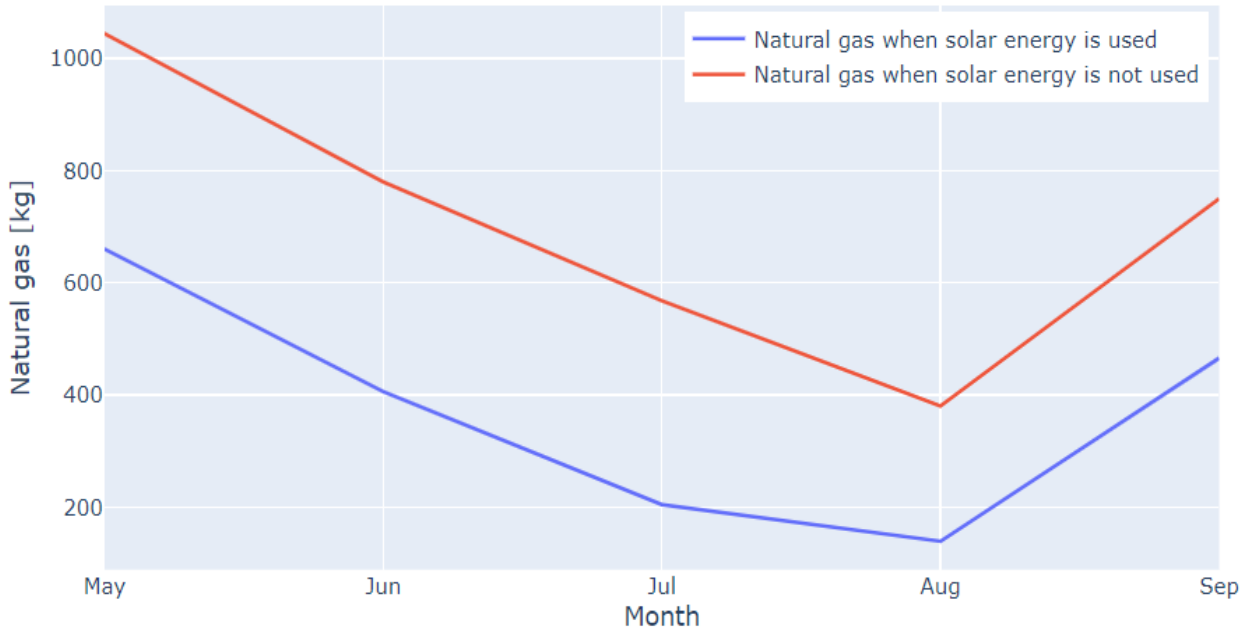

Figure 58: Natural gas usage comparison when Sunflower is used and not used to heat the pool water

Figure 59: Comparison of CO_2 generated between when Sunflower is used and when not

Table 15 highlights the key findings of the proposed system. To achieve the maximum energy output of the system, the number of Sunflowers is increased to 15 and 20 respectively. Table 16 shows the output results with different numbers of Sunflowers incorporated in the Sunflower model.

Table 15: Key findings of proposed system for Winnipeg

Characteristics	Percent
Total energy gain	67%
Total natural gas replacement	48%
Total GHG savings	48%

Table 16: Comparison of different number of Sunflowers for Winnipeg

Number of Sunflowers	10	15	20
Total energy gain	67%	71%	75%
Total natural gas replacement	48%	51%	56%
Total GHG savings	48%	51%	56%

After increasing the number of Sunflowers to 15, the energy production increases as well. The total surface area of pool is 32 m^2 and the mirror area of 1 Sunflower is 1 m^2. It is a magnification ratio when the target area is not equal to Sunflower area. Additionally, as the number of Sunflowers increases, the output energy beyond the required energy also increases. This is another reason of less increment in fuel and GHG emission savings percentage.

Furthermore, the proposed system is also conducted for Arviat, Nunavut location. The pool size, the target location, orientation, and location of Sunflowers set-up is the same as for Winnipeg. Due to cooler temperature in Arviat than Winnipeg, it is found that the 15 Sunflowers are more suitable to get the pool water temperature 25°C. Table 17 shows the energy calculations for the city of Arviat.

Table 17: Energy calculations for Arviat for pool energy use

Required energy and heat loss	Direct and energy from Sunflowers	Percent energy savings
62.5 MW	28.5 MW	46%

The Sunflower model for pool heating in Arviat demonstrated that for some hours, the energy provided by the proposed system is more than required. After not including this extra energy, the natural gas and GHG emission savings are 40%. The difference between energy savings and natural gas savings is significantly less for Arviat as compared to Winnipeg because of the difference in weather conditions for both the locations.

4.3. Cost analysis

The final assembled system will consist of parts that are designed and manufactured in-house and purchased from local part shops. Table 18 shows the parts needed for a Sunflower system.

Table 18: Part items and manufacturers

Items	Type	Manufacturer
Sunflower	3D printed	In house developed
Fence pole	Galvanized steel	Master Halco
Pool insulator cover	Bubble polycarbonate insulator	Qingdao Taiyue Composite Material Co., Ltd.

The cost analysis of the project is conducted for a system that can function independently. The system cost with more or fewer Sunflowers can be calculated by comparison with given system cost. Table 19 lists the list of items available in the market and the forecasted expenses for the parts designed and manufactured in house.

Table 19: Purchase/make prices of item

Item	Quantity	Price	Unit total
Sunflower	10	$50.00	$500.00
F. Pole	10	$20.00	$200.00
Pool insulator cover	1*32 m^2	$50	$50
System total			$750

The fuel comparison for the proposed project of pool heating with and without Sunflowers is conducted with natural gas. The residential average price of natural gas in Manitoba is $0.25/kg as per Manitoba Hydro [59]. Table 20 shows the fuel cost saving analysis of the system.

Table 20: Fuel cost saving analysis

Natural gas without Sunflowers	Natural gas with Sunflowers
$880/season	$468/season

The financial analysis of the project shows that the project yields 48% gain per season. It is concluded that this is a profitable project. The operating cost of natural gas pool heating system without using Sunflower is $880/season which reduces to $468/season when Sunflower system is being used. The projected lifetime of Sunflower is 25 years. The lifetime fuel cost savings for the pool heating using Sunflower in Winnipeg is $11,700.

5. Conclusion and recommendation

Conclusions: There is no information on the performance of small-scale reflective mirrors in the literature to contribute to building net-zero applications. Such systems do exist for large-scale applications that are optimized. For large-scale applications there is no restrictions on mirror placement, there is no redeployment of mirrors by the user, and the target is always north above the mirrors, and never below. A Sunflower model was developed which calculates the solar energy ratio allowing the user flexibility in placement of the mirrors and focus on seasonal applications. The Sunflower model was validated using Solartrace. The model was then used to investigate how Sunflower can be applied for heating a pool where it heats the water without the need of a heat transfer fluid, saves fuel costs, and reduces GHG emissions. Such a Sunflower application is aligned with THE RED CUP as it produces renewable heat at the personal scale (H-R-P) to help solve climate change.

The Sunflower model is developed in 2-steps:

- Step 1: Used for any applications and calculates the intensity and magnification ratio for user inputs for a given Sunflower project for different targets and seasonal relocation
- Step 2: A customized pool model required to be developed for pool heating application

The Step 1 of Sunflower model calculates the average direct energy from sun on a horizontal target is 148 W per meter of target area and the average redirect energy from Sunflower is 121 W per meter of target area. The total gain of energy is 81%. Furthermore, the base model results were validated with Solartrace calculations within an error of 2.35%. The total gain for a vertical surface is 77% and tilted surface at 50° to the ground is 63% for Winnipeg. Furtherly, the impact of different latitude and longitude on intensity ratio has been calculated. The total energy intensity gain for a horizontal target is 71% for Vancouver and 87% for Arviat. The total energy intensity gain for a vertical target is almost the same for all three cities.

When comparing the average intensity ratio for each month, the maximum intensity ratio in colder months is noticeably more than the warmer months for Winnipeg and Arviat. However, for

Vancouver the intensity ratio is almost the same throughout the year due to climate and sun's azimuth angle. The results demonstrated that the intensity ratio is more when place at a lower height or lower angle as compared to a higher height. The intensity ratio is highest when the Sunflower is placed in the north of the target and facing south. When the Sunflower is placed in the south of target and facing north, the average intensity ratio is approximately 23% lower as compared to the highest average intensity ratio. The average intensity ratio is approximately 1.60 when the Sunflower is placed in the east and north of the target. Additionally, the average intensity ratio is approximately 60% more on sunny days as compared to cloudy days due to only availability of only diffused solar energy.

Furthermore, the average magnification ratio of a Sunflower in Winnipeg is calculated by keeping either mirror area or the target area 10 times bigger than the other. The magnification ratio for 1 m^2 horizontal target with 10 m^2 of Sunflower mirror area, is 9.79 and is almost the same for a 1 m^2 vertical target. In case of the tilted target, the magnification ratio is 7.84 when the target area is 1 m^2 and the Sunflower mirror area is 10 m^2. The average magnification ratio is approximately 1.08 for all the target positions when the target area is 10 m^2 and mirror area is 1 m^2.

The overall trend of average intensity ratio is calculated by orienting the Sunflower at various combinations of vertical angles and horizontal angles for each month of 2014 for Winnipeg. The best combination to get most average intensity is when the Sunflower is placed in the south of the target, which is 180° horizontally and vertical angle is -30° in cooler months. Whereas the efficient combination of angles of Sunflower in summer is 180° horizontally and vertical angle of -50° for the horizontal target. The combination of angles of Sunflower location also depicts that there is no average intensity gain when the Sunflower is at the same height as the target because the sunlight vector is parallel to the plane. As the warmer months getting started the higher vertical angles give the lower average intensity ratio for all combinations with horizontal angle.

In step 2, the proposed pool heating application provides 67% of the required energy using 10 Sunflowers leading to 48% of the natural gas savings for Winnipeg. For Arviat, the total energy

saving is 46% and 40% of natural gas savings with 15 Sunflowers. The usage of 10 Sunflowers in Winnipeg provides 48% of financial gain per year without any need of operation cost. The projected life of this project is considered for 25 years. The GHG emission in Winnipeg is the 9.6 tCO_2eq seasonally to heat the pool by using natural gas but it deescalated to 5.1 tCO_{2eq}, when pool heating is done with Sunflowers.

The pool heating approach using Sunflower bypasses second law inefficiencies as the pool is heated by the irradiations directly from sun without the use of any intermediate thermal fluid. The temperature of pool water is raised by direct sun rays so there are no thermal losses. The heat from the solar rays is completely transferred to the pool water.

The evaporation losses are high as compared to the other losses. Additionally, for the cooler area like Arviat the heat transfer losses are more than Winnipeg, so the total gain for Arviat is more than Winnipeg as the extra energy is not much. The further research for reducing the heat losses due to evaporation, which is mainly due to high wind, can be done.

Recommendations: Additional Step-2 models need to be developed to allow users to redeploy Sunflower seasonally to optimize the energy generated to contribute to net-zero buildings:

- Heating windows with phase change materials
- Increase solar radiation into a greenhouse to reduce energy use and increase luminance
- Increase solar PV output
- Develop a single solar capture device and use multiple sunflowers to reduce cost for solar heating

Of research interest is to:

- Use fabric mirror filters to remove
    - UV to reduce skin cancer for applications involving people in the building like a sunroom
    - UV and IR leaving only PAR photons for growing plants

- Modify the mirror fabric to separate frequencies (diffraction) so that the target receives separated frequencies so that multiple applications can be used simultaneously at optimize the use of frequency ranges to better contribute to net-zero buildings.
- Estimate the contribution such mirrors can help building chive net-zero worldwide.

Bibliography

1. Toshiko Kaneda and Kristin Bietsch, “PRB Projects World Population Rising 33 Percent by 2050 to Nearly 10 Billion,” 2015 World Popul. Data Sheet, p. 23, 2016.
2. “World Energy Outlook 2017,” World Energy Outlook, 2017.
3. “Climate Change,” OECD Environmental Outlook to 2030 OECD Environmental Outlook, pp. 139–175, 2008.
4. E. P. Agency, “Atmospheric Concentrations of Greenhouse Gases,” pp. 1–13, Aug. 2016.
5. R. Harrington, “This incredible fact should get you psyched about solar power,” Business Insider, 29-Sep-2015.
6. “OECD Environmental Outlook to 2050 (Summary in Finnish),” OECD Environmental Outlook OECD Environmental Outlook to 2050, 2012.
7. . A. Som and S. Al-Alawi, “Characterisation And Evaluation Of Efficiency And Degradation Of Mono And Poly-Crystalline Photovoltaic Modules,” Energy and the Environment, pp. 361–365, 1990.
8. E. Trianti-Stourna, K. Spyropoulou, C. Theofylaktos, K. Droutsa, C. Balaras, M. Santamouris, D. Asimakopoulos, G. Lazaropoulou, and N. Papanikolaou, “Energy conservation strategies for sports centers: Part B. Swimming pools,” Energy and Buildings, vol. 27, no. 2, pp. 123–135, 1998.
9. “Affordable gas pool heaters,” Norwest Gas, 26-Jan-2021. [Online]. Available: https://www.norwestgas.com.au/pool-heating/gas-pool-heating/. [Accessed: 02-Apr-2021].
10. “Solar swimming pool heaters,” Energy.gov. [Online]. Available: https://www.energy.gov/energysaver/solar-swimming-pool-heaters. [Accessed: 29-Aug-2021].
11. About the author homestratosphere's editorial staff & writers, “What is the average size of residential in-ground swimming pools? Get all the details here,” Home Stratosphere, 16-Aug-2021.
12. “Residential solar pool heating systems.” Canada, Canada, 2001.

13. “Pool Heating Options Explained,” Pool Supplies Canada. [Online]. Available: https://www.poolsuppliescanada.ca/pool-heating-options-explained.html. [Accessed: 2021].
14. L. Lisell, T. Tetreault, and A. Watson, “Solar Ready Buildings Planning Guide,” 2009.
15. “Life Cycle Greenhouse Gas Emissions from Solar Photovoltaics (Fact Sheet),” 2012.
16. O. Nnaemeka and E. Bibeau, “Application of Low Temperature Phase Change Materials to Enable the Cold Weather Operability of B100 Biodiesel in Diesel Trucks,” ASME 2018 12th International Conference on Energy Sustainability, 2018.
17. T. Maridurai, A. A. Muhammad Irfan, E. Vengadesan, K. Loganathan, M. S. Mohamed Aminudeen, and K. Harish Ahamed, “Review on material aspects of solar thermal collectors,” Int. J. Mech. Eng. Technol., vol. 9, no. 7, pp. 286–292, 2018.
18. USGBC, “LEED.” USGBC. [Online]. Available: https://new.usgbc.org/leed [January 6, 2019]
19. J. C. Sattler, M. Röger, P. Schwarzbözl, R. Buck, A. Macke, C. Raeder, and J. Göttsche, “Review of heliostat calibration and tracking control methods,” Solar Energy, vol. 207, pp. 110–132, 2020.
20. A. Pfahl et al., “Progress in heliostat development,” Sol. Energy, vol. 152, pp. 3–37, 2017.
21. S. Zhang, A. M. Qwbaiban, J. Huh and T. G. Habetler, "Dimension and mechanical structure design of low-cost Heliostats in concentrated solar power plants," 2019 IEEE energy conversion congress and exposition (ECCE), 2019, pp. 3441-344.
22. H. Zhang, Y. Sun, L. Wu, X. Zhang, and Y. Xiang, “Tracking mechanism and cosine effect study of module-Heliostat solar collector,” in proceedings of the 2016 4th international conference on machinery, materials and information technology applications, 2016.
23. . G. López, G. López, C. A. Gueymard, and J. L. Bosch, “Evaluation of solar energy losses for the heliostat-to-receiver path of a tower solar plant for different aerosol models,” in Proceedings of SWC2017/SHC2017, 2017.
24. A. Pfahl, M. Randt, F. Meier, M. Zaschke, C. P. W. Geurts, and M. Buselmeier, “A holistic approach for low cost heliostat fields,” Energy Procedia, vol. 69, pp. 178–187, 2015.
25. J. A. Peterka, Z. Tan, J. E. Cermak, and B. Bienkiewicz, “Mean and peak wind loads on heliostats,” J. Sol. Energy Eng., vol. 111, no. 2, pp. 158–164, 1989.

26. A. Algarue, S. Mahmoud, and R. K. AL-Dadah, “Optical performance of low concentration ratio reflective and refractive concentrators for photovoltaic applications,” energy procedia, 12-Jan-2015.
27. L. Wood, “The science behind Heliostats and concentrated solar power (CSP) Heliostats,” HELIOSCSP, 27-Dec-2016.
28. A. Mousia and A. Dimoudi, “Energy performance of open air swimming pools in Greece,” energy and buildings, 10-Jan-2015.
29. Y. Li, N. Nord, G. Huang, and X. Li, “Swimming pool heating technology: A state-of-the-art review,” Building Simulation, vol. 14, no. 3, pp. 421–440, 2020.
30. R. Croy and F. A. Peuser, “Experience with solar systems for heating swimming pools in Germany,” Solar Energy, vol. 53, no. 1, pp. 47–52, 1994.
31. A. Dang, “A parametric study of swimming pool heating—I,” Energy Conversion and Management, vol. 26, no. 1, pp. 27–31, 1986.
32. A. Alkhamis and S. Sherif, “Performance analysis of a solar-assisted swimming pool heating system,” Energy, vol. 17, no. 12, pp. 1165–1172, 1992.
33. G. P. Greyvenstein and J. P. Meyer, “The viability of heat pumps for the heating of swimming pools in South Africa,” Energy, vol. 16, no. 7, pp. 1031–1037, 1991.
34. J. C. Lam and W. W. Chan, “Energy performance of air-to-water and water-to-water heat pumps in hotel applications,” Energy Conversion and Management, vol. 44, no. 10, pp. 1625–1631, 2003.
35. L. Yantong, Z. Quan, S. Xiaoqin, D. Yaxing, and L. Shuguang, “Optimization on Performance of the Latent Heat Storage Unit (LHSU) in Telecommunications Base Stations (TBSs) in China,” Energy Procedia, 28-Aug-2015.
36. Zimmermann@stlouisfed.org and M. C. & C. Argyrou, “Energy storage for electricity generation and related processes: Techn,” Renewable and Sustainable Energy Reviews, 01-Jan-1970.
37. R. Du, W. Li, T. Xiong, X. Yang, Y. Wang, and K. W. Shah, “Numerical investigation on the melting of nanoparticle-enhanced PCM in latent heat energy storage unit with spiral coil heat exchanger,” Building Simulation, 23-Apr-2019.
38. G. Zsembinszki, M. M. Farid, and L. F. Cabeza, “Analysis of implementing phase change materials in open-air swimming pools,” Solar Energy, 19-Nov-2011

39. E. Ruiz and P. J. Martinez, “Analysis of an open-air swimming pool solar heating system by using an experimentally validated TRNSYS model,” Solar Energy, 15-Jan-2010.
40. D. Govaer and Y. Zarmi, “Analytical evaluation of direct solar heating of swimming pools,” Solar Energy, 07-Aug-2003
41. “Fresnel Equations,” Internal Reflection and ATR Spectroscopy, pp. 39–54, 2012.
42. D. Rosenbloom and J. Meadowcroft, “Harnessing the Sun: Reviewing the potential of solar photovoltaics in Canada,” Renewable and Sustainable Energy Reviews, vol. 40, pp. 488–496, 2014.
43. M. Mousa, A. Bayomy, and M. Saghir, “Phase change materials effect on the thermal radius and energy storage capacity of energy piles: Experimental and numerical study,” International Journal of Thermofluids, vol. 10, p. 100094, 2021.
44. “Plastics & Elastomers - The Universal Selection Source,” SpecialChem. [Online]. Available: https://omnexus.specialchem.com/selectors?q=High-density polyethylene. [Accessed: 01-May-2021].
45. G. Szeicz and R. Mcmonagle, “The heat balance of urban swimming pools,” Solar Energy, vol. 30, no. 3, pp. 247–259, 1983.
46. M. Jobe, “Inground Pool Sizes: Three Questions to Ask Yourself,” Pool Pricer, 21-Apr-2020.
47. J. Carvill, “Thermodynamics and heat transfer,” Mechanical Engineers Data Handbook, pp. 102–145, 1993.
48. R. Serth, “Heat Conduction,” Process Heat Transfer, pp. 1–41, 2007.
49. Thermal Conductivity. [Online]. Available: http://hyperphysics.phy-astr.gsu.edu/hbase/Tables/thrcn.html. [Accessed: 23-May-2021].
50. L. L. C. Engineers Edge, “Convective Heat Transfer Convection Equation and Calculator: Engineers Edge,” Engineers Edge - Engineering, Design and Manufacturing Solutions. [Online]. Available: https://www.engineersedge.com/heat_transfer/convection.htm. [Accessed: 02-Oct-2021].
51. P. Kosky, R. Balmer, W. Keat, and G. Wise, “Mechanical Engineering,” Exploring Engineering, pp. 259–281, 2013.

52. M. Dresden, “Boltzmann constant,” Access Science, 01-Jan-1970. [Online]. Available: https://www.accessscience.com/content/boltzmann-constant/089800. [Accessed: 02-May-2021].
53. A. Garnysz-Rachtan and Z. Zapałowicz, “Effect of air parameters, water temperature, and number of pool occupants on moisture gains,” E3S Web of Conferences, vol. 70, p. 02006, 2018.
54. S. A. Kalogirou, “Solar Water-Heating Systems,” Solar Energy Engineering, pp. 257–321, 2014.
55. C. Lee and Y.-J. Wang, “A novel method to derive formulas for computing the wet-bulb temperature from relative humidity and air temperature,” Measurement, vol. 128, pp. 271–275, 2018.
56. Y. Huang, J. Pei, P. V. Nielsen, F. Bonthoux, S. Lechene, F.-X. Keller, S. Wu, C. Xu, and Z. Cao, “Experimental techniques,” Industrial Ventilation Design Guidebook, pp. 185–277, 2021.
57. I. Dincer, M. A. Rosen, and F. Khalid, “3.16 Thermal Energy Production,” Comprehensive Energy Systems, pp. 673–706, 2018.
58. Gas Pool Heaters & Pool Heat Pumps - Hayward Canada Pool Products. [Online]. Available: https://www.hayward-pool.ca/shop/en/canada/in-ground-product/can-heaters-info. [Accessed: 09-May-2021].
59. “Residential rates,” Manitoba Hydro. [Online]. Available: https://www.hydro.mb.ca/accounts_and_services/rates/residential_rates/. [Accessed: 01-May-2021].
60. “Evaporation from a water surface,” Engineering ToolBox. [Online]. Available: https://www.engineeringtoolbox.com/evaporation-water-surface-d_690.html. [Accessed: 27-Jan-2022].
61. L. Wald, Fundamentals of Solar Radiation. Boca Raton: CRC Press, 2018.
62. “Swimming pool heaters,” Engineering ToolBox. [Online]. Available: https://www.engineeringtoolbox.com/swimming-pool-heating-d_878.html. [Accessed: 06-Feb-2022].
63. F. Asdrubali, L. Evangelisti, G. Grazieschi, and C. Guattari, “Influence of sky temperatures on building energy needs,” Building Simulation Conference proceedings.

64. “Swimming Pool - NRCAN.” [Online]. Available: https://www.nrcan.gc.ca/sites/www.nrcan.gc.ca/files/energy/pdf/benchmarking-rendement/Swimming_Pool-ACC-EN.pdf. [Accessed: 22-Feb-2022].